2015-ENAM-0001

École doctorale n° 432 : Sciences des Métiers de l'Ingénieur

Doctorat ParisTech

T H È S E

pour obtenir le grade de docteur délivré par

l'École Nationale Supérieure d'Arts et Métiers

Spécialité " Mécanique - Matériaux "

présentée et soutenue publiquement par

Xiguang LI

le jeudi 15 janvier 2015

GRAPHENE / POLYMER NANOCOMPOSITES: VISCOELASTICITY, FORCED ASSEMBLY AND NANOSANDWICH

Directeur de thèse : **Gregory McKenna, Gilles REGNIER**
Co-encadrement de la thèse : **Guillaume Miquelard-Garnier**

Jury

M. Jinbo BAI	Professeur des Universités, MSSMAT, Ecole Centrale de Paris	Président
M. Micah GREEN	Associate Professeur, Texas AM University	Rapporteur
M. Olivier LAME	Professeur des Universités, MATEIS,, INSA	Rapporteur
M. Gregory MCKENNA	Professeur, TexasTech University	Examinateur
M. Guillaume MIQUELARD	Maître de conférences, PIMM, CNAM	Examinateur
M. Gilles REGNIER	Professeur des Universités, PIMM, Arts et Métiers ParisTech	Examinateur
M. Ronald C. HEDDEN	Associate Professeur, TexasTech University	Invité
M. Edward L. QUETEVIS	Professeur, TexasTech University	Invité

T H È S E

Arts et Métiers ParisTech - Centre de Paris
PIMM – Procédés et Ingénierie en Mécanique et Matériaux

ACKNOWLEDGEMENTS

I would like to express the deepest appreciation to my Texas Tech University supervisor, Professor Gregory B. McKenna, who guided and supported me in the area of rheology and mechanics. I have benefited a lot from his wealth of knowledge and from being exposed to his excellent professionalism in the past five years.

I would like to thank my Arts et Métiers ParisTech supervisor Professor Gilles Régnier. I benefited a lot from the discussion with him about the micromechanics and I really appreciate his help during my time in PIMM laboratory. I would like to thank my Arts et Métiers ParisTech co-supervisor Professor Guillaume Miquelard-Garnier. I have been gifted with his assistance throughout my time in Paris and really appreciate him for revising my research papers. I am also grateful to Dr Jinbo Bai for serving as my Arts et Métiers ParisTech committee.

I would like to thank Professor Ronald C. Hedden and Professor Edward L. Quitevis for serving as my Texas Tech University committee. I am also grateful to Professor Olivier Lame at INSA de Lyon and Professor Micah J. Green at Texas A&M University for spending their precious time being my Rapporteur.

I would like to acknowledge all members in Professor McKenna's group and all colleagues in PIMM laboratory for their help and friendship.

This dissertation is dedicated to my parents, my wife Zhen Zhang and my little son Lucas Li, for their love and support.

Finally, I would like to thank the National Science Foundation under Grant DMR-1207070, the John R. Bradford endowment at Texas Tech University, Chateaubriand Fellowship from the Embassy of France in the United States and PIMM laboratory at Arts et Métiers ParisTech, and each for partial support of this work.

TABLE OF CONTENTS

Chapter 7. Conclusions and Future work

Résumé de la thèse de doctorat de Xiguang Li

Nanocomposites graphène/polymères: rôle de la viscoélasticité, mise en œuvre par assemblage forcé, et étude de l'interface

Cette thèse ayant été rédigée en anglais, nous commençons ici par brièvement décrire les objectifs et principaux résultats de ce travail en français.

Ce travail a été réalisé dans le cadre d'une cotutelle entre Texas Tech University et Arts et Métiers ParisTech. Une partie du travail a donc été réalisée à Texas Tech University dans le département de Chemical Engineering, l'autre à Arts et Métiers ParisTech, plus précisément au laboratoire PIMM, grâce à l'obtention d'une bourse Châteaubriand.

Le travail de thèse est ici présenté, après deux chapitres introductifs, sous forme d'articles. 3 articles, ainsi qu'un acte de conférence dans une revue à comité de lecture, ont déjà été publiés (chapitres 3, 4 et 5) (voir références). Le chapitre 6 est également basé sur un article en cours de rédaction.

L'ajout de graphène et de nanoparticules dérivées de graphène pour renforcer des matrices polymères est une thématique de recherche en pleine expansion depuis l'isolation du graphène en 2004 et la caractérisation de ses propriétés exceptionnelles, du point de vue mécanique et électrique notamment. Cependant, comme il a pu être montré précédemment dans le cas d'autres nanocharges (montmorillonite ou nanotubes de carbone, par exemple), les nanocomposites polymères /graphène posent encore plusieurs questions qui doivent être abordées:

i. L'effet de renfort observé est-il lié aux propriétés intrinsèques de la nanocharge ou aux modifications structurales que la nanocharge peut amener au niveau de la matrice (modification de la cristallinité, par exemple). Dans le cas de polymères amorphes, le

renforcement apparent serait-il tout simplement dû à une variation de la transition vitreuse ? Dans ce cas, comment prendre en compte cet effet pour obtenir le renfort « réel » de la nanocharge ?

ii. Le graphène étant une particule plane, est-il possible d'obtenir cette orientation planaire des particules dans une matrice polymère, ceci afin d'obtenir un renfort à 2 dimensions?

iii. Comment étudier les mécanismes d'interface entre le graphène et les matrices polymères, avec l'utilisation d'une méthode directe pour obtenir des réponses mécaniques?

Ce travail de thèse apporte des éléments de réponses à ces questions.

Après un chapitre d'introduction présentant les particules de graphène et ses dérivés ainsi que leurs propriétés, puis les principales méthodes de mise en œuvre pour les nanocomposites, nous détaillerons brièvement dans le chapitre 2 les trois principales techniques expérimentales utilisées au cours de ce travail.

Pour répondre à la 1ère question, dans le chapitre 3, nous proposerons de nouveaux résultats expérimentaux pour la transition vitreuse et le module de cisaillement dynamique de poly (méthacrylate d'éthyle) / nanocomposites d'oxyde de graphène (PEMAGO), et utiliserons également des données de la littérature pour des nanocomposites de poly(méthacrylate de méthyle) et d'oxyde de graphène (PMMAGO). Une approche micromécanique thermo-visco-élastique est présentée pour expliquer le renforcement des nanocomposites polymères de graphène.

Ci-dessous sont résumés les principaux résultats de ce chapitre :

- L'oxyde de graphène a été incorporé dans le poly (méthacrylate d'éthyle) de la matrice (PEMA) à 0,25 % en poids (Figure 1) et près de 15 K d'augmentation de la température de transition vitreuse T_g ont été observés. (Figure 2)
- Après avoir remplacé le module en fonction de la température par le module en fonction de $T-T_g$ afin de donner les renforts expérimentaux corrigés, notre approche micromécanique thermo-viscoélastique montre que la plupart des renforts apparents extrêmes décrits dans la littérature pour les nanocomposites polymères / oxyde de graphène peuvent être attribués à l'augmentation de la T_g du polymère. Ainsi nous montrons que le renforcement mécanique corrigé à partir de l'oxyde de graphène, permettant d'obtenir le renfort « réel » induit par la nanoparticule, est beaucoup plus faible que précédemment. (Figure 3)

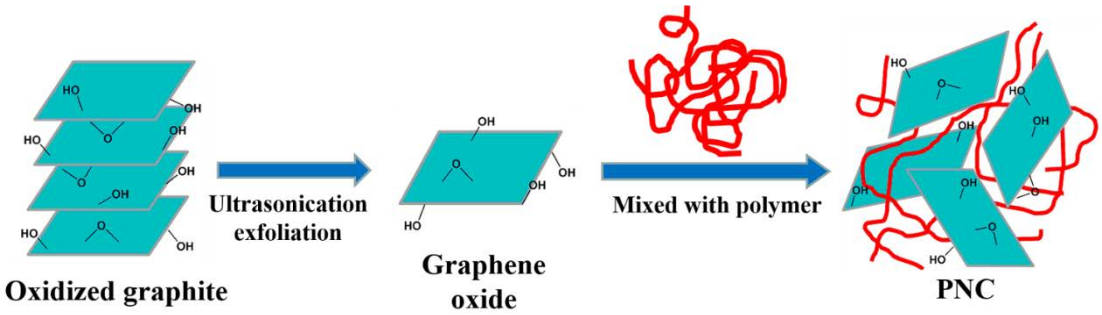

Figure 1. Procédé de fabrication de nanocomposites polymères / oxyde de graphène

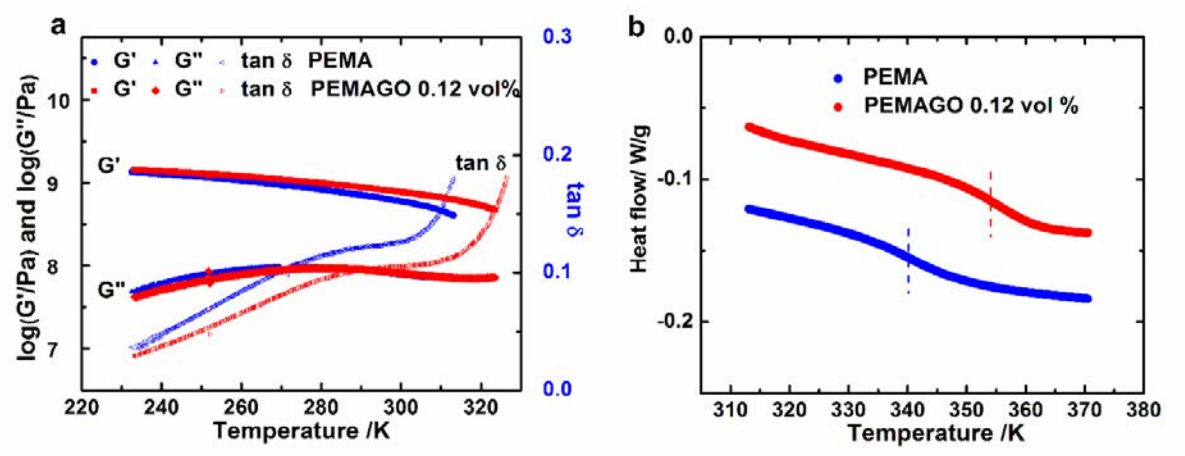

Figure 2. Module de conservation (G') et de perte (G'') en rampe de température pour (a) PEMA et PEMAGO 0,12% en volume (b) Détermination de la T_g pour les 2 systèmes

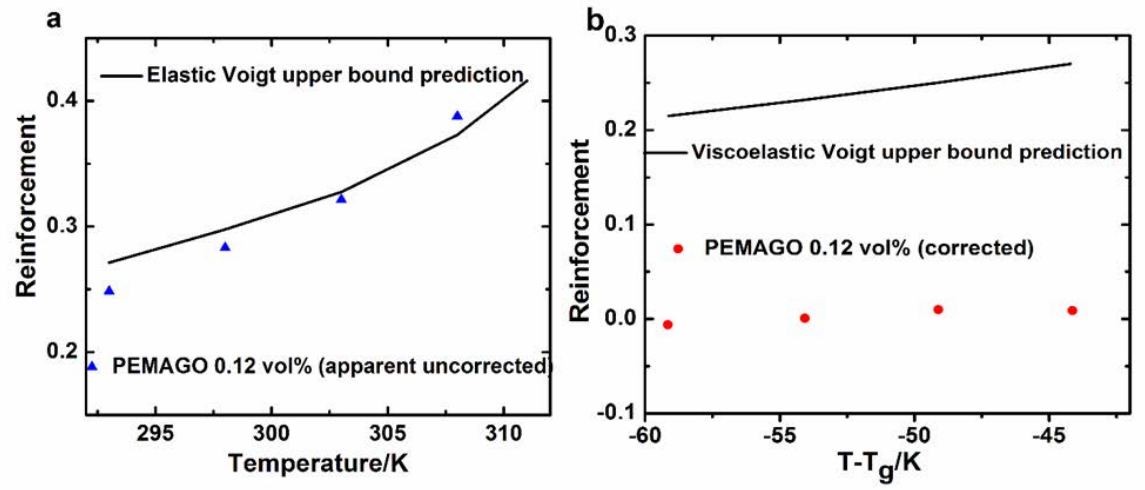

Figure 3. Prédictions apparentes et renforcement corrigé et limite supérieure suivant le modèle de Voigt (a, b) pour le système PEMAGO 0,12% en volume

Dans le chapitre 4, pour répondre à la 2ème question, l'assemblage forcé est utilisé pour orienter les nanoplaquettes de graphène dans les films multinanocouches poly (méthacrylate de méthyle) / polystyrène (PMMA / PS) et PMMA / PMMA produits par co-extrusion multicouche, procédé innovant disponible au laboratoire PIMM. (Figure 4). Comme montré dans la figure 4, ce procédé innovant permet par l'utilisation d'éléments multiplicateurs de couches, en théorie, d'obtenir des films constitués de milliers de couches alternées d'un ou plusieurs polymères, éventuellement chargés. Ici, on s'en sert pour favoriser la dispersion et l'alignement des particules de graphène, en les confinant dans des couches d'épaisseur de l'ordre de la dizaine de nanomètres suivant la configuration illustrée dans la Figure 4. La morphologie des couches et

l'orientation des nanoplaquettes de graphène ont été caractérisées par microscopie optique et électronique. Les propriétés mécaniques des matériaux ont été déterminées et reliées à l'orientation des nanoplaquettes de graphène dans les films multicouches. Les principaux résultats sont donnés ci-dessous :

- Dans les films multicouches PMMA graphène / PMMA, les couches renforcées (épaisseur 35 ~ 40 nm) montrent le graphène orienté dans la direction d'extrusion et partiellement orienté dans la direction transversale. (Figure 5)
- L'orientation de nanoplaquettes de graphène au sein des nanocouches (2 % en poids), conduit à un renforcement significatif de la couche renforcée. On a pu estimer une augmentation de 118% dans le module de traction le long de la direction d'écoulement. Contrairement à l'étude faite dans le chapitre 3, l'effet sur la T_g des particules de graphène est moins important : en tenant compte de l'augmentation de la T_g, le renforcement corrigé est d'environ 101 % comparé à la matrice de polymère pur. (Figure 6).

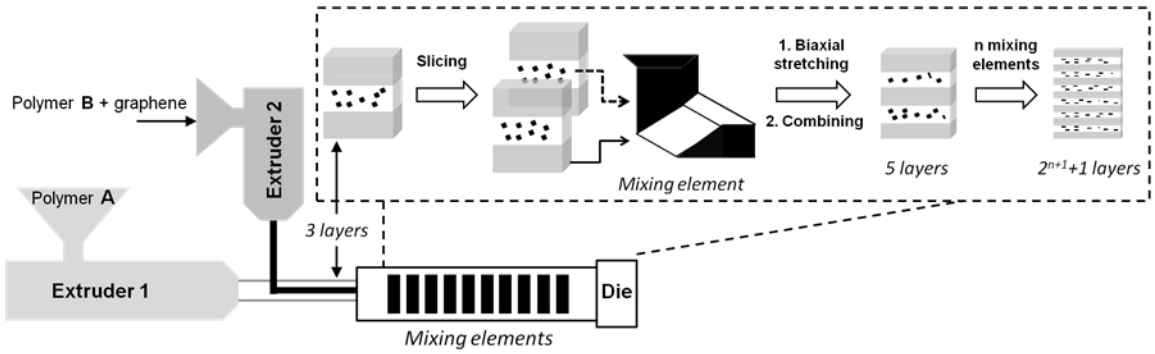

Figure 4. Schéma du procédé de coextrusion multinanocouches

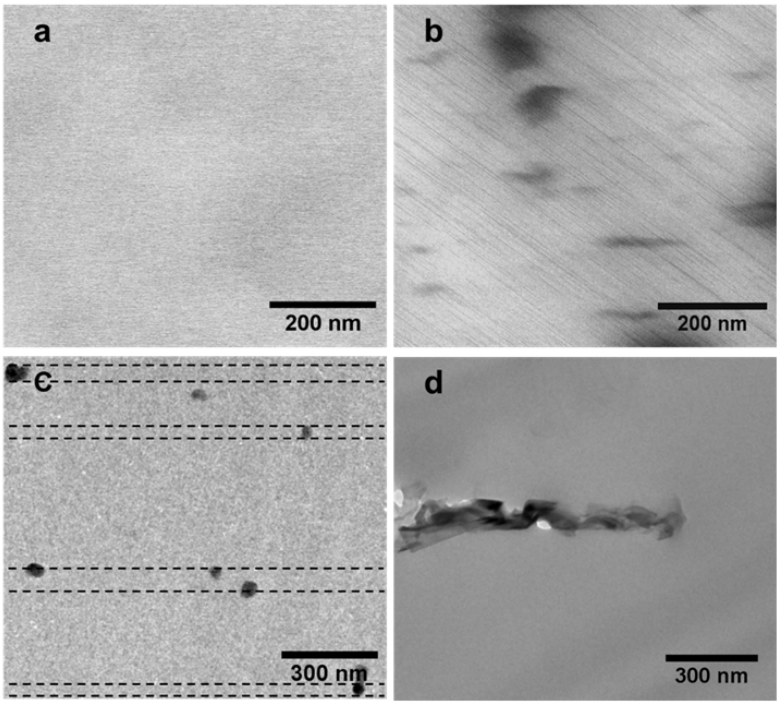

Figure 5. Images en coupe de films constitués de 2049 couches de PMMA graphène / PMMA (a) 0 % poids (sans graphène); (b) 0,1 % en poids de graphène (1% dans les couches chargées); Images TEM à 0,2% en poids de graphène (2,0 % dans les couches chargées) (c) montrant des particules de graphène « froissées » (les lignes pointillées représentent les positions estimées des couches minces de PMMA) (d) montrant une particule unique de graphène alignée.

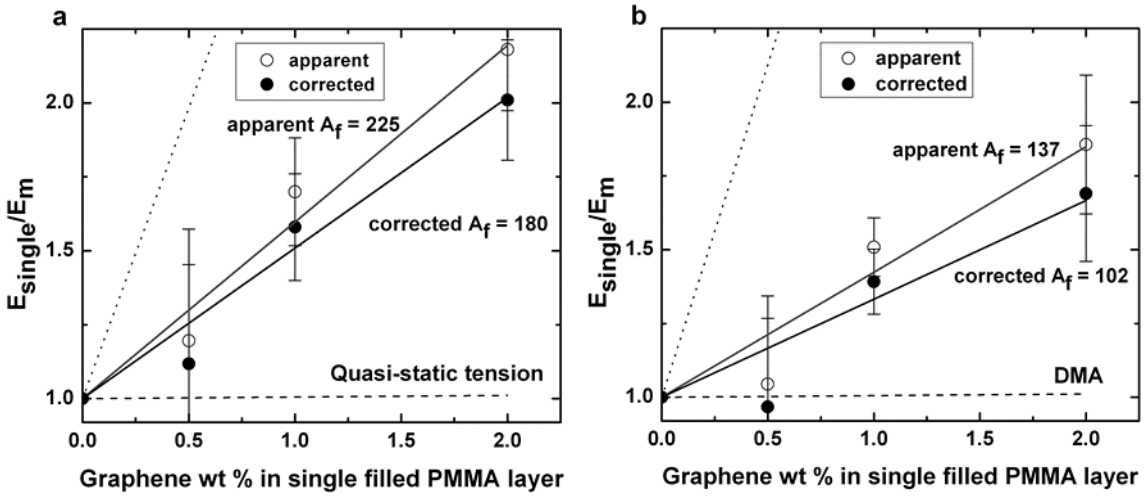

Figure 6. Renforcement expérimental et extrapolations en utilisant le modèle de Mori-Tanaka pour les couches renforcées au sein d'un film PMMA-graphène / PMMA de 2049 couches (Cercles vides: renforcement apparent / cercles pleins: corrigés pour tenir compte de l'effet du graphène sur la T_g; ligne solide: prédiction Mori-Tanaka, en trait pointillé: borne supérieure du modèle de Voigt; ligne pointillée: borne inférieure du modèle de Reuss.

Dans le Chapitre 5, pour répondre à la 3ème question, une nouvelle structure dite de « nano-sandwich » fait de couche mince de PEMA / couche simple de graphène CVD / couche mince de PEMA a été créé (Figure 7), et la méthode expérimentale d'inflation de nano-bulles a été appliquée à ce système pour obtenir les réponses mécaniques et obtenir des informations sur les mécanismes d'interface entre le graphène et les polymères:

- Des renforcements mécaniques (rigidité) importants ont été observés à des petites déformations, tant dans le domaine caoutchoutique (45,9 fois pour 0,52% en volume de graphène) que pour l'état vitreux (2,5 fois pour 0,48% en volume) pour le PEMA (Figure 8).
- Au-dessus de déformations critiques (0,18% pour le régime caoutchoutique et 0,23% pour le régime vitreux dans le PEMA), un phénomène similaire à de la plasticité a été observé et a été interprété comme étant dû à un glissement interfacial. La force de cisaillement à l'interface a pu ainsi être estimée en utilisant une analyse de décalage de cisaillement. (Figure 9)

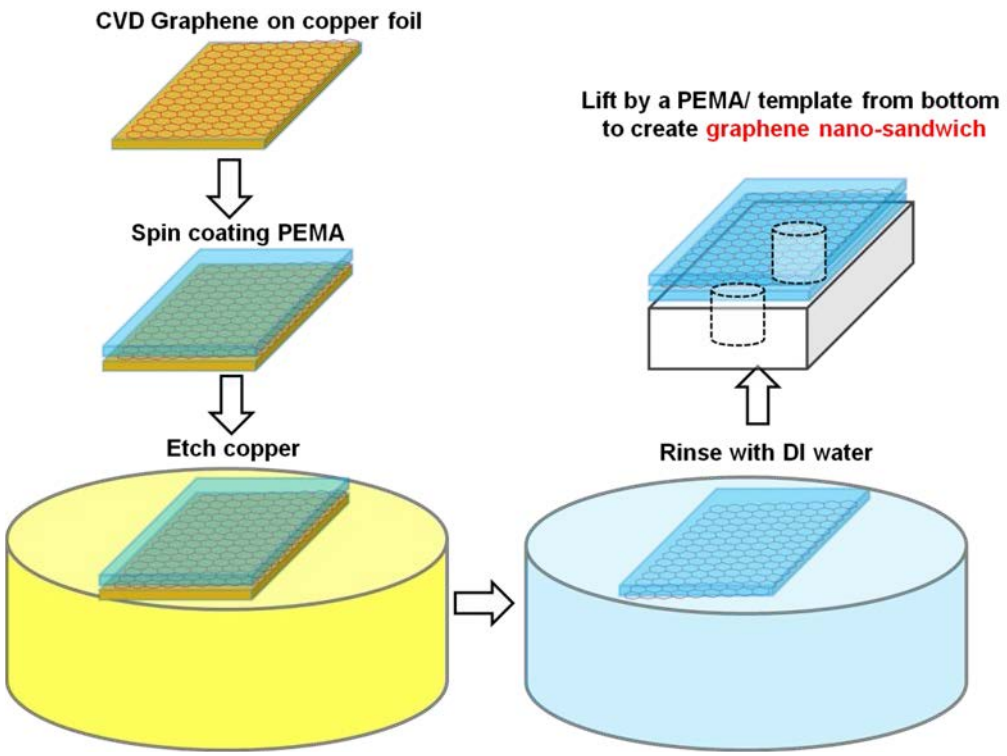

Figure 7. Protocole expérimental pour créer les nano-sandwichs polymère / graphène

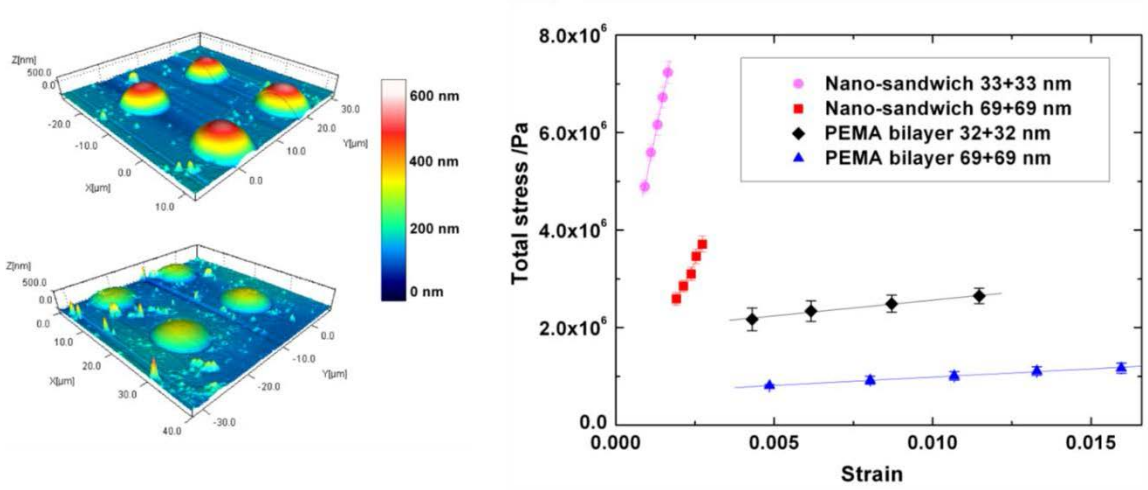

Figure 8. Gauche: images AFM en trois dimensions de bulles de diamètre 10 µm sur une bicouche de PEMA d'épaisseur de 62 nm (image du haut) et sur un nano-sandwich PEMA/graphène/PEMA de 64 nm d'épaisseur (image du bas) à 80 °C avec une pression de 13,0

kPa. Droite: Réponses en contrainte-déformation pour le nano-sandwich et le bicouche PEMA à 80 ° C

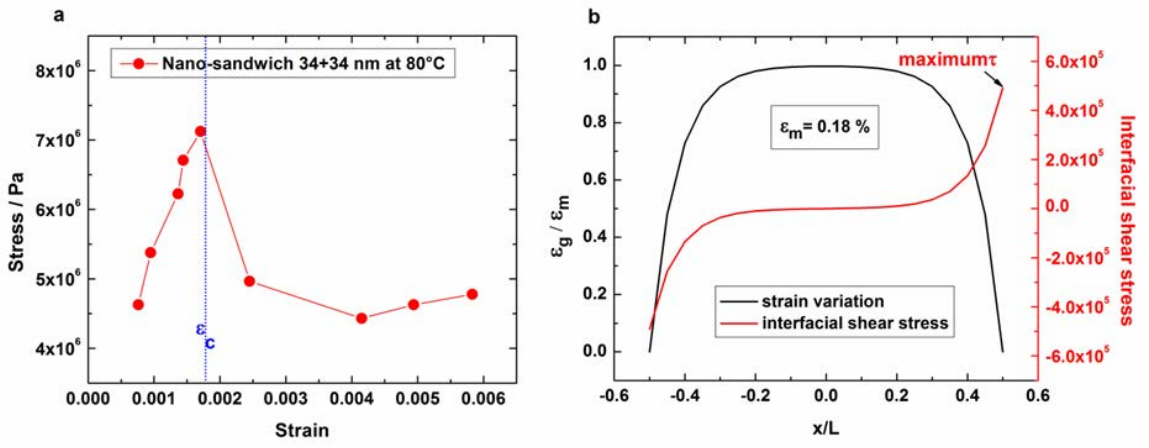

Figure 9. (a) Le comportement contrainte-déformation d'un nano sandwich de 68 nm d'épaisseur montrant une instabilité similaire à de la plasticité liée au glissement à l'interface entre le graphène et le PEMA à 80 °C; (b) la variation de contrainte et la contrainte de cisaillement interfaciale pour une déformation de la matrice de 0,18% pour un nano-sandwich de 68 nm d'épaisseur en utilisant l'analyse de décalage de cisaillement.

En conclusion, nous avons montré au cours de cette thèse l'importance du rôle du graphène et de ses dérivés sur la visco-élasticité des matrices amorphes, et la nécessité de tenir compte de ces changements de visco-élasticité pour appréhender le renfort mécanique pur de nanocomposites polymère / graphène. Nous avons ensuite illustré les capacités d'un procédé de mise en œuvre innovant, la coextrusion multinanocouches, pour l'obtention de nanocomposites graphène dans lesquels les particules sont partiellement orientées dans la direction de l'extrusion par le biais du nanoconfinement. Enfin nous avons développé un système expérimental permettant de caractériser l'importance du renfort dû au graphène au niveau de l'interface polymère-graphène.

Référence:

1. Li, X.; McKenna, G. B., *Considering Viscoelastic Micromechanics for the Reinforcement of Graphene Polymer Nanocomposites*. *ACS Macro Letters* **2012,** *1* (3), 388-391.
2. Li, X.; McKenna, G. B.; Miquelard-Garnier, G.; Guinault, A.; Sollogoub, C.; Regnier, G.; Rozanski, A., *Forced assembly by multilayer coextrusion to create oriented graphene reinforced polymer nanocomposites*. *Polymer* **2014,** *55* (1), 248-257.
3. Li, X.; McKenna, G. B.; Miquelard-Garnier, G.; Guinault, A.; Regnier, G.; Rozanski, A. In *Graphene-based Multilayered Poly(methyl methacrylate) Nanocomposites via Forced Assembly Coextrusion*, Society of Plastics Engineers' Annual Technical Conference, Las Vegas, US, **2014**; pp 609-613.
4. Li, X.; Warzywoda, J.; McKenna, G. B., *Mechanical responses of a polymer graphene-sheet nano-sandwich*. *Polymer* **2014,** *55* (19), 4976-4982.

Abstract

Graphene is an atomically thick, two-dimensional nano-sheet with advanced mechanical, electrical, and thermal properties. As a result, the addition of graphene and graphene derivative nanoparticles to polymer matrices has been a major strategy towards development of new materials in the field of composites. However, from a fundamental point of view, the origins of the advanced properties of graphene-based nanocomposites have been little investigated. In particular, changes in the viscoelastic properties of the polymer matrix due to specific interactions between the polymer and the graphene reinforcing elements can cause higher than expected apparent reinforcement. In addition, there is little work on characterizing the strength of the interface between the graphene used for reinforcement and the polymer matrixes. From a more engineering point of view, the design of polymer nanocomposites made of in-plane oriented graphene to create a two-dimensionally reinforced structure has also not been previously undertaken. The present dissertation is composed of three major works focusing on these problems.

The first part focuses on how to use a viscoelastic micromechanics approach to account for the effects of glass transition temperature T_g changes to correct the apparent stiffening of graphene oxide nanocomposites. It is found that graphene oxide stiffens the polymer matrices by increasing the T_g, which significantly modifies their thermo-viscoelasticity. This leads to apparent reinforcements that are not due to the stiffness of the graphene oxide itself, and largely explains anomalously high moduli reported in the literature for such graphene oxide/polymer matrix nanocomposites.

The second part focuses on a forced assembly multi-layer co-extrusion method to create films made of alternating layers of neat polymer / oriented graphene nanoplatelet filled polymer.

The morphology of the layers (35 ~ 40 nm thick) containing oriented graphene was established by electron microscopy. Mechanical properties of the materials were determined and the two-dimensional stiffening could be related to the oriented graphene nanoplatelets in the layered films. Taking into account the change of T_g, more than 100% intrinsic reinforcement was estimated for 2 wt % of graphene in the nanolayers. The results were analyzed and interpreted via an analytical model based on Mori-Tanaka analysis.

The third part focuses on extending a nano-bubble inflation method to the investigation of a novel graphene nano-sandwich with the purpose of investigation of the graphene / polymer interface. At small strains, significant mechanical reinforcement was observed for both graphene-reinforced rubbery and glassy PEMA layers. The interfacial mechanics between graphene and polymer layers was investigated and a "yield-like" interfacial slip was observed in the mechanical response of the nano-sandwich structures. The nano-bubble inflation method was also used to investigate the viscoelastic responses of poly(ethyl methacrylate) (PEMA) ultra-thin films over thicknesses ranging from 112 to 21 nm. A reduction in glass transition temperature with stiffening of the rubbery regime as decreasing film thickness was observed.

List of Tables

List of Figures

Chapter 1. Background & Introduction

1.1 Graphene

Graphene is an atomically thick, two-dimensional sheet composed of sp^2 carbon atoms, arranged in a hexagonal lattice (Figure 1.1a).[1] Graphite, an abundant naturally occurring material, has been viewed as constructed by graphene sheets stacked on top of each other. Attempts to study graphene can be traced back to Brodie's work[2] in 1859, and studies of single layer graphene became possible with the development by Novoselov and Geim in 2004, who used the "Scotch-tape method" to produce large isolated graphene sheets from graphite (Figure 1.1b).[3-5] Because of the unique properties of graphene, the area of graphene research grows extremely fast around the world and the number of research publications with the title containing the word "graphene" is more than 66,600 between 2005 and 2014.(Searched by ISI-Web of Science on November 4th, 2014)

Graphene has many unique properties so as to draw such a high research interest in fields to utilize its mechanical, electrical, thermal, and gas barrier properties. Graphene has been found with a Young's modulus of 0.5 - 1 TPa[6-7] and ultimate strength of 130 GPa[7]. It has also been reported with a high electrical conductivity up to 6000 S/cm[8] and a thermal conductivity of 4840 - 5300 W/(m.K), which is above the reported value for carbon nanotubes.[9] Moreover, the theoretically high surface area of 2630 m^2/g[10] and gas impermeability[11] arouse high interest of graphene application in a variety of fields.

Methods to create graphene are being researched intensively. There are two major strategies: Top-down and bottom-up. In top-down methods, graphene sheets are exfoliated from graphite. A micromechanical cleavage technique, called the "Scotch-tape method", ignited the original interest of graphene research and so far is still the most reliable method for producing

high-quality graphene sheets, although in limited quantities.[3] Chemical exfoliation with sonication is also widely used, and graphene dispersion can be stabilized by specific surfactants[12-13]and ionic liquid[14]. Oxidation of graphite[15] is also a useful method for this process. Another method is heating graphite oxide with inert gas at 1000 °C to produce thermally reduced graphene oxide in one step.[16] On the other hand, surface science provides new strategies to grow graphene using "bottom-up" methods. Chemical vapor deposition (CVD) on metal substrates[17-18] and epitaxial growth on SiC[19-20] can produce large graphene sheets in small amounts. Most of these techniques produce few-layer graphene (2~5 layers) with thicknesses around 0.7~1.7 nm, rather than single layer graphene with a thickness of 0.34 nm. The major methods to produce graphene are summarized in Table 1.1.

It is necessary to obtain the information of the size, thickness and quality of graphene produced by the different methods described above. Therefore the techniques to characterize graphene are also important. To obtain the thickness (the number of layers), Raman spectroscopy[21] and Atomic Force Microscopy (AFM)[22] can be used. And AFM[22] and transmission electron microscopy (TEM)[23] can be used to measure the lateral size.

To identify the chemical structure, X-ray photoelectron spectroscopy (XPS)[24] and infrared absorption[25] can identify the carbon oxygen bonds, and element analysis can measure the oxidation degree. NMR and Raman spectroscopy can distinguish and quantify chemical modifications, such as identifying oxygen functional groups[26], and the transformation of sp^3 to sp^2 hybridized carbons[24].

1.2 Graphene oxide and graphene nanoplatelets

A variety of graphene derivative nanoparticles have been created to enlarge the "Graphene Family", such as graphene oxide,[27] fluorographene[28] and graphene nanoplatelets.[29-30]

(Figure 1.2) Since graphene oxide and graphene nanoplatelets were used in the work of the present dissertation, these two graphene derivative nanoparticles will be discussed.

Graphene oxide (GO) is one of the most studied graphene derivative nanoparticles. It is exfoliated from graphite oxide, with a carbon/oxygen/hydrogen ratio of 2/1/0.8.[31] There has been much work on the structure of graphene oxide and it is found that it contains 1~3 layers (0.34 ~ 1.0 nm thick) with carboxyl, hydroxyl, epoxide and ketone groups.[26-27] Although graphene oxide is electrically insulating, its good dispersion in water and polar organic solvent, and the ease of mixing it with polar polymer matrices make it of interest in the production of polymer nanocomposites.[32]

For practical use, graphene nanoplatelets (GNP) have been used to improve the mechanical and electrical properties of polymer matrices.[30, 33] GNP is exfoliated from graphite by rapid heating and pulverization, to produce the platelets with thicknesses 2~10 nm (6~30 layers), with different lateral sizes.[29] Although GNP is indeed stacks of graphene, and much thicker than a single layer graphene, hence less surface area and lower tensile strength, GNP can still provide excellent electrical conductivity and good mechanical reinforcement. The reason is that the GNP has a large lateral size (5~15 μm) therefore high aspect ratios are still achieved.[33-34]

1.3 Graphene/Polymer Nanocomposites: Preparation and properties

Polymers are used in a broad range of applications, especially due to their light weight, low cost, flexibility and easy processing. However, compared to ceramics and metals, polymers have weaknesses in terms of low stiffness and strength, limiting their use. Therefore, the addition of rigid fillers in nanometer size to reinforce the polymer matrices, leading to a new class of materials, polymer nanocomposites, has been a major strategy from 1920s, when carbon black

was first added to stiffen rubbers.[35-36] And Toyota Motors first used layered silicates (plate-like nano-fillers) to stiffen nylon 6 in the late 1980s.[37] Compared to conventional micro meter sized fillers, nano-fillers have the advantage of much higher surface area, which can increase the interface between the polymer matrix and the filler and lead to better load transfer from the matrix to the filler, for example. However, in spite of large promise of nanofillers, only a few nanofillers have successful practical applications, e.g. carbon black in rubbery industry. The reasons are the aggregations of nanofillers, high cost and environment concern[38].

1.3.1 Preparation methods

Since the properties of polymer nanocomposites depend on how well the nanofillers are dispersed in the polymer matrices, the methods to disperse graphene and graphene derivative nanoparticles are of significant interest and we summarize them in Table 1.2 and describe them next.

Solvent blending with the aid of sonication has been broadly used to produce nanocomposites of polymer / graphene oxide,[32, 39-41] polymer / reduced graphene oxide,[42-43] and polymer / pristine graphene with surfactants[44-45]. Generally solvent dispersion methods give good dispersion, however, the cost of the solvents, their potential hazards, and solvent removal hinder their industrial use.[10] Another dispersion strategy is in situ polymerization of monomers with graphene and it has succeeded in several polymers, e.g. epoxy,[46] PMMA,[47] PU[48] and PDMS,[45] and some nanocomposites prepared by in situ polymerization have been reported to contain covalent bonding[48] between graphene and the polymer chains which enhance the properties of nanocomposites. The limitation of the technique is still the use of solvent since bulk-phase polymerization with graphene is difficult due to high viscosity of the graphene filled

monomer systems.

Melt blending is the most economical and scalable dispersion method.[10, 32] Under high shear conditions, graphene and polymer melts can be mixed on a large scale without the use of solvent. Reduced graphene oxide and graphene nanoplatelets have been reported to mix with polymers using extrusion.[34, 49] The major shortcoming is that the dispersion of the graphene in polymer melts is not as good as that achieved by solvent mixing, mainly due to the high viscosities of the polymer melts.[48] Also the thermal instability of some graphene derivative nanoparticles limits this method.[10]

1.3.2 Mechanical properties

Because graphene has reported Young's modulus between 0.5 - 1 TPa and ultimate strength of 130 GPa, it is thought that graphene is an excellent candidate for mechanical reinforcement of polymer in the area of nanocomposites. To this end, there is significant research in which graphene has been added into a variety of polymers to make nanocomposites, with varying level of success.[32-34, 39-41, 48, 50-52] Table 1.3 is a summary of mechanical properties of graphene polymer nanocomposites. Interestingly, besides the mechanical properties of graphene, there are two additional stiffening mechanisms for graphene and graphene derivative nanoparticles to stiffen certain polymer matrices. With hydrogen bonding, graphene oxide (GO) generally interacts with polar polymers to give higher glass transition temperature, and this leads to apparently superior mechanical reinforcements due to the change in viscoelasticity of the polymer matrix, rather than the extraordinary reinforcement by the graphene.[39-41] (We discuss this in details in Chapter 3) For semi-crystalline polymers[53], graphene can enhance the degree of

crystallinity as a nucleating agent, and therefore stiffens the polymer matrix by increasing the crystallinity.

In addition to stiffness change, tensile strength and elongation at break of graphene polymer nanocomposites have also been reported. With good dispersion, tensile strength increases with the addition of graphene,[51, 53-54] although usually elongation at break decreases, hence leading to increased brittleness.[53-54]

1.3.3 Electrical conductivity

Graphene can provide electrical percolation (network) above a critical concentration (threshold) to make the polymers electrically conductive. The threshold concentration is significantly lower than that needed for carbon black to percolate. Although graphene oxide is electrically insulating, reduced graphene oxide (RGO), thermally reduced graphene (TRG) and graphene nanoplatelets (GNP) have been widely used to increase the electrical conductivity of polymers.[33, 42, 45, 48, 55-57] Here we summarize typical polymer nanocomposites with their electrical conductivities in Table 1.4. Although the electrical conductivities of graphene polymer nanocomposites are still much lower than that of copper, they still have some applications,[58] such as antistatic coating[59] and electromagnetic shielding[60].

1.3.4 Gas barrier properties

As a two dimensional nanofiller, graphene is impermeable to most gas molecules in the direction perpendicular to the plane of the graphene.[11] Therefore the incorporation of graphene and graphene derivatives into polymer matrices can enhance the gas barrier properties,[29, 48, 50, 61] e.g. a 60 % reduction of H_2 permeability for polyethylene naphthalate (PEN) using 1.8 vol % graphene was observed by Macosko and co-workers.[61] Due to the two dimensional

characteristics of graphene, higher aspect ratios and better orientation are important to reduce the gas permeability.[48]

1.4 Stiffening mechanics of graphene polymer nanocomposites

1.4.1 Elastic micromechanics theories

Over several decades, micromechanics theories have been developed for evaluating the influence of stiffness, geometry, aspect ratio and orientation of nanofillers, and predict the mechanical properties of nanocomposites. The most widely used elastic micromechanics theories are Voigt upper bound[62] and Reuss lower bound[63] mixing rules, Halpin-Tsai model[64] and Mori-Tanaka model[65].

Voigt upper bound and Reuss lower bound mixing rules have been used for composites for almost a hundred years.[62-63, 66] By neglecting the Poisson effects, filler size and geometry, a set of bounds on the Young's modulus of the composite are given from equation 1, 2 and 3:

$$E_{Voigt} = V_m E_m + V_f E_f \quad (\mathbf{1})$$

$$\frac{1}{E_{Reuss}} = \frac{V_m}{E_m} + \frac{V_f}{E_f} \quad (\mathbf{2})$$

$$E_{Reuss} \leq E \leq E_{Voigt} \quad (\mathbf{3})$$

where E is Young's modulus and V is volume fraction of each component. Subscripts are m for the polymer matrix and f for fillers. To further incorporate the influence of geometry and aspect ratio of nanofillers, Halpin and Tsai developed a theory for disk-like platelet fillers[64, 67] from equations 4 and 5:

$$\frac{E}{E_m} = \frac{1 + \eta\xi V_f}{1 - V_f} \quad (\mathbf{4})$$

$$\eta = \frac{E_f/E_m - 1}{E_f/E_m + \xi} \quad (5)$$

where η is the stiffness contrast between the filler and the polymer and the shape factor ξ (ξ = 2l/t). l and t are the diameter and thickness of platelet fillers.

Mori and Tanaka developed the Mori-Tanaka average stress theory[65] and Tandon and Weng derived complete analytical solutions for the elastic modulus of composites with unidirectionally aligned isotropic platelets as equation 6,[68]

$$\frac{E}{E_m} = \frac{1}{(1+V_f(-2\nu_m A_3-(1-\nu_m A_4+(1+\nu_m)A_5 A))/2A)} \quad (6)$$

where E_m , ν_m, and V_f are tensile modulus of the polymer, Poisson's ratio of the polymer and volume fraction of the filler, respectively. A and A_i are functions of V_f, ν_m and the Eshelby tensors provided by Tandon and Weng.[68] Comparing to Halpin-Tsai model, the treatment of filler geometry is different in Mori-Tanaka model and Paul and co-worker reported that for clay/nylon 6 nanocomposites, Halpin-Tsai model slightly overpredicts the experimental results compared to Mori-Tanaka model.[67] In Chapter 4, we use the Mori-Tanaka theory to analyze the graphene reinforcement in PMMA/PMMA-graphene multilayer films.

1.4.2 Current challenges

As already stated, because of its high mechanical strength and stiffness, graphene has been thought to have the potential of achieving excellent mechanical reinforcement for polymer nanocomposites. Also because of the two dimensional structure of graphene, if graphene can be oriented in the plane of the polymer matrix, the mechanical reinforcement along two dimensions

at a significantly lower loading can be achieved than for randomly dispersed graphene in the polymer matrix.[52]

To date, significant stiffening by graphene or graphene derivative nanoparticles in polymer matrices have been reported widely,[39, 41, 51, 69-70] such as PMMA/ graphene oxide (33% enhancement of Young's modulus E at only 0.005 vol %) reported by Brinson and co-workers.[39] The apparent high reinforcement of Brinson and co-workers' work exceeds the Voigt upper bound prediction (the limit of infinite aspect ratio of filler and perfect alignment)[62, 66] and these striking results have lead to great enthusiasm for the prospect of graphene polymer nanocomposites. At the same time, Macosko and co-workers[71] have questioned Brinson and co-workers' results and claimed that most of the reinforcements and T_g increase they observed are due to the removal of low molecular additives in the original PMMA during the solvent mixing procedure used to prepare nanocomposites. Therefore their comparison of the properties of neat PMMA containing additives with that of the nanocomposites without additives leads to apparently higher T_g and stiffness values. [71]

Because its chemical structure contains carboxyl, hydroxyl, epoxide and ketone groups,[26-27] graphene oxide (GO) generally interacts with polar polymers via hydrogen bonding, hence the nanocomposites frequently have a higher glass transition temperature T_g than the neat resins.[39, 41, 70] The increases of T_g cause a change in thermo-viscoelastic properties of the polymer matrices, hence graphene oxide has an additional stiffening mechanism when incorporated into polymer matrices, when compared to graphene. Consequently, investigation of the mechanical reinforcement of polymer graphene nanocomposites requires a viscoelastic micromechanics approach to account for the effect of T_g change to correct the apparent stiffening. This is

especially important because polymers generally are used relatively close to their glass transition temperatures.[72] We will discuss this in details in Chapter 3.

Another challenge is how to align the graphene in a plane of the polymer matrix, to achieve the two dimensional reinforcement. The development of methods to create in-plane oriented graphene in a polymer matrix have not been undertaken. Kim and Macosko[50] reported the production of slightly oriented polycarbonate/ graphene nanocomposites with only weak reinforcement, using injection molding. We will show how to use multilayer co-extrusion to orient graphene in polymer thin layers by forced assembly in Chapter 4.

1.5 Interfacial mechanics between graphene and polymer matrices

It has been commonly thought that nanoparticle / polymer interfaces are important in the reinforcement of nanocomposites since the observation of the bound rubber[73] (immobilized layer adhered to fillers) in carbon black reinforced rubbers. In the area of graphene polymer nanocomposites, the understanding of interfacial interaction between graphene and the polymer matrices at generally small amount of graphene in polymer matrices, is very important but challenging, due to the limitation of experimental techniques. Recently, however, there has been an attempt to understand the interfacial mechanics of single and multilayer graphene sheets in polymers using Raman spectroscopy[21, 74-75]. Single layer graphene has several characteristic peaks in Raman spectroscopy (Figure 1.3a), and the shift of the Raman peaks of graphene upon stretching the graphene can be used to characterize the deformation of the graphene.[76-79] Under tension the Raman 2D peak at 2645 cm^{-1} shifts to lower wavenumbers. (Figure 1.3b)

Young and co-workers used Raman spectroscopy to study graphene supported on polymeric substrates using a bending/stretching test.[21, 74, 80] (Figure 1.4a) Their work provided

the first measurement of interfacial mechanics of a graphene/polymer system, and they created a strain map for graphene on a PMMA (Figure 1.4b). They also observed what appeared to be an interfacial slip. Using a shear lag analysis, they estimated the shear strength of the interface between the polymer and graphene. The interfacial slip and interfacial shear strength results were interpreted to mean that the graphene and the polymer matrix are bonded by van der Waals forces, i.e. the interface is formed by a relatively poor adhesion, but can transfer interfacial stress at very small strains (< 0.4 %).[21]

The interface study based on Raman spectroscopy has been used to probe the reinforcement mechanism and to study the effect of the chemical modification on the interface between graphene derivatives and polymer matrices.[81] In addition, AFM has also been used to investigate the interfacial adhesion in polymer graphene nanocomposites.[82-83] However, most of these techniques still have limitations. For the AFM techniques, it is necessary to convert the morphology of the interface after peeling[82] into mechanical information, therefore these are indirect measurements of the mechanical properties of the interface. Although the Raman spectroscopy[21, 75] is not as "indirect" as AFM, it requires specific instrumentation and spectroscopy expertise. We will show the measurement of a novel graphene nano-sandwich using a nanobubble inflation method, to add a new technique to the investigation of graphene / polymer interface in Chapter 5.

1.6 Motivation and overview

The addition of graphene and graphene derivative nanoparticles to reinforce polymer matrices has been widely studied. However, as discussed above, graphene polymer nanocomposites still pose several questions which need to be addressed:

i. How to use a viscoelastic micromechanics approach to account for the effects of a T_g change in the apparent stiffening of graphene nanocomposites?

ii. How to achieve planar orientation of graphene in the polymer matrices to realize two dimensional reinforcement?

iii. How to develop a method to investigate the interfacial mechanics between graphene and polymer matrices, using a novel graphene nano-sandwich structure?

The understanding of these topics is so important that it helps researchers to evaluate, design and improve nanocomposites. The present dissertation addresses them and provides some answers to these problems. Viscoelasticity, orientation of graphene and interfacial mechanics are investigated using three different experimental techniques: rheology, forced assembly multilayer co-extrusion and nano-bubble inflation methods. Chapter 2 describes briefly the three major experimental methods used in this dissertation.

Chapter 3 describes the study of the mechanical properties and viscoelasticity including glass transition and β relaxation of graphene oxide/polymer nanocomposites. A viscoelastic micromechanics approach is applied to explain the reinforcement of graphene oxide in PEMA and PMMA matrices and we describe an investigation in which to account for the apparent stiffening, which is due to T_g changes in the polymer matrix.

In Chapter 4, forced assembly was used to orient graphene nanoplatelets in poly (methyl methacrylate)/polystyrene (PMMA/PS) and PMMA/PMMA multilayer films produced through multilayer co-extrusion. The morphology of the layers and orientation of the graphene nanoplatelets were characterized with optical and electron microscopies. Mechanical properties of the materials were determined and related to the oriented graphene nanoplatelets in the layered films.

In Chapter 5, the creation of a nano-sandwich model structure composed of ultrathin polymer layer/monolayer graphene/ultrathin polymer layer is described. A nano-bubble inflation method was used to study the interfacial mechanics. Interfacial shear strength and internal residual stress were also estimated.

In Chapter 6, the nano-bubble inflation method was used to investigate another topic of interest: the viscoelastic responses of poly(ethyl methacrylate) (PEMA) ultra-thin films over thicknesses ranging from 112 to 21 nm. A reduction in glass transition temperature with stiffening of the rubbery regime as decreasing film thickness was observed.

Finally, Chapter 7 summarizes all key results of the dissertation and provides perspectives for future work.

Parts of the information in Chapters 3-5 are from the journal manuscripts and the permission has been obtained from the journals to incorporate them into the present dissertation. Detailed information of published journal articles and a conference proceeding related to Chapters 3-5 is as follows: Chapter 3, entitled "*Considering Viscoelastic Micromechanics for the Reinforcement of Graphene Polymer Nanocomposites*", was published under a slightly different form in **ACS Macro Letters, 2012, 1, 388-391**. Chapter 4, a part of work entitled "*Forced Assembly by Multilayer Coextrusion to Create Oriented Graphene Reinforced Polymer Nanocomposites*", was published in **Polymer, 2014, 55, 248-257**. Another part of the work contained in chapter 4, entitled "*Graphene-based Multilayered Poly (methyl methacrylate) Nanocomposites via Forced Assembly Coextrusion*", was published in **Society of Plastics Engineers' Annual Technical Conference, 2014, Las Vegas. ISBN 978-0-9850112-4-6, pp. 609-613**. Chapter 5, entitled "*Mechanical Responses of A Polymer Graphene Sheet Nano-sandwich*" was published in **Polymer, 2014, 55, 4976-4982**.

1.7. References

1. Novoselov, K. S., *Nobel Lecture: Graphene: Materials in the Flatland*. *Reviews of Modern Physics* **2011,** *83* (3), 837-849.
2. Brodie, B. C., *On the Atomic Weight of Graphite*. *Philosophical Transactions of the Royal Society of London* **1859,** *149* (0), 249-259.
3. Novoselov, K. S.; Geim, A. K.; Morozov, S. V.; Jiang, D.; Zhang, Y.; Dubonos, S. V.; Grigorieva, I. V.; Firsov, A. A., *Electric field effect in atomically thin carbon films*. *Science* **2004,** *306* (5696), 666-9.
4. Geim, A. K.; Novoselov, K. S., *The rise of graphene*. *Nat Mater* **2007,** *6* (3), 183-191.
5. Geim, A. K., *Graphene: Status and Prospects*. *Science* **2009,** *324* (5934), 1530-1534.
6. Frank, I. W.; Tanenbaum, D. M.; van der Zande, A. M.; McEuen, P. L., *Mechanical properties of suspended graphene sheets*. *Journal of Vacuum Science & Technology B: Microelectronics and Nanometer Structures* **2007,** *25* (6), 2558.
7. Lee, C.; Wei, X. D.; Kysar, J. W.; Hone, J., *Measurement of the elastic properties and intrinsic strength of monolayer graphene*. *Science* **2008,** *321* (5887), 385-388.
8. Du, X.; Skachko, I.; Barker, A.; Andrei, E. Y., *Approaching ballistic transport in suspended graphene*. *Nat Nano* **2008,** *3* (8), 491-495.
9. Balandin, A. A.; Ghosh, S.; Bao, W.; Calizo, I.; Teweldebrhan, D.; Miao, F.; Lau, C. N., *Superior Thermal Conductivity of Single-Layer Graphene*. *Nano Letters* **2008,** *8* (3), 902-907.
10. Kim, H.; Abdala, A. A.; Macosko, C. W., *Graphene/Polymer Nanocomposites*. *Macromolecules* **2010,** *43* (16), 6515-6530.
11. Bunch, J. S.; Verbridge, S. S.; Alden, J. S.; van der Zande, A. M.; Parpia, J. M.; Craighead, H. G.; McEuen, P. L., *Impermeable atomic membranes from graphene sheets*. *Nano Lett* **2008,** *8* (8), 2458-2462.
12. Bourlinos, A. B.; Georgakilas, V.; Zboril, R.; Steriotis, T. A.; Stubos, A. K., *Liquid-Phase Exfoliation of Graphite Towards Solubilized Graphenes*. *Small* **2009,** *5* (16), 1841-1845.
13. Parviz, D.; Das, S.; Ahmed, H. S. T.; Irin, F.; Bhattacharia, S.; Green, M. J., *Dispersions of Non-Covalently Functionalized Graphene with Minimal Stabilizer*. *ACS Nano* **2012,** *6* (10), 8857-8867.
14. Bari, R.; Tamas, G.; Irin, F.; Aquino, A. J. A.; Green, M. J.; Quitevis, E. L., *Direct exfoliation of graphene in ionic liquids with aromatic groups*. *Colloids and Surfaces A: Physicochemical and Engineering Aspects* **2014,** *463*, 63-69.
15. Hummers, W. S.; Offeman, R. E., *Preparation of Graphitic Oxide*. *Journal of the American Chemical Society* **1958,** *80* (6), 1339-1339.
16. McAllister, M. J.; Li, J.-L.; Adamson, D. H.; Schniepp, H. C.; Abdala, A. A.; Liu, J.; Herrera-Alonso, M.; Milius, D. L.; Car, R.; Prud'homme, R. K.; Aksay, I. A., *Single Sheet Functionalized Graphene by Oxidation and Thermal Expansion of Graphite*. *Chem Mater* **2007,** *19* (18), 4396-4404.
17. Wang, X.; You, H.; Liu, F.; Li, M.; Wan, L.; Li, S.; Li, Q.; Xu, Y.; Tian, R.; Yu, Z.; Xiang, D.; Cheng, J., *Large-Scale Synthesis of Few-Layered Graphene using CVD*. *Chemical Vapor Deposition* **2009,** *15* (1-3), 53-56.
18. Li, X.; Cai, W.; An, J.; Kim, S.; Nah, J.; Yang, D.; Piner, R.; Velamakanni, A.; Jung, I.; Tutuc, E.; Banerjee, S. K.; Colombo, L.; Ruoff, R. S., *Large-Area Synthesis of High-Quality and Uniform Graphene Films on Copper Foils*. *Science* **2009,** *324* (5932), 1312-1314.

19. Rollings, E.; Gweon, G. H.; Zhou, S. Y.; Mun, B. S.; McChesney, J. L.; Hussain, B. S.; Fedorov, A. V.; First, P. N.; de Heer, W. A.; Lanzara, A., *Synthesis and characterization of atomically thin graphite films on a silicon carbide substrate*. *Journal of Physics and Chemistry of Solids* **2006,** *67* (9–10), 2172-2177.
20. Sutter, P. W.; Flege, J.-I.; Sutter, E. A., *Epitaxial graphene on ruthenium*. *Nat Mater* **2008,** *7* (5), 406-411.
21. Gong, L.; Kinloch, I. A.; Young, R. J.; Riaz, I.; Jalil, R.; Novoselov, K. S., *Interfacial Stress Transfer in a Graphene Monolayer Nanocomposite*. *Adv Mater* **2010,** *22* (24), 2694.
22. Schniepp, H. C.; Kudin, K. N.; Li, J.-L.; Prud'homme, R. K.; Car, R.; Saville, D. A.; Aksay, I. A., *Bending Properties of Single Functionalized Graphene Sheets Probed by Atomic Force Microscopy*. *ACS Nano* **2008,** *2* (12), 2577-2584.
23. Meyer, J. C.; Geim, A. K.; Katsnelson, M. I.; Novoselov, K. S.; Obergfell, D.; Roth, S.; Girit, C.; Zettl, A., *On the roughness of single- and bi-layer graphene membranes*. *Solid State Commun* **2007,** *143* (1–2), 101-109.
24. Stankovich, S.; Dikin, D. A.; Piner, R. D.; Kohlhaas, K. A.; Kleinhammes, A.; Jia, Y.; Wu, Y.; Nguyen, S. T.; Ruoff, R. S., *Synthesis of graphene-based nanosheets via chemical reduction of exfoliated graphite oxide*. *Carbon* **2007,** *45* (7), 1558-1565.
25. Szabó, T.; Berkesi, O.; Dékány, I., *DRIFT study of deuterium-exchanged graphite oxide*. *Carbon* **2005,** *43* (15), 3186-3189.
26. Gao, W.; Alemany, L. B.; Ci, L.; Ajayan, P. M., *New insights into the structure and reduction of graphite oxide*. *Nat Chem* **2009,** *1* (5), 403-408.
27. Dreyer, D. R.; Park, S.; Bielawski, C. W.; Ruoff, R. S., *The chemistry of graphene oxide*. *Chemical Society Reviews* **2010,** *39* (1), 228-240.
28. Robinson, J. T.; Burgess, J. S.; Junkermeier, C. E.; Badescu, S. C.; Reinecke, T. L.; Perkins, F. K.; Zalalutdniov, M. K.; Baldwin, J. W.; Culbertson, J. C.; Sheehan, P. E.; Snow, E. S., *Properties of Fluorinated Graphene Films*. *Nano Letters* **2010,** *10* (8), 3001-3005.
29. Kalaitzidou, K.; Fukushima, H.; Drzal, L. T., *Multifunctional polypropylene composites produced by incorporation of exfoliated graphite nanoplatelets*. *Carbon* **2007,** *45* (7), 1446-1452.
30. Li, B.; Zhong, W.-H., *Review on polymer/graphite nanoplatelet nanocomposites*. *J Mater Sci* **2011,** *46* (17), 5595-5614.
31. Herrera-Alonso, M.; Abdala, A. A.; McAllister, M. J.; Aksay, I. A.; Prud'homme, R. K., *Intercalation and Stitching of Graphite Oxide with Diaminoalkanes*. *Langmuir* **2007,** *23* (21), 10644-10649.
32. Potts, J. R.; Dreyer, D. R.; Bielawski, C. W.; Ruoff, R. S., *Graphene-based polymer nanocomposites*. *Polymer* **2011,** *52* (1), 5-25.
33. Kalaitzidou, K.; Fukushima, H.; Drzal, L. T., *A new compounding method for exfoliated graphite–polypropylene nanocomposites with enhanced flexural properties and lower percolation threshold*. *Compos Sci Technol* **2007,** *67* (10), 2045-2051.
34. Kalaitzidou, K.; Fukushima, H.; Drzal, L. T., *Mechanical properties and morphological characterization of exfoliated graphite–polypropylene nanocomposites*. *Composites Part A: Applied Science and Manufacturing* **2007,** *38* (7), 1675-1682.
35. Kraus, G., *Swelling of filler-reinforced vulcanizates*. *J Appl Polym Sci* **1963,** *7* (3), 861-871.
36. Kraus, G., *Interactions of Elastomers and Reinforcing Fillers*. *Rubber Chemistry and Technology* **1965,** *38* (5), 1070-1114.

37. Kojima, Y.; Usuki, A.; Kawasumi, M.; Okada, A.; Fukushima, Y.; Kurauchi, T.; Kamigaito, O., *Mechanical properties of nylon 6-clay hybrid*. *Journal of Materials Research* **1993,** *8* (05), 1185-1189.
38. Anisa, M.; Abdallah, S. D.; Peter, A. S., *'Mind the gap': science and ethics in nanotechnology*. *Nanotechnology* **2003,** *14* (3), R9.
39. Ramanathan, T.; Abdala, A. A.; Stankovich, S.; Dikin, D. A.; Herrera-Alonso, M.; Piner, R. D.; Adamson, D. H.; Schniepp, H. C.; Chen, X.; Ruoff, R. S.; Nguyen, S. T.; Aksay, I. A.; Prud'Homme, R. K.; Brinson, L. C., *Functionalized graphene sheets for polymer nanocomposites*. *Nat Nanotechnol* **2008,** *3* (6), 327-31.
40. Salavagione, H. J.; Gómez, M. n. A.; Martínez, G., *Polymeric Modification of Graphene through Esterification of Graphite Oxide and Poly(vinyl alcohol)*. *Macromolecules* **2009,** *42* (17), 6331-6334.
41. Li, X. G.; McKenna, G. B., *Considering Viscoelastic Micromechanics for the Reinforcement of Graphene Polymer Nanocomposites*. *ACS Macro Letters* **2012,** *1* (3), 388-391.
42. Pang, H.; Chen, T.; Zhang, G.; Zeng, B.; Li, Z.-M., *An electrically conducting polymer/graphene composite with a very low percolation threshold*. *Materials Letters* **2010,** *64* (20), 2226-2229.
43. Wang, D.; Zhang, X.; Zha, J.-W.; Zhao, J.; Dang, Z.-M.; Hu, G.-H., *Dielectric properties of reduced graphene oxide/polypropylene composites with ultralow percolation threshold*. *Polymer* **2013,** *54* (7), 1916-1922.
44. Das, S.; Irin, F.; Tanvir Ahmed, H. S.; Cortinas, A. B.; Wajid, A. S.; Parviz, D.; Jankowski, A. F.; Kato, M.; Green, M. J., *Non-covalent functionalization of pristine few-layer graphene using triphenylene derivatives for conductive poly (vinyl alcohol) composites*. *Polymer* **2012,** *53* (12), 2485-2494.
45. Parviz, D.; Yu, Z.; Hedden, R. C.; Green, M. J., *Designer stabilizer for preparation of pristine graphene/polysiloxane films and networks*. *Nanoscale* **2014,** *6* (20), 11722-11731.
46. Wang, S.; Tambraparni, M.; Qiu, J.; Tipton, J.; Dean, D., *Thermal Expansion of Graphene Composites*. *Macromolecules* **2009,** *42* (14), 5251-5255.
47. Jang, J. Y.; Kim, M. S.; Jeong, H. M.; Shin, C. M., *Graphite oxide/poly(methyl methacrylate) nanocomposites prepared by a novel method utilizing macroazoinitiator*. *Compos Sci Technol* **2009,** *69* (2), 186-191.
48. Kim, H.; Miura, Y.; Macosko, C. W., *Graphene/Polyurethane Nanocomposites for Improved Gas Barrier and Electrical Conductivity*. *Chem Mater* **2010,** *22* (11), 3441-3450.
49. Zhang, H.-B.; Zheng, W.-G.; Yan, Q.; Yang, Y.; Wang, J.-W.; Lu, Z.-H.; Ji, G.-Y.; Yu, Z.-Z., *Electrically conductive polyethylene terephthalate/graphene nanocomposites prepared by melt compounding*. *Polymer* **2010,** *51* (5), 1191-1196.
50. Kim, H.; Macosko, C. W., *Processing-property relationships of polycarbonate/graphene composites*. *Polymer* **2009,** *50* (15), 3797-3809.
51. Rafiee, M. A.; Rafiee, J.; Wang, Z.; Song, H.; Yu, Z.-Z.; Koratkar, N., *Enhanced Mechanical Properties of Nanocomposites at Low Graphene Content*. *ACS Nano* **2009,** *3* (12), 3884-3890.
52. Li, X.; McKenna, G. B.; Miquelard-Garnier, G.; Guinault, A.; Sollogoub, C.; Regnier, G.; Rozanski, A., *Forced assembly by multilayer coextrusion to create oriented graphene reinforced polymer nanocomposites*. *Polymer* **2014,** *55* (1), 248-257.

53. Song, P.; Cao, Z.; Cai, Y.; Zhao, L.; Fang, Z.; Fu, S., *Fabrication of exfoliated graphene-based polypropylene nanocomposites with enhanced mechanical and thermal properties*. *Polymer* **2011,** *52* (18), 4001-4010.
54. Liang, J.; Huang, Y.; Zhang, L.; Wang, Y.; Ma, Y.; Guo, T.; Chen, Y., *Molecular-Level Dispersion of Graphene into Poly(vinyl alcohol) and Effective Reinforcement of their Nanocomposites*. *Advanced Functional Materials* **2009,** *19* (14), 2297-2302.
55. Chen, G.; Weng, W.; Wu, D.; Wu, C., *PMMA/graphite nanosheets composite and its conducting properties*. *European Polymer Journal* **2003,** *39* (12), 2329-2335.
56. Stankovich, S.; Dikin, D. A.; Dommett, G. H.; Kohlhaas, K. M.; Zimney, E. J.; Stach, E. A.; Piner, R. D.; Nguyen, S. T.; Ruoff, R. S., *Graphene-based composite materials*. *Nature* **2006,** *442* (7100), 282-6.
57. Yoonessi, M.; Gaier, J. R., *Highly Conductive Multifunctional Graphene Polycarbonate Nanocomposites*. *ACS Nano* **2010,** *4* (12), 7211-7220.
58. Chung, D. D. L., *Electrical applications of carbon materials*. *J Mater Sci* **2004,** *39* (8), 2645-2661.
59. Crain, J. M.; Lettow, J. S.; Aksay, I. A.; Prud'homme, R. K.; Korkut, S. *Coatings containing functionalized graphene sheets and articles coated therewith.* US20110049437 A1, **2011**.
60. Liang, J.; Wang, Y.; Huang, Y.; Ma, Y.; Liu, Z.; Cai, J.; Zhang, C.; Gao, H.; Chen, Y., *Electromagnetic interference shielding of graphene/epoxy composites*. *Carbon* **2009,** *47* (3), 922-925.
61. Kim, H.; Macosko, C. W., *Morphology and Properties of Polyester/Exfoliated Graphite Nanocomposites*. *Macromolecules* **2008,** *41* (9), 3317-3327.
62. Voigt, W., *Ueber die Beziehung zwischen den beiden Elasticitätsconstanten isotroper Körper*. *Annalen der Physik* **1889,** *274* (12), 573-587.
63. Reuss, A., *Berechnung der Fließgrenze von Mischkristallen auf Grund der Plastizitätsbedingung für Einkristalle*. *ZAMM - Journal of Applied Mathematics and Mechanics / Zeitschrift für Angewandte Mathematik und Mechanik* **1929,** *9* (1), 49-58.
64. Halpin, J. C.; Kardos, J. L., *HALPIN-TSAI EQUATIONS: A REVIEW*. *Polymer Engineering and Science* **1976,** *16* (5), 344-352.
65. Mori, T.; Tanaka, K., *Average stress in matrix and average elastic energy of materials with misfitting inclusions*. *Acta Metallurgica* **1973,** *21* (5), 571-574.
66. Liu, B.; Feng, X.; Zhang, S.-M., *The effective Young's modulus of composites beyond the Voigt estimation due to the Poisson effect*. *Compos Sci Technol* **2009,** *69* (13), 2198-2204.
67. Fornes, T. D.; Paul, D. R., *Modeling properties of nylon 6/clay nanocomposites using composite theories*. *Polymer* **2003,** *44* (17), 4993-5013.
68. Tandon, G. P.; Weng, G. J., *The Effect of Aspect Ratio of Inclusions on the Elastic Properties of Unidirectionally Aligned Composites*. *Polym Composite* **1984,** *5* (4), 327-333.
69. Zhao, X.; Zhang, Q.; Chen, D.; Lu, P., *Enhanced Mechanical Properties of Graphene-Based Poly(vinyl alcohol) Composites*. *Macromolecules* **2010,** *43* (5), 2357-2363.
70. Potts, J. R.; Lee, S. H.; Alam, T. M.; An, J.; Stoller, M. D.; Piner, R. D.; Ruoff, R. S., *Thermomechanical properties of chemically modified graphene/poly(methyl methacrylate) composites made by in situ polymerization*. *Carbon* **2011,** *49* (8), 2615-2623.
71. Liao, K.-H.; Kobayashi, S.; Kim, H.; Abdala, A. A.; Macosko, C. W., *Influence of Functionalized Graphene Sheets on Modulus and Glass Transition of PMMA*. *Macromolecules* **2014**, 141028074543005.

72. McKenna, G. B., Dynamics of Materials at the Nanoscale: Small-Molecule Liquids and Polymer Films. In *Polymer Physics*, John Wiley & Sons, Inc.: 2010; pp 191-223.
73. Dannenberg, E. M., *Bound Rubber and Carbon Black Reinforcement*. *Rubber Chemistry and Technology* **1986,** *59* (3), 512-524.
74. Young, R. J.; Kinloch, I. A.; Gong, L.; Novoselov, K. S., *The mechanics of graphene nanocomposites: A review*. *Compos Sci Technol* **2012,** *72* (12), 1459-1476.
75. Jiang, T.; Huang, R.; Zhu, Y., *Interfacial Sliding and Buckling of Monolayer Graphene on a Stretchable Substrate*. *Advanced Functional Materials* **2014,** *24* (3), 396-402.
76. Tsoukleri, G.; Parthenios, J.; Papagelis, K.; Jalil, R.; Ferrari, A. C.; Geim, A. K.; Novoselov, K. S.; Galiotis, C., *Subjecting a graphene monolayer to tension and compression*. *Small* **2009,** *5* (21), 2397-402.
77. Frank, O.; Tsoukleri, G.; Riaz, I.; Papagelis, K.; Parthenios, J.; Ferrari, A. C.; Geim, A. K.; Novoselov, K. S.; Galiotis, C., *Development of a universal stress sensor for graphene and carbon fibres*. *Nature Communications* **2011,** *2*, 255.
78. Zabel, J.; Nair, R. R.; Ott, A.; Georgiou, T.; Geim, A. K.; Novoselov, K. S.; Casiraghi, C., *Raman spectroscopy of graphene and bilayer under biaxial strain: bubbles and balloons*. *Nano Lett* **2012,** *12* (2), 617-21.
79. Raju, A. P. A.; Lewis, A.; Derby, B.; Young, R. J.; Kinloch, I. A.; Zan, R.; Novoselov, K. S., *Wide-Area Strain Sensors based upon Graphene-Polymer Composite Coatings Probed by Raman Spectroscopy*. *Advanced Functional Materials* **2014**, n/a-n/a.
80. Young, R. J.; Gong, L.; Kinloch, I. A.; Riaz, I.; Jalil, R.; Novoselov, K. S., *Strain Mapping in a Graphene Monolayer Nanocomposite*. *ACS Nano* **2011,** *5* (4), 3079-3084.
81. Li, Z.; Young, R. J.; Kinloch, I. A., *Interfacial Stress Transfer in Graphene Oxide Nanocomposites*. *ACS Applied Materials & Interfaces* **2012,** *5* (2), 456-463.
82. Cai, M.; Glover, A. J.; Wallin, T. J.; Kranbuehl, D. E.; Schniepp, H. C., *Direct Measurement of the Interfacial Attractions between Functionalized Graphene and Polymers in Nanocomposites*. *AIP Conference Proceedings* **2010,** *1255* (1), 95-97.
83. Aoyama, S.; Park, Y. T.; Macosko, C. W.; Ougizawa, T.; Haugstad, G., *AFM Probing of Polymer/Nanofiller Interfacial Adhesion and Its Correlation with Bulk Mechanical Properties in a Poly(ethylene terephthalate) Nanocomposite*. *Langmuir* **2014**.
84. Cai, W.; Piner, R. D.; Stadermann, F. J.; Park, S.; Shaibat, M. A.; Ishii, Y.; Yang, D.; Velamakanni, A.; An, S. J.; Stoller, M.; An, J.; Chen, D.; Ruoff, R. S., *Synthesis and Solid-State NMR Structural Characterization of 13C-Labeled Graphite Oxide*. *Science* **2008,** *321* (5897), 1815-1817.
85. Miao, M., *Electrical conductivity of pure carbon nanotube yarns*. *Carbon* **2011,** *49* (12), 3755-3761.
86. He, H.; Klinowski, J.; Forster, M.; Lerf, A., *A new structural model for graphite oxide*. *Chemical Physics Letters* **1998,** *287* (1–2), 53-56.
87. Reatto, L.; Galli, D. E.; Nava, M.; Cole, M. W., *Novel behavior of monolayer quantum gases on graphene, graphane and fluorographene*. *Journal of physics. Condensed matter : an Institute of Physics journal* **2013,** *25* (44), 443001.
88. Wei, T.; Song, L.; Zheng, C.; Wang, K.; Yan, J.; Shao, B.; Fan, Z.-J., *The synergy of a three filler combination in the conductivity of epoxy composites*. *Materials Letters* **2010,** *64* (21), 2376-2379.
89. Wang, Y. Y.; Burke, P. J., *A large-area and contamination-free graphene transistor for liquid-gated sensing applications*. *Appl Phys Lett* **2013,** *103* (5).

Table 1.1 Typical methods to produce graphene

Strategy	Methods	Advantage	Disadvantage
Top-down	Micromechanical cleavage[3]	Large size High quality Single and few layers	Very small quantity
	Exfoliation of graphite with surfactants[12-13]	High quality Low cost Few layers;	Low yield; Contamination by surfactants
	Sonication exfoliation of graphite oxide and chemical reduction[26, 84]	Large quantity Few layers	Low electrical conductivity; Hazardous procedure
	Thermal exfoliation and reduction of graphite oxide in one step[16]	Large quantity; Few layers; No solvent; Fast process with one step exfoliation/reduction	High temperature process; Relatively smaller size
Bottom-up	Chemical vapor deposition[17-18]	Large size; Single and few layers; High quality	Small quantity
	Epitaxial growth on SiC[19-20]	Large size; Few layers High quality	Very small quantity

Table 1.2 Dispersion methods to produce graphene polymer nanocomposites

Method	Advantage	Disadvantage
Solvent mixing[32, 39]	Good dispersion	Cost / removal of solvent
In situ polymerization[48, 70]	Good dispersion; Enable covalent bonding	Solvent using
Melt blending[10, 50]	No solvent	Poor dispersion due to high viscosities; Degradation of polymer and graphene derivatives

Table 1.3 Mechanical properties of typical polymer graphene nanocomposites

Nanocomposites		Graphene wt. %	Increase in Young's modulus	Increase in tensile strength	T_g change / °C
PMMA[39]	GO	0.01	33 %	N/A	+13
PMMA[52]	GNP	2.0	118 %	N/A	+2
PEMA[41]	GO	0.25	25 %	N/A	+15
PP[53]	RGO	0.85	74 %	54 %	+2.5
Epoxy[51]	TRG	0.1	31 %	40 %	N/A
PVA[54]	GO	0.7	62 %	76 %	+3.3
Polyurethane[48]	TRG	3.0	680 %	N/A	N/A

GO: graphene oxide; RGO: reduced graphene oxide; TRG: thermally reduced graphene oxide; GNP: graphene nanoplatelet

Table 1.4 Typical electrically conductive polymer graphene nanocomposites and other conductive materials

Nanocomposites		Lowest percolation threshold / wt. %	Maximum conductivity/ S/cm
PS[56]	Treated GO	0.2	0.01 at 5 wt. %
Polyurethane[48]	TRG	0.5	N/A
Polycarbonate[57]	TRG	0.3	0.5 at 4.8 wt. %
PMMA[55]	GNP	0.7	1 at 10 wt. %
PE[42]	RGO	0.2	0.1 at 1.3 wt.%
PP[33]	GNP	0.7	0.005 at 10 wt.%
PDMS[45]	Pristine graphene	N/A	2.2 at 3.4 wt. %
Other materials			
Copper		N/A	5.85×10^5
Graphite		N/A	2.5×10^3
Graphene[8]		N/A	6.0×10^3
Carbon nanotube[85]		N/A	4.0×10^2 ~ 5.0×10^3

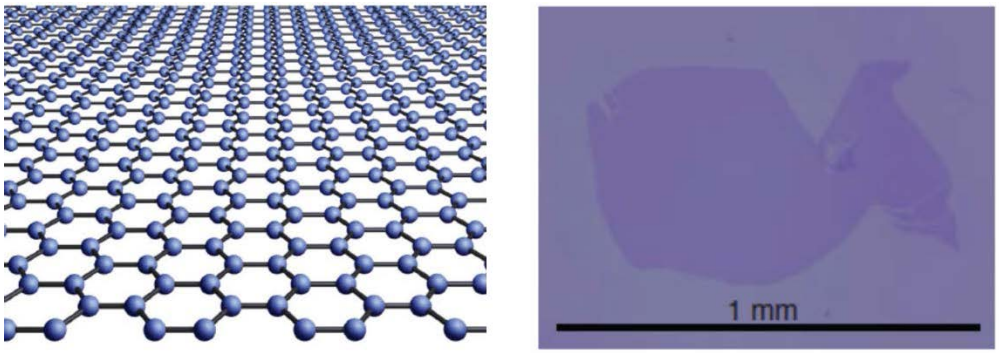

Figure 1.1 Left: The structure of graphene; Right: Large graphene pieces placed on SiO_2 wafer prepared by "Scotch-tape method" (Adapted from Reference[1, 5])

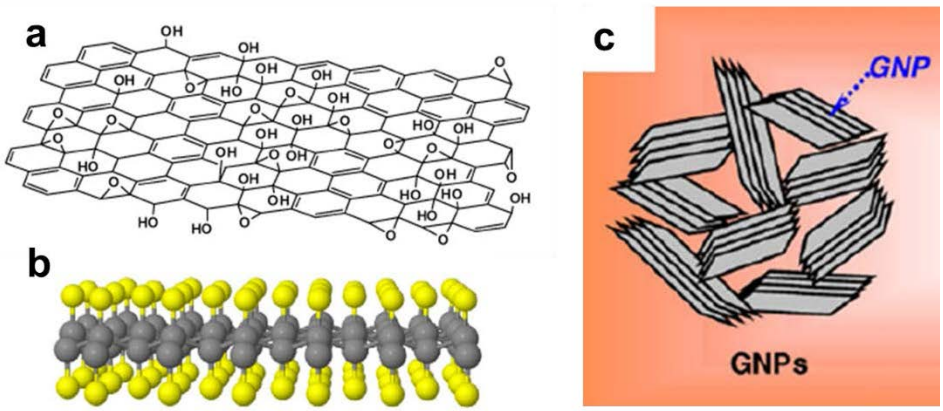

Figure 1.2 Graphene derivative nanoparticles: (a) Graphene oxide (GO), adapted from Reference[86]; (b) Fluorographene, adapted from Reference[87]; (c) Graphene nanoplatelets (GNP), adapted from Reference[88]

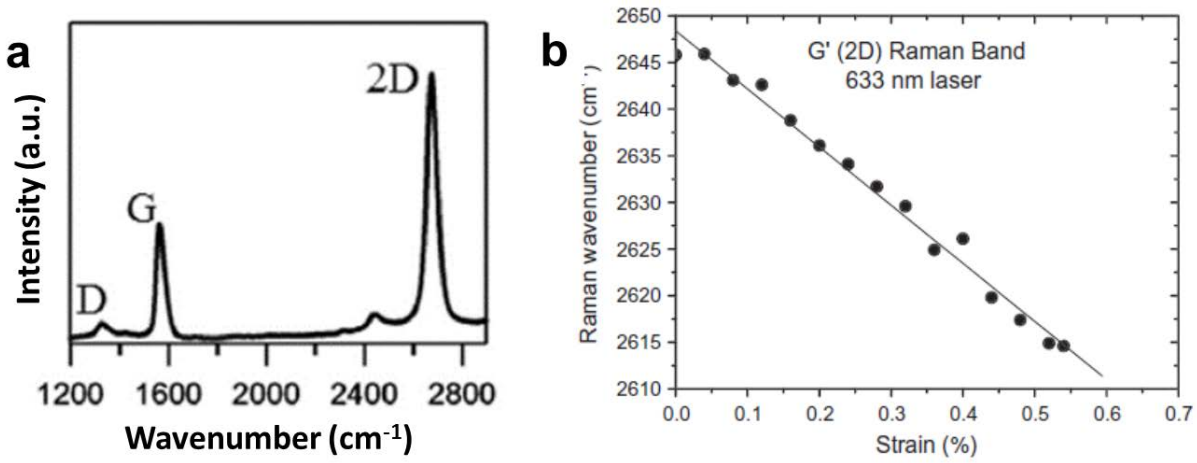

Figure 1.3 (a) Raman spectrum of single graphene, adapted from Reference[89]; (b) Shift of 2D peak as a function of strain, adapted from Reference[74]

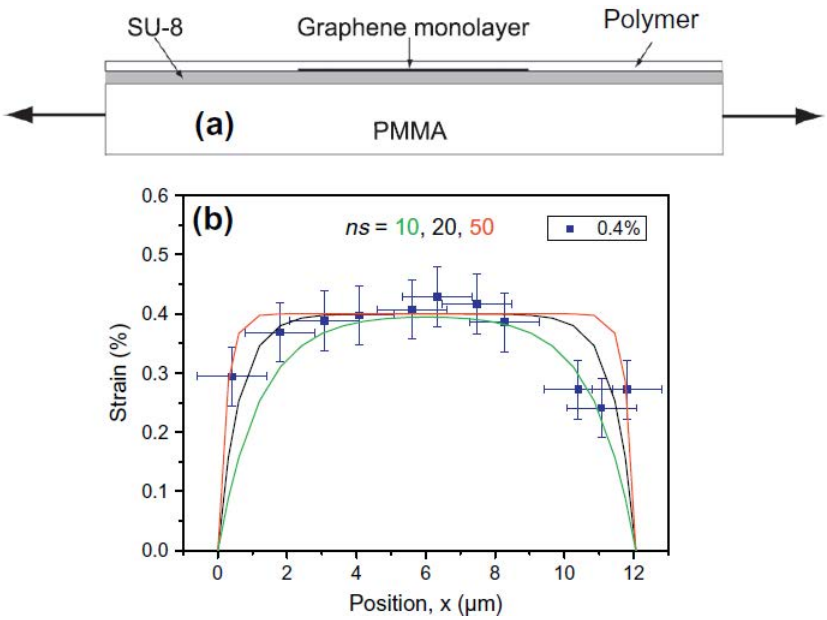

Figure 1.4 (a) Stretching test on a PMMA beam with graphene on top of it; (b) Strain map of a single layer graphene in the direction of tensile axis at 0.4 % strain (Adapted from Reference[74])

Chapter 2. Experimental Methodology

In this chapter, we describe briefly the three main experimental methods used to prepare or investigate the graphene oxide nanocomposites, oriented graphene nanoplatelets in multilayer films, and graphene nano-sandwich.

2.1 Rheometry

Viscoelastic behavior of polymer can be measured by rheometers, using dynamic tests, stress relaxation and creep test. In the dissertation, the dynamic test on rheometers is the major experimental method. Using the rheometer, when a sinusoidal strain or stress is applied to a sample, the corresponding stress or strain can be measured. If the sample is elastic, the resulting signal is also sinusoidal and in phase. If a sample is purely viscous, the resulting signal is out of phase with a 90° angle. However, for polymers, due to their viscoelastic characteristics, the resulting signal is out of phase with a shift called phase angle δ ($0° < \delta < 90°$).

When the rheometer is applying a sinusoidal strain onto the sample, as equation 1,

$$\gamma = \gamma^0 \sin(\omega t) \qquad (\mathbf{1})$$

where ω is the frequency, γ^0 is the maximum strain applied. The resulting stress response can be described as equation 2,[1]

$$\tau_0(t) = \gamma^0\big(\sin(\omega t)\, G'(\omega) + \cos(\omega t)\, G'(\omega)\big) \qquad (\mathbf{2})$$

where G'(ω) and G"(ω) are the storage modulus to measure the elasticity and loss modulus to measure the energy lost by viscous dissipation, respectively.[1] Then the phase angle δ is defined as equation 3,

$$\tan(\delta) = \frac{G"(\omega)}{G'(\omega)} \qquad (\mathbf{3})$$

Dynamic frequency test and Dynamic temperature test are generally used to test the polymeric samples. In dynamic frequency test, the temperature is fixed and the resulting

responses as a function of frequency are measured. (Usually 100 – 0.01 rad/s). In linear regime, the response of amorphous polymers at lower temperature is equivalent to that within short time / large frequency, and the response at higher temperature is equivalent to that within long time / small frequency in the same way. Therefore, a time-temperature superposition (TTS) can be applied, in the way that all curves of responses can be shifted to a reference temperature to construct a continuous curve (master curve). Using TTS, experiments on a commercial rheometer can be designed to collect data for up to 15 decades.

A shift factor a_T was defined as equation 4,[1]

$$a_T = \frac{\tau(T)}{\tau(T_0)} \tag{4}$$

where τ is the relaxation time and T_0 is the reference temperature. In the temperature ranging from T_g to T_g+100 K, the shift factors a_T can be typically fit to the Williams-Landel-Ferry (WLF) equation,[2]

$$log(a_T) = \frac{-C_1(T - T_0)}{C_2 + (T - T_0)} \tag{5}$$

where C_1 and C_2 are material-dependent constants, and generally the reference temperature T_0 equals to T_g.

The Vogel-Fulcher-Tammann (VFT) equation[3-5] is equivalent to the Williams-Landel-Ferry (WLF) equation, with a T_∞ rather than reference temperature:

$$\tau = \tau_\infty \exp(\frac{B}{T - T_\infty}) \tag{6}$$

where τ_∞ and B are material-dependent constants, and T_∞ is the temperature at which the viscosity becomes infinite.

Dynamic temperature tests are often used to characterize some transition temperatures of polymers, such as glass transition temperature T_g,[6] and β relaxation temperature T_β.[7] The testing

frequency is fixed, and the resulting response is measured as a function of the temperatures. The glass transition temperature T_g can be estimated as the corresponding temperature of the peak of tan(δ), or G" in the glass transition region, and T_β can be obtained in the same way (Figure 2.1). However, the value of T_g and T_β also depend on the testing frequency and heating/cooling rate. Generally 6.28 rad/s (1Hz) and 1 K/min are used for most dynamic temperature tests.

2.2 Forced assembly multilayer coextrusion

Melting extrusion has been used to disperse nanoparticles into polymer matrices and is especially relevant for industrial applications, due to cost and simplicity compared to other techniques such as in-situ polymerization and solvent mixing.[8-11] However, nanoparticles tend to aggregate due to van der Waals forces and high specific areas, and the high viscosity of polymer melts often leads to the poor dispersion of nanoparticles, especially when there are no strong interactions between the nanoparticles and polymer matrices. Forced assembly multilayer coextrusion, also named layered multiplying coextrusion, is an attractive technique to produce up to thousands of layers in films, and the individual layer thicknesses can be ranged from micron meter to nano-meter scale.[12-16] Figure 2.2 illustrates the procedure: Two polymeric melts are extruded from two single-screw extruders and combined, then flow through a series of n mixing elements, each of which doubles the number of layers by the process of vertical slicing, spreading and recombining,[14, 17] to make the layers in the number of 2^{n+1}. For example, with up to n=11, a 30 μm thick film with 4096 layers can be produced, with the layer thickness less than 10 nm.[14, 18]

In pioneering work, Baer and coworkers used this "forced assembly" technique to force immiscible polymer pairs to construct unique multilayer structures (Figure 2.3), such as designed

architectures leading to interesting confined crystallization (EAA / PEO),[16] optical properties (PMMA / SAN)[14] and combined glass transition temperature (PMMA / PC).[18] They also reported that multilayer coextrusion requires a reasonable viscosity match between the two polymeric melts.[14]

The idea of using forced assembly multilayer coextrusion to disperse particles into polymer matrices takes the advantage of layer thickness theoretically smaller than the typical size of the aggregates of particle (often in the micron scale). (Figure 2.4) During the co-extrusion, the confined layer structure forces the breaking of aggregates by shear stress. Up to recently, only micro-fillers such as talc micro-platelets,[19] phosphate glass spherical particles (diameter is 2~4 μm)[20] have been dispersed into multilayered films with layers in micron meter thicknesses, leading to materials presenting enhanced gas barrier and mechanical properties. Studies on carbon black[17] and carbon nanotubes[17, 21] dispersed into multilayered polypropylene films with layers in nano-scale thicknesses were published very recently and showed potential to prepare nanocomposites using this technique.

2.3 Nanobubble inflation method

The classical bubble inflation technique has been used in the study both the elastic and viscoelastic properties of polymeric membranes[22-23]. In 2005, O'Connell and McKenna[24] developed a nano-bubble inflation method which is a miniaturization of the membrane inflation experiment to study the viscoelastic properties of ultrathin polymeric films. Using atomic force microscopy (AFM) they imaged the time-changing bubble profile of membranes as small as 1.2 μm in diameter and of thickness to 27 nm.[24] In 2008, Bunch et al[25] used a bulge test technique[26] and AFM to study the elastic properties and gas permeability of graphene by inflating a 4.75 μm

square graphene membrane with helium. The nano-bubble inflation method of McKenna and co-workers[24, 27-30] has also been expanded recently to measure the mechanical properties of 800 nm × 2.6 μm rectangular ultrathin polymer films[31] as well as to polycarbonate films as thin as 3 nm.[30] More recently Maillard, *et al.*[32] used a laser confocal microscope profilometer to image 500 μm x 5 mm rectangular near-nanometric scale thickness films of a glassy polystyrene filled with silica nanoparticles.

In the nano-bubble inflation method, a polymer thin film was prepared by spin coating the polymer solution onto mica sheets and floated onto the water surface, then transfer on top of a filter template. The filter template holding the film was mounted in a custom pressure cell using adhesives and pressurized dry air was applied into the pressure cell to inflate the sample films under AFM.[27] The details of experiments will be described in Chapter 5. Figure 2.5 illustrates the bubble inflation for a single bubble and three-dimension AFM images of inflated bubbles.

When the bubble deflections are larger than three times the film thickness (membrane limit[33]), the bending contribution can be neglected and the bubble deformation is dominated by the stretching stress.[28] In this case, the bubble shape can be described by a hemisphere. By fitting the bubble profile data to the equation of a circle, the radius of curvature R is calculated as,

$$R^2 = (x - a)^2 + (y - b)^2 \quad \textbf{(7)}$$

where x and y are the x-position and height data, and a and b are offset constants for a circle not centered on the coordinate axes. The stress σ is related to the pressure P, the film thickness t_0 and the radius of curvature R of the bubble as equation 8:

$$\sigma_{11} = \sigma_{22} = \frac{PR}{2t_0} \quad \textbf{(8)}$$

The biaxial strain $\varepsilon_{11}=\varepsilon_{22}$ at the pole of the bubbles is related to the geometry of the bubble by Equation 9 and 10,[24, 27]

$$\varepsilon_{11} = \varepsilon_{22} = \frac{s}{2R_0} - 1 \quad \textbf{(9)}$$

$$s = 2R \sin^{-1}\left({R_0}/{R}\right) \quad \textbf{(10)}$$

where R_0 is hole radius and s is the segment length of the bubble. The total stress σ_{total} in the bubble is the sum of the elastic stress and pre-stress σ_0 as given in Equation 11.[29]

$$\sigma_{total} = \sigma_{11} = E_{biax}\varepsilon_{11} + \sigma_0 \quad \textbf{(11)}$$

Therefore, a plot of σ_{total} versus ε_{11} should be a straight line and the biaxial modulus E_{biax} and pre-stress σ_0 can be obtained as the slope and intercept, respectively. σ_0 is generated by the surface energy of polymers as:

$$\sigma_0 = \frac{2\gamma}{t_0} \quad (\mathbf{12})$$

where t_0 is the film thickness and γ is the surface energy of polymers.

To study the viscoelastic properties, creep tests can be performed with constant pressure at different temperatures, to construct a master curve using time – temperature superposition. Then temperature shift factors can be collected and fitted using Williams-Landel-Ferry (WLF) equation,[2] or the Vogel-Fulcher-Tammann (VFT) equation[3-5], therefore to obtain the glass transition temperature T_g.[30, 34]

2.4 References

1. Ferry, J. D., *Viscoelastic Properties of Polymers*. Wiley: New York, 1980.
2. Williams, M. L.; Landel, R. F.; Ferry, J. D., *The Temperature Dependence of Relaxation Mechanisms in Amorphous Polymers and Other Glass-forming Liquids*. *Journal of the American Chemical Society* **1955,** *77* (14), 3701-3707.
3. Vogel, H., *The law of relation between the viscosity of liquids and the temperature*. *Phys. Z.* **1921,** *22*.
4. Fulcher, G. S., *ANALYSIS OF RECENT MEASUREMENTS OF THE VISCOSITY OF GLASSES*. *Journal of the American Ceramic Society* **1925,** *8* (6), 339-355.
5. Tammann, G.; Hesse, W., *The dependence of viscosity upon the temperature of supercooled liquids*. *Z. Anorg. Allg. Chem.* **1926,** *156*.
6. Badrinarayanan, P.; Zheng, W.; Li, Q.; Simon, S. L., *The glass transition temperature versus the fictive temperature*. *Journal of Non-Crystalline Solids* **2007,** *353* (26), 2603-2612.
7. Robeson, L. M.; Faucher, J. A., *Secondary loss transitions in antiplasticized polymers*. *Journal of Polymer Science Part B: Polymer Letters* **1969,** *7* (1), 35-40.
8. Kim, H.; Macosko, C. W., *Morphology and Properties of Polyester/Exfoliated Graphite Nanocomposites*. *Macromolecules* **2008,** *41* (9), 3317-3327.
9. Kim, H.; Macosko, C. W., *Processing-property relationships of polycarbonate/graphene composites*. *Polymer* **2009,** *50* (15), 3797-3809.
10. Fornes, T. D.; Paul, D. R., *Modeling properties of nylon 6/clay nanocomposites using composite theories*. *Polymer* **2003,** *44* (17), 4993-5013.
11. Kalaitzidou, K.; Fukushima, H.; Drzal, L. T., *Multifunctional polypropylene composites produced by incorporation of exfoliated graphite nanoplatelets*. *Carbon* **2007,** *45* (7), 1446-1452.
12. Ivan'kova, E. M.; Krumova, M.; Michler, G. H.; Koets, P. P., *Morphology and toughness of coextruded PS/PMMA multilayers*. *Colloid & Polymer Science* **2004,** *282* (3), 203-208.
13. Liu, R. Y. F.; Bernal-Lara, T. E.; Hiltner, A.; Baer, E., *Interphase materials by forced assembly of glassy polymers*. *Macromolecules* **2004,** *37* (18), 6972-6979.
14. Ponting, M.; Hiltner, A.; Baer, E., *Polymer Nanostructures by Forced Assembly: Process, Structure, and Properties*. *Macromolecular Symposia* **2010,** *294* (1), 19-32.
15. Liu, R. Y. F.; Bernal-Lara, T. E.; Hiltner, A.; Baer, E., *Polymer interphase materials by forced assembly*. *Macromolecules* **2005,** *38* (11), 4819-4827.
16. Wang, H. P.; Keum, J. K.; Hiltner, A.; Baer, E.; Freeman, B.; Rozanski, A.; Galeski, A., *Confined Crystallization of Polyethylene Oxide in Nanolayer Assemblies*. *Science* **2009,** *323* (5915), 757-760.
17. Wen, M.; Sun, X.; Su, L.; Shen, J.; Li, J.; Guo, S., *The electrical conductivity of carbon nanotube/carbon black/polypropylene composites prepared through multistage stretching extrusion*. *Polymer* **2012,** *53* (7), 1602-1610.
18. Liu, R. Y. F.; Jin, Y.; Hiltner, A.; Baer, E., *Probing Nanoscale Polymer Interactions by Forced-Assembly*. *Macromolecular Rapid Communications* **2003,** *24* (16), 943-948.
19. Sekelik, D. J.; Stepanov, E. V.; Nazarenko, S.; Schiraldi, D.; Hiltner, A.; Baer, E., *Oxygen barrier properties of crystallized and talc-filled poly(ethylene terephthalate)*. *J Polym Sci Pol Phys* **1999,** *37* (8), 847-857.
20. Gupta, M.; Lin, Y.; Deans, T.; Baer, E.; Hiltner, A.; Schiraldi, D. A., *Structure and Gas Barrier Properties of Poly(propylene-graft-maleic anhydride)/Phosphate Glass Composites Prepared by Microlayer Coextrusion*. *Macromolecules* **2010,** *43* (9), 4230-4239.

21. Miquelard-Garnier, G.; Guinault, A.; Fromonteil, D.; Delalande, S.; Sollogoub, C., *Dispersion of carbon nanotubes in polypropylene via multilayer coextrusion: Influence on the mechanical properties*. *Polymer* **2013,** *54* (16), 4290-4297.
22. Green, A. E., *Large Elastic Deformations*. Oxford University Press: London, 1970.
23. Wineman, A. S., *LARGE AXISYMMETRIC INFLATION OF A NONLINEAR VISCOELASTIC MEMBRANE BY LATERAL PRESSURE*. *Trans. Soc. Rheol.* **1976,** *20*, 203.
24. O'Connell, P. A.; McKenna, G. B., *Rheological measurements of the thermoviscoetastic response of ultrathin polymer films (vol 307, pg 1760, 2005)*. *Science* **2005,** *310* (5753), 1431-1431.
25. Bunch, J. S.; Verbridge, S. S.; Alden, J. S.; van der Zande, A. M.; Parpia, J. M.; Craighead, H. G.; McEuen, P. L., *Impermeable atomic membranes from graphene sheets*. *Nano Lett* **2008,** *8* (8), 2458-2462.
26. Beams, J. W., Mechanical Properties of Thin Films of Gold and Silver. In *Structure and Properties of Thin Films*, Neugebauer, D. A. N., J.B.; Vermilyea, D.A., Ed. Wiley: New York, 1959; pp 183-192.
27. O'Connell, P. A.; McKenna, G. B., *Novel nanobubble inflation method for determining the viscoelastic properties of ultrathin polymer films*. *Rev Sci Instrum* **2007,** *78* (1), 013901.
28. O'Connell, P. A.; McKenna, G. B., *A novel nano-bubble inflation method for determining the viscoelastic properties of ultrathin polymer films*. *Scanning* **2008,** *30* (2), 184-196.
29. Xu, S.; O'Connell, P. A.; McKenna, G. B., *Unusual elastic behavior of ultrathin polymer films: Confinement-induced/molecular stiffening and surface tension effects*. *The Journal of Chemical Physics* **2010,** *132* (18), 184902.
30. O'Connell, P. A.; Wang, J.; Ishola, T. A.; McKenna, G. B., *Exceptional Property Changes in Ultrathin Films of Polycarbonate: Glass Temperature, Rubbery Stiffening, and Flow*. *Macromolecules* **2012,** *45* (5), 2453-2459.
31. Xu, S.; O'Connell, P. A.; McKenna, G. B.; Castagnet, S., *Nanomechanical properties in ultrathin polymer films: Measurement on rectangular versus circular bubbles*. *Journal of Polymer Science Part B: Polymer Physics* **2012,** *50* (7), 466-476.
32. Maillard, D.; Kumar, S. K.; Fragneaud, B.; Kysar, J. W.; Rungta, A.; Benicewicz, B. C.; Deng, H.; Brinson, L. C.; Douglas, J. F., *Mechanical properties of thin glassy polymer films filled with spherical polymer-grafted nanoparticles*. *Nano Lett* **2012,** *12* (8), 3909-14.
33. Timoshenko, S. P.; Woinowsky-Krieger, S., *Theory of Plates and Shells*. McGraw-Hill: New York, 1969.
34. O'Connell, P. A.; Hutcheson, S. A.; McKenna, G. B., *Creep behavior of ultra-thin polymer films*. *Journal of Polymer Science Part B: Polymer Physics* **2008,** *46* (18), 1952-1965.
35. Li, Q.; Hutcheson, S. A.; McKenna, G. B.; Simon, S. L., *Viscoelastic properties and residual stresses in polyhedral oligomeric silsesquioxane-reinforced epoxy matrices*. *Journal of Polymer Science Part B: Polymer Physics* **2008,** *46* (24), 2719-2732.

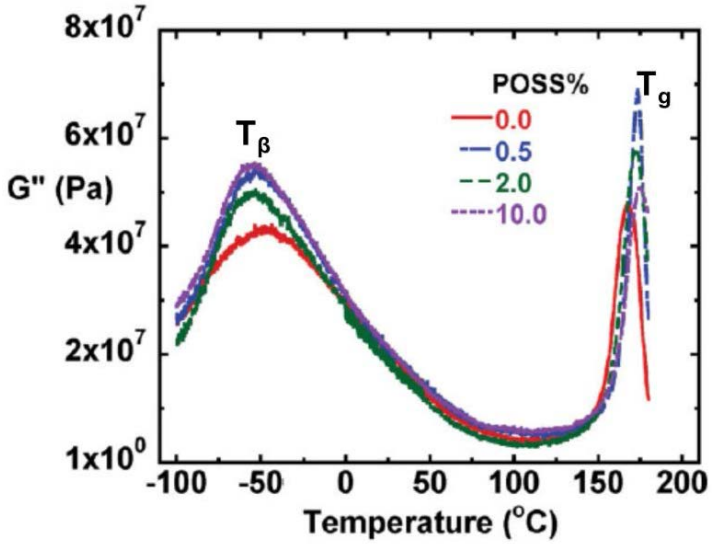

Figure 2.1 An example of a dynamic temperature test: T_g and T_β of epoxy / POSS composites by the test with the condition of 1K /min and 1Hz (Adapted from Reference[35])

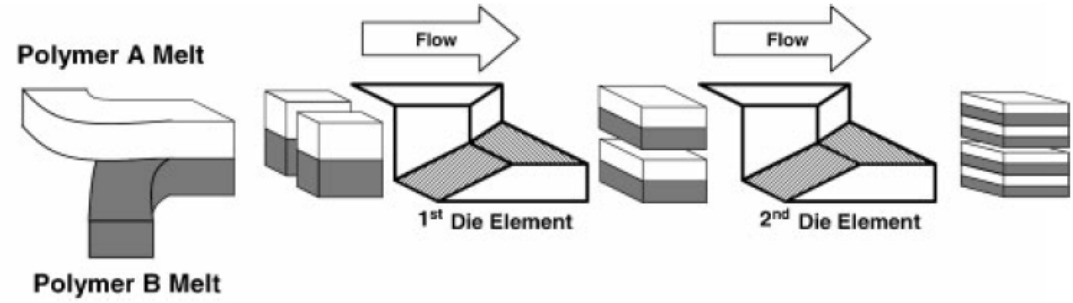

Figure 2.2 Schematic of forced assembly multilayer coextrusion (Adapted from Reference[18])

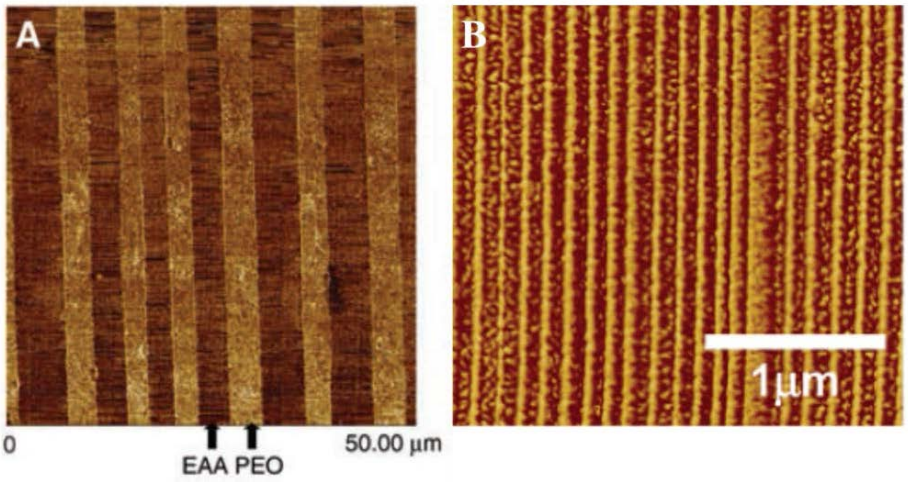

Figure 2.3 AFM images of multilayer films: (Left) EAA/PEO (Adapted from Reference[16]) and (Right) PMMA/PS (Adapted from Reference[15])

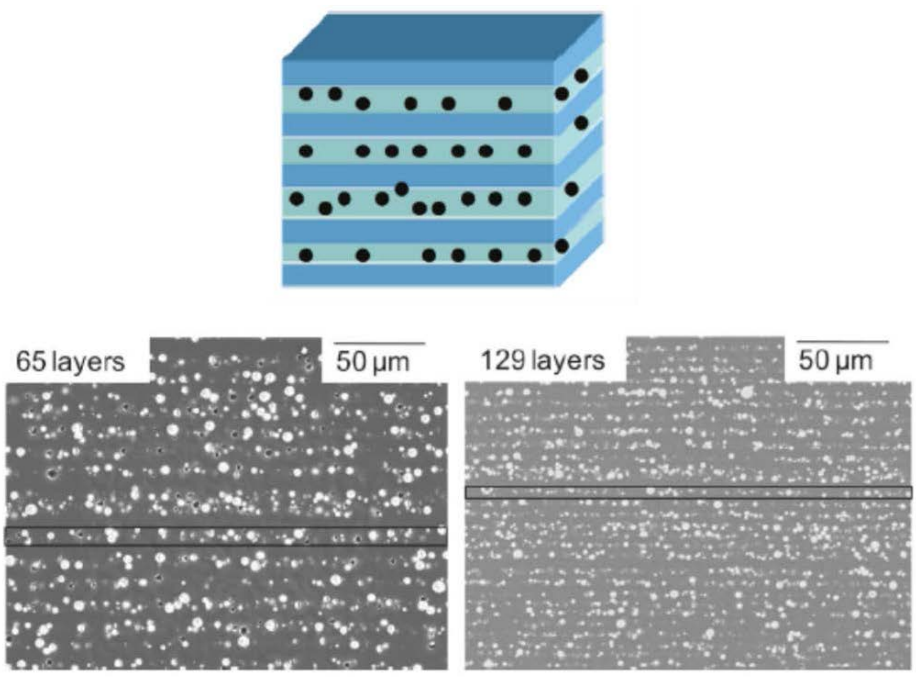

Figure 2.4 Schematic and SEM images of multilayered PP/PP filled with phosphate glass particles (Adapted from Reference[20])

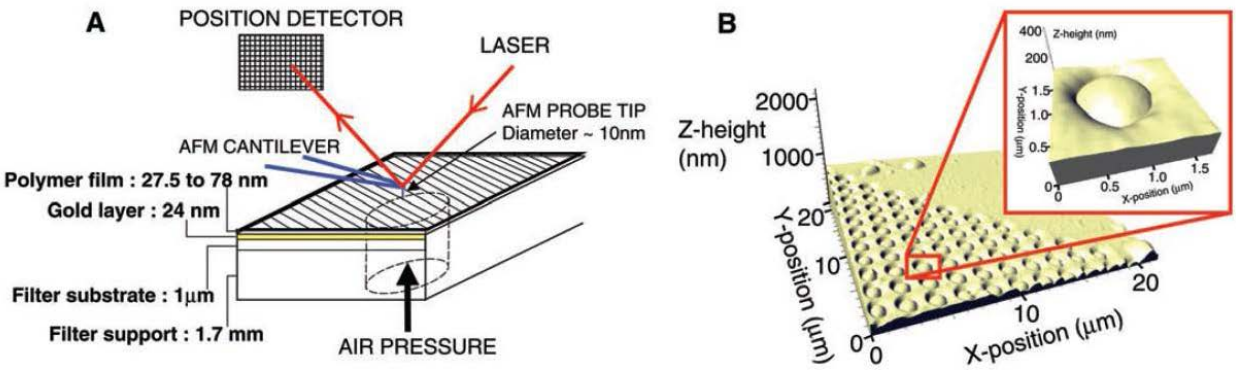

Figure 2.5. Schematic of bubble inflation and three-dimension AFM images (Adapted from Reference[24])

Chapter 3. Viscoelastic Micromechanics for the Reinforcement of Graphene oxide Polymer Nanocomposites

3.1 Overview and Introduction

Recently, it has been reported[1-3] that dispersing graphene or graphene oxide into polymer matrices at low loading (< 0.50 vol %) can lead to excellent mechanical reinforcement of polymer nanocomposites (PNC). In some instances, such as PMMA/ graphene oxide (33% enhancement of Young's modulus E at only 0.005 vol %)[1], results were interpreted to exceed the idealized Voigt upper bound prediction (the limit of infinite aspect ratio of filler and perfect alignment)[4-5]. The Halpin-Tsai model prediction[6] has also been exceeded in an epoxy/graphene system (31% increment of Young's modulus at 0.05 vol %).[2] The authors attributed this high reinforcement to a hydrogen-bonding interaction[1] or an enhanced nanofiller-polymer mechanical interlocking due to the wrinkled morphology of graphene.[1-2] These striking results exceeding elastic micromechanics predictions lead to a great enthusiasm for the prospect of graphene polymer nanocomposites. However, Macosko and co-workers have questioned the surprising results of PMMA/ graphene oxide[1] and claimed that their most of the reinforcements and T_g increase is due to the removal of low molecular additives in the original PMMA during the solvent mixing procedure to prepare nanocomposites.[7-8]

An interesting phenomenon to be considered in what follows, is that associated with the reported striking reinforcement is a significant increase in the glass transition temperature (T_g): 17 K at 0.005 vol% (PMMA/ graphene oxide)[1] and 10 K at 0.05 vol% (epoxy/graphene).[2, 9] In Figure 3.1, constructed from Ruoff's data,[3] we can see that the increase of T_g and reinforcement for PMMA/ graphene oxide nanocomposites share a similar trend. This hint that T_g and modulus increases are correlated leads us to consider that the thermo-viscoelasticity of the polymer

matrix change with the addition of the graphene or graphene oxide, and we propose that incorporation of viscoelastic micromechanics rather than conventional elastic micromechanics is necessary to describe the reinforcement of PNCs especially if the T_g of the matrix is changed by the addition of a nanofiller. The reason is that polymer nanocomposites are frequently used at high fractions of their T_g, e.g. the room temperature 298 K is around 78 % for the T_g of PMMA (383 K). In this case, the time dependence of the polymers is significant so as to influence their mechanical properties.[10]

The most widely used elastic micromechanics theories are the Voigt upper bound mixing rule[5, 11], Halpin-Tsai equation[6] and Mori-Tanaka model[12], and they are used to predict elastic properties of composites.[4, 13] To account for the polymer matrix viscoelasticity in composite materials, Hashin defined a viscoelastic micromechanics model for the modulus behavior,[14-15]

$$E_C^* = V_m E_m^*(i\omega) + V_f E_f$$

$$E_m^*(i\omega) = E_m'(\omega) + iE_m^{"}(\omega) \qquad (\mathbf{1})$$

where E^* is the complex modulus; V is the volume fraction of components; subscript: m for the polymer matrix , f for filler, and c for composites. Following Hashin's work, finite element analysis and Mori-Tanaka model have been extended to the viscoelastic materials.[16-17] And the interphase around the fillers has also been considered in viscoelastic micromechanics model of composites (Three-phase model).[17-18]

In the present work, we examine the influence of viscoelasticity of the polymer matrix on the PNCs' reinforcement and especially consider changes in the viscoelastic properties induced by the changing T_g upon the addition of graphene oxide. We provide new experimental results for the glass transition and complex modulus of poly(ethyl methacrylate) / graphene oxide nanocomposites (PEMAGO) and consider literature data[3] for poly(methyl methacrylate) /

graphene oxide nanocomposites (PMMAGO). A convenient thermo-viscoelastic micromechanics approach is presented to explain the reinforcement of graphene polymer nanocomposites. As shown below, apparently high reinforcement can be attributed to the changing thermo-viscoelasticity of the polymer matrix.

3.2 Experiments

3.2.1 Materials

The graphite oxide was purchased from Graphene Laboratories, Inc. Poly(ethyl methacrylate) (PEMA) was supplied by Sigma-Aldrich (Mw = 515 Kg/mol, PDI = 1.52).

3.2.2 Methods

Using a solution procedure, graphene oxide was exfoliated from graphite oxide in THF by ultra-sonication using a Misonix sonicator (XL 2000), then mixed with PEMA / THF solution and precipitated by MeOH.[1] (Figure 3.2) The graphene oxide was added to the system as 0.25 wt % (0.12 vol %). Rectangular bar samples ($1.3\times8.0\times45$ mm^3) and cylindrical samples (8.0 mm diameter, 1.1 mm height) were prepared through compression molding using a hot-press at 453 K. Dynamic mechanical properties were characterized using an ARES rheometer with rectangular torsion fixtures. The glass transition temperature T_g was determined from the absolute heat capacity measurement as the limiting fictive temperature[19] T_f'. Using the step-scan method in Koh and Simon's work,[29,30] the absolute heat capacity was measured by a PerkinElmer Pyris 1 differential scanning calorimeter (DSC) with multiple temperature ramp/isothermal steps. Each step is in 2 K size, with a 10 K/ min heating rate between each isothermal hold temperature, and holding for 0.8 min at each temperature. The temperature range of measurement is from -30 °C to 125°C.

3.3 Results and Discussions

As seen in Figure 3.3a, a significant increase in the glass transition temperature T_g (nearly 11 K) was observed for the 0.12 vol % PEMAGO. Generally this could be attributed to hydrogen bonding between the hydroxyl groups in graphene oxide and the carbonyl groups of PEMA (Figure 3.3b), leading to a strong interaction of graphene oxide with the PEMA, as postulated for the PMMA/graphene oxide system.[1] This is also similar to the increased T_g values that have been reported in thin polymer films on substrates with strong interactions,[20] such as PMMA on native silicon oxide.[21] Here absolute heat capacity measurement for both glassy and liquid states can provide better understanding of the reinforcement. It is found that the addition of graphene oxide leads to a slight depression of the absolute heat capacity in both glassy and liquid states.(Figure 3.3a) Another interesting phenomenon is that a larger depression is observed in the liquid state than the glassy state, indicating a reduced ΔC_p at the glass transition. The magnitude of the heat capacity change (ΔC_p) at the glass transition depends on the amount of polymer involved in the transition.[31] Therefore Figure 3.3a shows the evidence of an imobilized polymer layer around the graphene oxide. A lower ΔC_p for the 0.12 vol % PEMAGO suggests that 25 % of the PEMA is imobilized on the surface of graphene oxide. However, the glass transition doesn't seem to be significantly broadened, hence the reduction in ΔC_p due to the reinforcement with the graphene oxide does not fully explain the results and further investigation would be necessary to examine possible reasons, such as all of the polymer is confined but in a way that the liquid loses mobility uniformly. Koh and Simon reported a similar result of the greater reduced absolute heat capacity in liquid states for stacked ultra-thin polystyrene films due to the nano-confinment.[29,30]

Figure 3.4 shows dynamic temperature ramp results for both the PEMAGO from this work and the PMMAGO from reference[3]. The addition of graphene oxide causes a shift in the

curves towards higher temperatures for both materials, consistent with a nearly 15 K increment in T_g for the PEMAGO 0.12 vol%, 14 K for the PMMAGO 0.13 vol%, and 17 K for the PMMAGO 1.0 vol%. Therefore, the polymer matrix with the graphene oxide seems to behave as the pure polymer at lower temperatures, showing the importance of the matrix thermo-viscoelasticity.

Dynamic frequency sweep results for the PEMA and PEMAGO at different temperatures are shown in Figure 3.5**.** At 298 K (room temperature), the curves for *G'* and *G"* for the 0.12 vol % PEMAGO (solid square and solid diamond) overlap the curves of pure PEMA at 283 K (open circle and open triangle), which is consistent with the increase of 15 K in the T_g and for the frequency – temperature behavior of the polymer matrix.

To further explore the influence of the matrix thermo-viscoelasticity and elasticity on the reinforcement for graphene polymer nanocomposites, the dynamic temperature ramp data were shifted to the same value of T-T_g in Figure 3.6. It is found that for the PEMA the curves for storage modulus *G'* coincide well though the loss modulus *G"* curves don't overlap well due to the β relaxation[22] (Figure 3.6a). In the case of the PMMA, it is found that *E'* and *E"* for the PMMAGO 0.13 vol% nearly overlap the PMMA curves, but the PMMAGO 1.0 vol% shows a slight vertical shift (Figure 3.6b).

The apparent experimental reinforcements can be obtained using equation 2 for the data of Figure 3.4. However, upon considering the thermo-viscoelasticity, equation 2 was modified to equation 3 by replacing the modulus as function of temperature by the modulus as function of T-T_g, to give corrected experimental reinforcements from the shifted data of Figure 3.6. In a similar manner the reinforcement prediction from the elastic Voigt upper bound (equation 4)[11] was modified to the viscoelastic Voigt upper bound (equation 5).

$$\frac{E_c(T)}{E_m(T)} - 1 \quad (\mathbf{2})$$

$$\frac{E_c(T - T_g)}{E_m(T - T_g)} - 1 \quad (\mathbf{3})$$

$$\frac{V_m E_m(T) + V_f E_f}{E_m(T)} - 1 \quad (\mathbf{4})$$

$$\frac{V_m E_m(T - T_g) + V_f E_f}{E_m(T - T_g)} - 1 \quad (\mathbf{5})$$

It is worth noting that the interest in the Voigt bounds arises because properties that exceed these bounds are considered to be evidence for "extreme reinforcement" or synergistic reinforcement, which could be evidence for novel behavior in such nanocomposites.

The influence of viscoelasticity is more clearly illustrated in Figure 3.7, where the apparent experimental reinforcements (obtained by equation 2) are plotted for different temperatures and compared to the elastic Voigt upper bound predictions (equation 4) (Figure 3.7a and 3.7c). The corrected reinforcements obtained from equation 3 are also shown to compare with the viscoelastic Voigt upper bound predictions (from equation 5) in Figure 3.7b and 3.7d. Although the apparent uncorrected reinforcement is close to or even exceeds the elastic Voigt upper bound prediction, it is clear that the corrected reinforcements are much weaker than the viscoelastic upper bound prediction.

Figure 3.7 demonstrates that in polymer nanocomposites, the apparent reinforcement can be attributed to the changed viscoelasticity of the polymer induced by the T_g change. The corrected effect of the graphene oxide reinforcement on PEMA and PMMA at ultra-low loading is not as high as has been reported and accounting for the viscoelastic response indicates less reinforcement than estimated from the elastic bound, hence providing a reason to Macosko and co-workers' skepticism concerning claims of extreme reinforcement. It may also explain Ruoff's

work with polycarbonate/graphene oxide that exhibits weak reinforcement, where little T_g change (< 1 K) is seen.[23]

The results presented here show that it is necessary to consider the thermo-viscoelastic response of the polymer matrix in nanocomposites (PNCs) to fully understand the reinforcement of the filler. This is especially so because polymer nanocomposites are frequently used at high fractions of the T_g, where the time dependence of the polymer is significant.[10] Therefore it is a conceptual error to examine the modulus behavior of PNCs via only elastic micromechanics. When the glass transition temperature increases, the polymer matrix in the PNCs behaves as the pure polymer at a lower temperature, contradicting the inherent assumption in elastic micromechanics.[4] Consequently, it is more reasonable to use Hashin's viscoelastic micromechanics model, taking into account changes in matrix response due to the addition of the filler, to estimate the bounds on modulus behavior of PNCs.[14-15] At temperatures much farther below T_g, or when there is no change of T_g , the changes in the viscoelasticity of the polymer matrix are less important and the elastic micromechanics might be considered to capture the approximate reinforcement behavior of PNCs.

Another topic of interest is the β relaxation of graphene polymer nanocomposites. As the first relaxation below glass transition temperature T_g, β relaxation has been related to the side group motion of the poly (n-alkyl methacrylates),[24] and it is important for a material's mechanical properties, i.e. brittleness.[25-26] In Figure 3.4, we can see for the PEMA peak of the loss shear modulus *G"* around 274 K, the addition of graphene oxide can increase the relaxation temperature by 6~7 K but doesn't change the intensity of β relaxation peak, which means the graphene oxide does not reinforce the PEMA by suppressing the β relaxation as an antiplasticizer.[27] Considering the increase of 14~15 K in the glass transition temperature T_g, the

incorporation of graphene oxide splits the glass transition and β relaxation, similar to the result reported for an epoxy/ POSS nanocomposite system.[28]

3.4 Conclusion

In summary, we have demonstrated in this chapter that the ultra-low loading of graphene oxide raises the T_g of PEMA and PMMA significantly and leads to a large shift of the frequency–temperature properties of the polymer matrix. In such a condition, it is necessary to consider the influence of thermo-viscoelasticity on the expected reinforcement in graphene oxide polymer nanocomposites, and our thermo-viscoelastic approach shows that apparent extreme reinforcements can be attributed to the changing T_g of the polymer, and the corrected mechanical reinforcement from graphene oxide is much weaker than previously reported. It is also found that incorporation of graphene oxide splits the glass transition and β relaxation, instead of suppressing the β relaxation.

3.5 References

1. Ramanathan, T.; Abdala, A. A.; Stankovich, S.; Dikin, D. A.; Herrera-Alonso, M.; Piner, R. D.; Adamson, D. H.; Schniepp, H. C.; Chen, X.; Ruoff, R. S.; Nguyen, S. T.; Aksay, I. A.; Prud'Homme, R. K.; Brinson, L. C., *Functionalized graphene sheets for polymer nanocomposites*. *Nat Nanotechnol* **2008,** *3* (6), 327-31.
2. Rafiee, M. A.; Rafiee, J.; Wang, Z.; Song, H.; Yu, Z.-Z.; Koratkar, N., *Enhanced Mechanical Properties of Nanocomposites at Low Graphene Content*. *ACS Nano* **2009,** *3* (12), 3884-3890.
3. Potts, J. R.; Lee, S. H.; Alam, T. M.; An, J.; Stoller, M. D.; Piner, R. D.; Ruoff, R. S., *Thermomechanical properties of chemically modified graphene/poly(methyl methacrylate) composites made by in situ polymerization*. *Carbon* **2011,** *49* (8), 2615-2623.
4. Fornes, T. D.; Paul, D. R., *Modeling properties of nylon 6/clay nanocomposites using composite theories*. *Polymer* **2003,** *44* (17), 4993-5013.
5. Liu, B.; Feng, X.; Zhang, S.-M., *The effective Young's modulus of composites beyond the Voigt estimation due to the Poisson effect*. *Compos Sci Technol* **2009,** *69* (13), 2198-2204.
6. Halpin, J. C.; Kardos, J. L., *HALPIN-TSAI EQUATIONS: A REVIEW*. *Polymer Engineering and Science* **1976,** *16* (5), 344-352.
7. Kim, H.; Abdala, A. A.; Macosko, C. W., *Graphene/Polymer Nanocomposites*. *Macromolecules* **2010,** *43* (16), 6515-6530.
8. Liao, K.-H.; Kobayashi, S.; Kim, H.; Abdala, A. A.; Macosko, C. W., *Influence of Functionalized Graphene Sheets on Modulus and Glass Transition of PMMA*. *Macromolecules* **2014**, 141028074543005.
9. Yavari, F.; Rafiee, M. A.; Rafiee, J.; Yu, Z. Z.; Koratkar, N., *Dramatic Increase in Fatigue Life in Hierarchical Graphene Composites*. *ACS Applied Materials & Interfaces* **2010,** *2* (10), 2738-2743.
10. McKenna, G. B., Dynamics of Materials at the Nanoscale: Small-Molecule Liquids and Polymer Films. In *Polymer Physics*, John Wiley & Sons, Inc.: 2010; pp 191-223.
11. Voigt, W., *Ueber die Beziehung zwischen den beiden Elasticitätsconstanten isotroper Körper*. *Annalen der Physik* **1889,** *274* (12), 573-587.
12. Mori, T.; Tanaka, K., *Average stress in matrix and average elastic energy of materials with misfitting inclusions*. *Acta Metallurgica* **1973,** *21* (5), 571-574.
13. Tucker Iii, C. L.; Liang, E., *Stiffness predictions for unidirectional short-fiber composites: Review and evaluation*. *Compos Sci Technol* **1999,** *59* (5), 655-671.
14. Hashin, Z., *Viscoelastic Behavior of Heterogeneous Media*. *Journal of Applied Mechanics* **1965,** *32* (3), 630-636.
15. Hashin, Z., *Complex moduli of viscoelastic composites—II. Fiber reinforced materials*. *International Journal of Solids and Structures* **1970,** *6* (6), 797-807.
16. Brinson, L. C.; Lin, W. S., *Comparison of micromechanics methods for effective properties of multiphase viscoelastic composites*. *Composite Structures* **1998,** *41* (3–4), 353-367.
17. Fisher, F. T.; Brinson, L. C., *Viscoelastic interphases in polymer–matrix composites: theoretical models and finite-element analysis*. *Compos Sci Technol* **2001,** *61* (5), 731-748.
18. Matzenmiller, A.; Gerlach, S., *Micromechanical modeling of viscoelastic composites with compliant fiber–matrix bonding*. *Computational Materials Science* **2004,** *29* (3), 283-300.
19. Badrinarayanan, P.; Zheng, W.; Li, Q.; Simon, S. L., *The glass transition temperature versus the fictive temperature*. *Journal of Non-Crystalline Solids* **2007,** *353* (26), 2603-2612.

20. Alcoutlabi, M.; McKenna, G. B., *Effects of confinement on material behaviour at the nanometre size scale*. *Journal of Physics: Condensed Matter* **2005,** *17* (15), R461-R524.
21. Keddie, J. L.; Jones, R. A. L.; Cory, R. A., *Interface and surface effects on the glass-transition temperature in thin polymer films*. *Faraday Discussions* **1994,** *98* (0), 219-230.
22. Kulik, A. S.; Beckham, H. W.; Schmidt-Rohr, K.; Radloff, D.; Pawelzik, U.; Boeffel, C.; Spiess, H. W., *Coupling of .alpha. and .beta. Processes in Poly(ethyl methacrylate) Investigated by Multidimensional NMR*. *Macromolecules* **1994,** *27* (17), 4746-4754.
23. Potts, J. R.; Murali, S.; Zhu, Y.; Zhao, X.; Ruoff, R. S., *Microwave-Exfoliated Graphite Oxide/Polycarbonate Composites*. *Macromolecules* **2011,** *44* (16), 6488-6495.
24. Heijboer, J., *In Physics of Non-crystalline Solids*. Wiley: New York, 1965.
25. Boyer, R. F., *Dependence of mechanical properties on molecular motion in polymers*. *Polymer Engineering & Science* **1968,** *8* (3), 161-185.
26. Flory, A. L.; McKenna, G. B., *Chemical structure—normal force relationships in polymer glasses*. *Polymer* **2005,** *46* (14), 5211-5217.
27. Robeson, L. M.; Faucher, J. A., *Secondary loss transitions in antiplasticized polymers*. *Journal of Polymer Science Part B: Polymer Letters* **1969,** *7* (1), 35-40.
28. Li, Q.; Hutcheson, S. A.; McKenna, G. B.; Simon, S. L., *Viscoelastic properties and residual stresses in polyhedral oligomeric silsesquioxane-reinforced epoxy matrices*. *Journal of Polymer Science Part B: Polymer Physics* **2008,** *46* (24), 2719-2732.
29. Koh, Y. P.; McKenna. G. B.; Simon, S. L., *Calorimetric glass transition temperature and absolute heat capacity of polystyrene ultrathin films. Journal of Polymer Science Part B: Polymer Physics* **2006**, 44, 3518–3527.
30. Koh, Y. P.; Simon, S. L., *Structural relaxation of stacked ultrathin polystyrene films. Journal of Polymer Science Part B: Polymer Physics* **2008**, 46, 2741–2753.
31. Grady, B. P.; Paul, A.; Peters, J. E.; Ford, W. T., *Glass transition behavior of single-walled carbon nanotube-polystyrene composites. Macromolecules* **2009**, 42, 6152–6158.

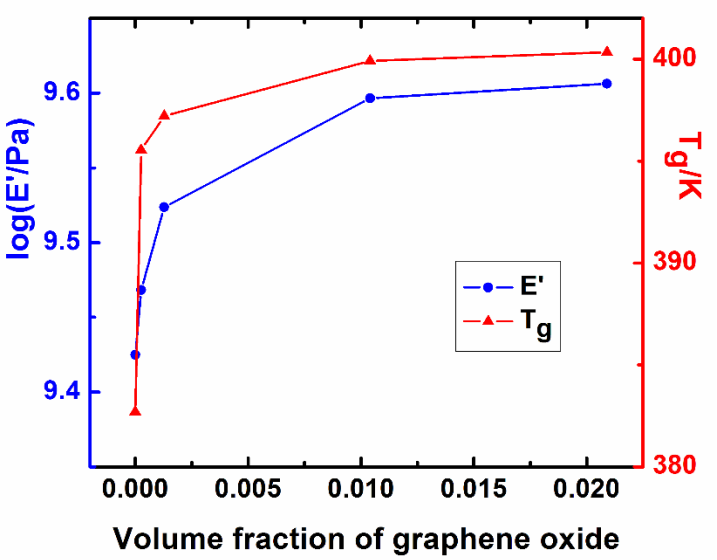

Figure 3.1 Glass transition temperature and storage tensile modulus *E'* of PMMA/ graphene oxide at 313 K vs. graphene oxide loading. (Data from reference[3]).

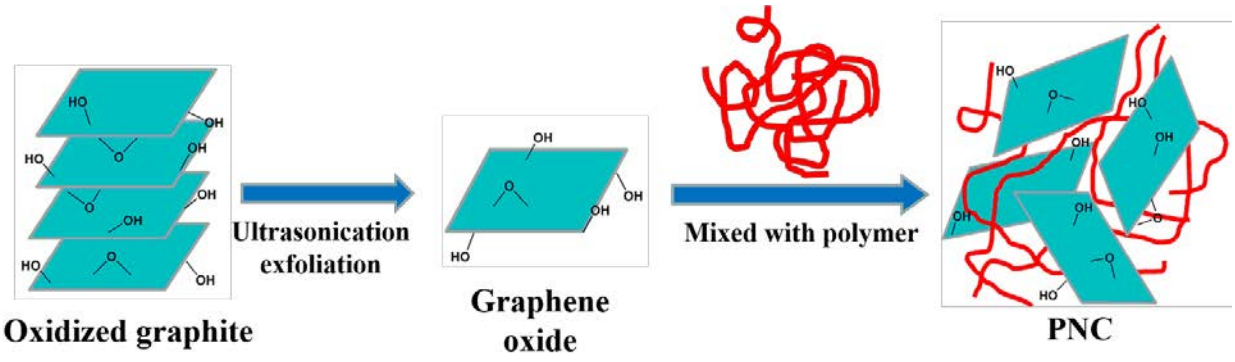

Figure 3.2 Schematic to make graphene oxide polymer nanocomposites (PNC)

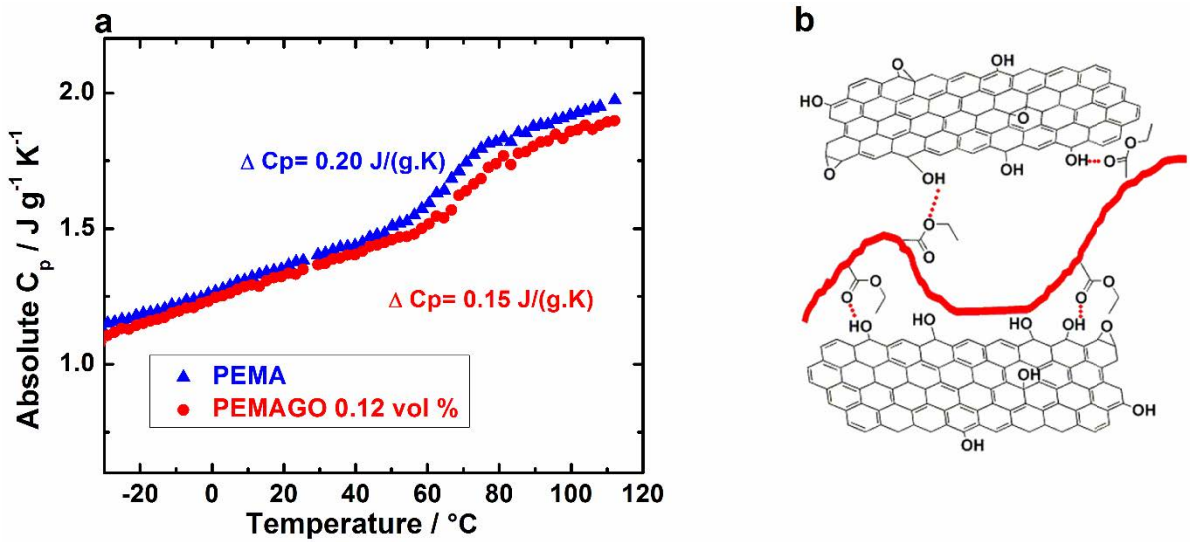

Figure 3.3 (a) Absolute C_p vs. temperature for PEMA and PNC (b) Interaction between graphene oxide and PEMA

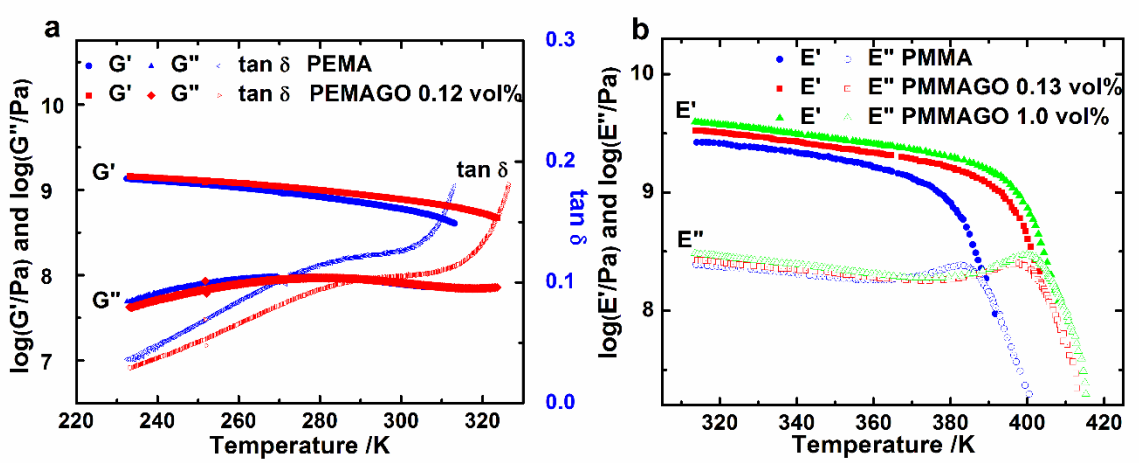

Figure 3.4 Loss and storage moduli during temperature ramp for (a) PEMA and PEMAGO 0.12 vol % from 230K to 330 K (Heating rate at 1K/min; ω= 6.28 rad/s; strain is 0.02%) and (b) PMMA and PMMAGO (data from reference[3]).

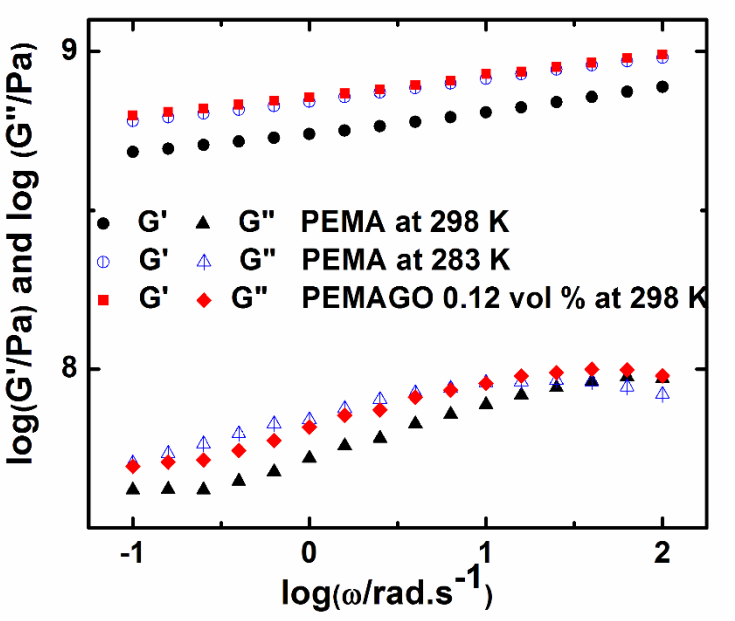

Figure 3.5 Dynamic frequency sweep of PEMA and PEMAGO 0.12 vol% at 283K and 298 K (Strain is 0.02%)

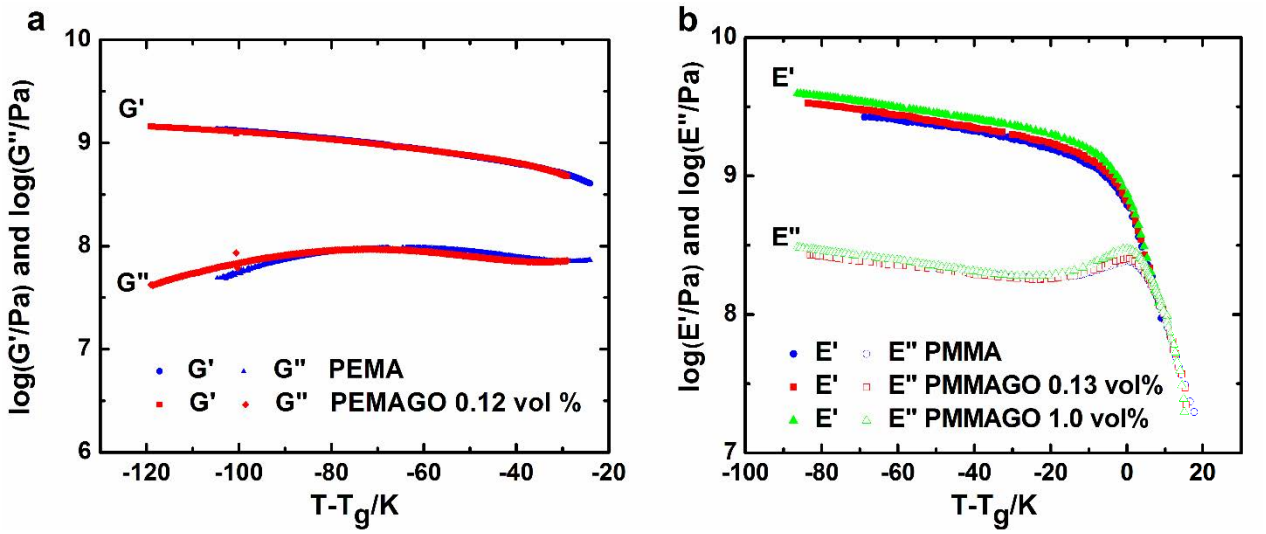

Figure 3.6 Storage modulus and loss modulus versus T-T_g of (a) PEMA and PEMAGO 0.12 vol % and (b)PMMA and PMMAGO (data from ref[3])

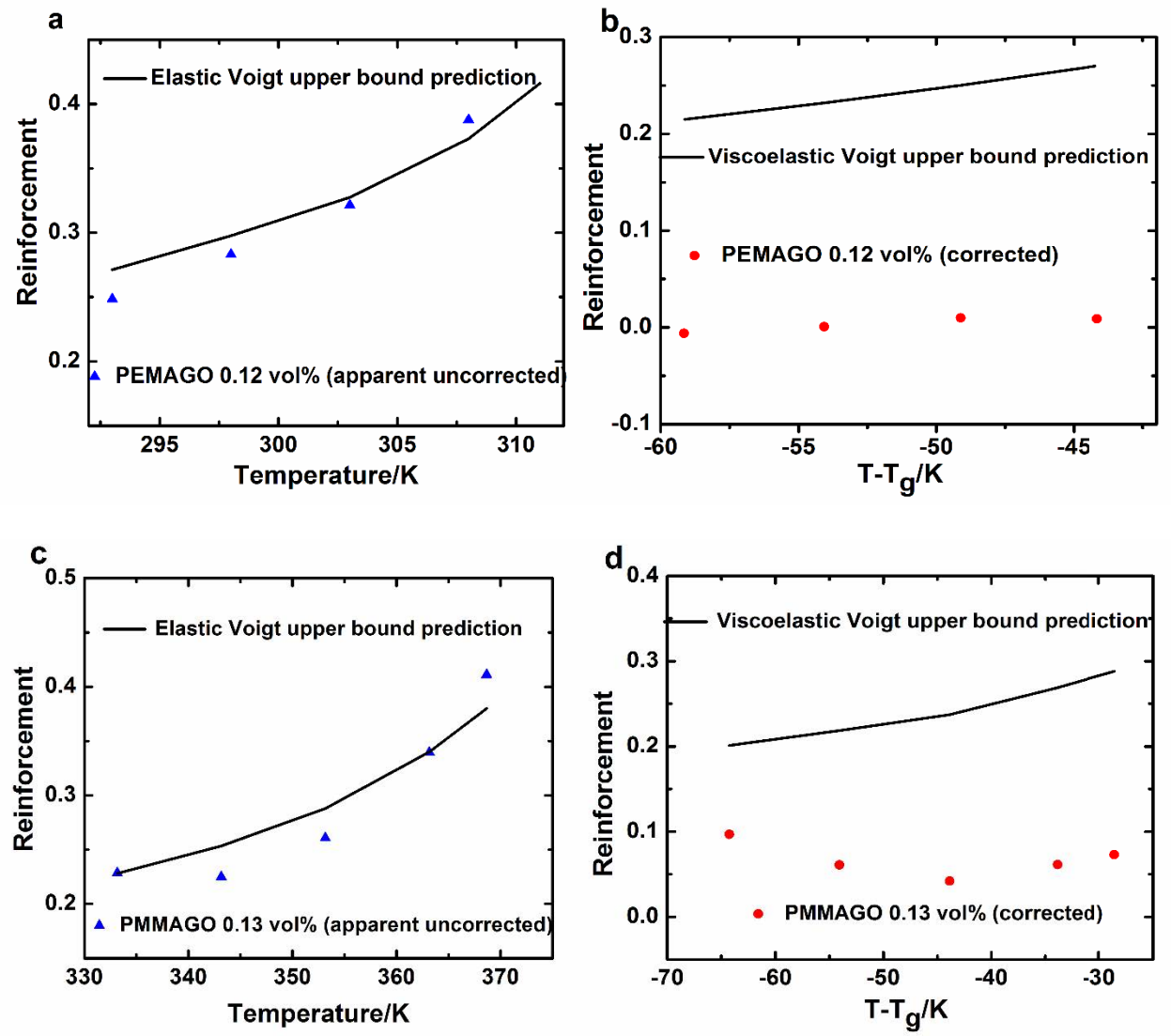

Figure 3.7 Apparent and corrected reinforcement and Voigt upper bound predictions for (a, b) PEMAGO 0.12 vol % and (c, d) PMMAGO 0.13 vol % (data from reference[3]).

Chapter 4. Forced assembly by multilayer co-extrusion to create oriented graphene nanoplatelets reinforced polymer nanocomposites

4.1 Overview and Introduction

To date, most work on graphene polymer nanocomposites has focused on isotropic or random dispersion of the graphene in the polymer matrix,[1-3] giving limited reinforcement.[4] If platelet-like fillers can be oriented in a plane of the polymer matrix, they provide the possibility of two-dimensional reinforcement in the plane of orientation.[5] Theoretically, if the requirements of both high volume fraction of filler and in-plane alignment of the platelets are met, the mimicking of nacre-like[6] structures might be achieved. Therefore, methods to create such structures, especially with a potentially industrially useful method, are desirable and important.

In the general case, graphene nanocomposites have been made in ways that emphasize good dispersion and have not examined heavily the possibility of creating oriented structures. For example, as already stated in the previous chapter, it has been reported[7-8] that dispersing graphene or graphene oxide into a polymer matrix at low loadings (< 1 wt %) can lead to good mechanical reinforcement for polymer nanocomposites, such as PMMA/graphene oxide[7] (33% enhancement of Young's modulus at only 0.01 wt %). One reason that has been given for the apparent strong reinforcement is that, via a solution mixing method, graphene and graphene oxide are dispersed with a wrinkled topology in the host polymer matrix.[7] Some researchers think that this provides strong interfacial adhesion between graphene and the polymer chains with a consequent significant increase in the glass transition temperature (T_g) of the polymer matrix.[7-8] If this is the case, we showed in chapter 2 that much of the high degree of reinforcement might be attributed to the changing thermo-viscoelasticity of the polymer matrix due to the changing T_g[9] rather than to a mechanical reinforcement *per se*, although such strong reinforcement is still

impressive and could lead to many applications. In addition to bench scale solution mixing, graphene nanoplatelets can also be dispersed into a polymer matrix via melt mixing, e.g. in most cases through extrusion, which is the most relevant tool for exploring potential industrial applications.[4, 10-12] However, due to the high viscosities of polymer melts, melt extrusion usually falls short of providing effective dispersion of nanofillers and results in filler aggregation.[12] Recently it has been shown that this method can be improved by multiplying the number of extrusion steps: a concentrated solid mixture of filler in polymers (or "master batch") is produced by melt mixing then further dilution one or more times with the same polymer to the desired concentration.[13-14] It has been found that this technique can result in better dispersion of the nanofiller with consequently better composite mechanical properties.

To the best of our knowledge, the development of methods to create in-plane oriented graphene in a polymer matrix in order to realize two-dimensional reinforcement have not been undertaken either for bench scale solution mixing or for melt extrusion. Kim and Macosko reported the production of slightly oriented polycarbonate/graphene nanocomposites obtained from injection molding. However, they also reported that wrinkling of the graphene in the polymer matrix resulted in only weak reinforcement.[10]

Multilayer coextrusion, which has been briefly described before, is an attractive technique to produce up to thousands of alternating layers in films with individual layer thicknesses from 10 nm to multiple μm.[15-16] In pioneering work, Baer and coworkers have used this "forced assembly" technique and have shown that immiscible polymer pairs and filled/unfilled polymers can be forced to combine into a unique multilayer structure, accompanied with interesting confined crystallization effects,[17] gas barrier properties,[18] and

optical properties.[19] In addition, Koets et al report the toughening of immiscible amorphous polymer pairs by multilayer coextrusion.[20]

Since multilayer coextrusion is scalable to industrial processing and alignment of anisotropic nanofillers can make desirable composites, it offers an attractive approach to orient nanoparticles with high aspect ratio A_f, such as graphene nanoplatelets, in the layer plane. What we search to achieve in the present study is evidence that the forced assembly, by creating a structure with extremely thin layers filled with graphene, has the potential of creating a new type of nanocomposites in which in-plane oriented graphene is the reinforcing element. Figure 4.1 shows a schematic of the multilayer coextrusion method of forced assembly and how the geometric constraints and the complex flow that includes biaxial stretching[21] may create the oriented graphene layers in the multilayer film.

To date the idea of dispersing and orienting anisotropic nanofillers through multilayer coextrusion has been only briefly investigated. In 1999, the Baer group reported incorporating talc micro-platelets into poly(ethylene terephthalate) micro-layer films to reduce oxygen permeability.[21] Very recently, Guo et al [22] reported that enhanced electrical conductivity can result from oriented carbon nanotubes in layers with carbon black in polypropylene films formed through multilayer coextrusion. And Miquelard-Garnier et al[23] have also reported on nanocomposites with improved mechanical properties through the dispersion of carbon nanotubes in polypropylene via multilayer coextrusion. However, to the best of our knowledge, multilayer coextrusion has not been exploited to orient platelet-like nanofillers, such as graphene, to reinforce polymer matrixes, with particular thought to creating a biaxially reinforced medium.

In the present study, we use forced assembly by multilayer coextrusion to develop a new class of polymer nanocomposites with planar oriented graphene nanoplatelets to achieve two-dimensional reinforcement. To this end we prepared and studied two different nanocomposites made using the amorphous polymers polystyrene (PS) and poly(methyl methacrylate) (PMMA). The PMMA/PS couple is a typical alternating layered film structure used in multilayer coextrusion studies.[20, 24] Furthermore, commercial polystyrene /graphene master batch materials are now available in reasonable quantities. Therefore, the immiscible PMMA/graphene filled PS (PMMA/PS-graphene) system was the first that we investigated. In this instance we used a commercial PS/graphene master batch and compared the films obtained with similar films using a lab-made PS/graphene masterbatch. As poor strength of the films was observed, possibly due to the poor bonding between graphene and PS, and the weak interface between the PS and PMMA layers, we also made our own master batch of PMMA/graphene and used this to investigate the properties of PMMA/PMMA-graphene nanocomposites.

The morphology of the continuous layers and orientation of the graphene nanoplatelets were characterized with electron microscopy. Quasi-static mechanical and dynamic mechanical properties of the materials were determined. Differential scanning calorimetry was used to determine the glass transition temperatures of the systems, hence permitting us to evaluate the magnitude of any apparent reinforcement due to the changing viscoelasticity of the matrix materials due to a change in T_g.[9]

4.2 Experiments

4.2.1 Materials

Neat poly(methyl methacrylate) was supplied by *Altuglas International* (PMMA V920T, MFI is 6 g/ 10 min at 230°C /3.8 kg; GPC using tetrahydrofuran and calibrated with polystyrene standards gives Mw = 110k, PDI = 2.15) and neat polystyrene was obtained from *Total Petrochemicals* (PS 1340, MFI is 4 g/ 10 min at 200°C /5 kg; GPC in THF gives Mw = 286k, PDI = 1.66). The graphene nanoplatelets came from two sources: virgin graphene nanoplatelets obtained from *ACS Materials* were used to make PS/graphene and PMMA/graphene master batches in our laboratories. Prior to extrusion the PMMA systems were dried in a SOMOS dry air dryer T20 eco system at 80 °C for 4 hours. A commercial polystyrene/15% graphene nanoplatelet filled master batch was obtained from *Ovation Polymers Company*. The characteristics of the master batches and the graphene nanoplatelets are presented in Table 4.1.

4.2.2 Preparation of lab made polymer/graphene master batches

The lab-made PMMA/20 wt % graphene master batch was prepared from the Altuglas PMMA and the *ACS Materials* graphene nanoplatelets following a solution mixing method used by Ramanathan et al[7] and adapted here for bigger quantities. 15 g graphene and 60 g PMMA were dissolved in 600 mL THF (*Emparta ACS)* at 40 °C and the mixture was mechanically stirred for 2 h to assure good dispersion. The mixture was precipitated by adding 6 L water and vacuum dried at 80 °C for 24 h. The lab-made PS/graphene master batch (20 wt %) was prepared using the same method.

4.2.3 Preparation of the polymer/graphene formulations

Prior to multilayer coextrusion, the relevant PMMA-graphene formulations (0.5, 1.0 and 2.0 wt %) to be used in extruder 2 (see Figure 4.1) were prepared by diluting the PMMA-20 wt % graphene with the neat PMMA using a Thermo Haake PTW 16-40D co-rotating twin-screw extruder at 600 rpm and 215 °C. The PS-graphene formulations (0.5, 2.0 and 4.0 wt %) were prepared by diluting the commercial PS/ 15 wt % graphene master batch from *Ovation Polymers Company* with the *Total Petrochemicals* PS, using the same twin-screw extruder at 200 °C with co-rotating mixing, again, at 600 rpm. The specific mechanical energy (SME = torque × screw speed of the extruder / throughput of the mixing) was around 5000 kJ/Kg for the PMMA systems and 8000 kJ/kg for the PS systems. For the two systems, this value was fixed as high as possible, following studies by Pötschke[25] and others[23] showing that a high SME value for twin-screw extrusion results in better dispersion of nanofillers in polymers.

Multilayer coextrusion requires a reasonable viscosity match between the polymer melt streams.[16] In the present study, because the films were prepared with different amounts of graphene nanoplatelets, the viscosity ratio between the two melt streams ($\eta_{\text{graphene filled polymer}}$ / η_{PMMA}) could not be maintained constant. The viscosity ratios were obtained from the apparent steady shear viscosities of all polymers and graphene formulations as a function of temperature to choose acceptable operating conditions. And 240°C and 225 °C were chosen for PMMA/ PS-graphene systems and PMMA/PMMA-graphene systems, respectively, considering both viscosity match and degradation.. The zero shear viscosity increases with increasing concentration of graphene. However, at the shear rate of $4s^{-1}$ to simulate the flow condition in the extrusion, the graphene enhances shear thinning therefore decrease the viscosity of polymers.

4.2.4 Fabrication of multilayer polymer/polymer-graphene films

Using a multilayer coextrusion process (Figure 4.1), the primary polymer melt A (in this study always PMMA) and the secondary polymer melt B (PMMA or PS) filled with graphene, were extruded from two single-screw extruders (Extruder 1: Mapre, 30 mm diameter with a barrel of length-to-diameter ratio of 33 and speed fixed at 37 rpm; Extruder 2: Scamex, 20 mm diameter with a barrel of length-to-diameter ratio of 20 and speed between 30 and 45 rpm) respectively, combined in a classical three layer coextrusion feed block (ABA). In this study, the percentage of polymer B in the film was kept constant at 10 wt %. Exact values for this ratio were calculated after extrusion by measuring the mass flow rate and always found to be between 9.3 and 10.8%.

The three-layer melt block flows through a series of mixing elements with the process of vertical slicing, biaxial stretching and recombining[22-23] shown in Figure 4.1 to produce $2^{n+1}+1$ layers (n being the number of mixing elements). In this study, 0, 6 and 10 mixing elements were used, giving films containing respectively 3, 129 and 2049 layers. These are then spread through a flat die (width = 100mm, thickness = 1mm) and onto a chill roll drawn at 1.7 m/min and maintained at 80 °C to allow relaxation of the PMMA. The result is a rectangular film made up of the alternating layers. For the two single-screw extruders, mixing elements and die were set to 225 °C for the PMMA/PMMA systems and 240°C for the PMMA/PS systems. The residence time for the melts in the mixing element segment, estimated using the throughput of the extruder, is approximately 2 minutes.

The final concentration of graphene was then 0.05, 0.1 and 0.2 wt % in the PMMA/PMMA films, and 0.05, 0.2 and 0.4 wt % in the PMMA/PS films if both filled and unfilled layers are counted.

4.2.5 Morphological analysis

Optical microscopy: 20 μm thick slices were obtained using a Leica RM 2225 microtome. The cuts were made perpendicular to the extrusion flow direction. They were then observed by transmission optical microscopy using an Olympus BH2-UMA. Images were analyzed using ImageJ (an open source image processing software developed by the National Institutes of Health) and at least five images were used for quantitative analysis.

Electron microscopy:

- Scanning electron microscopy (SEM) and scanning transmission electron microscopy (STEM): 70-80 nm thick slices from the films were obtained using a LKB BROMMA 2088 ultratome with a glass knife at the speed of 2 mm/s. The cuts were perpendicular to the extrusion flow direction. Images were collected using a HITACHI 4800 SEM in SEM and STEM modes.

- Transmission electron microscopy (TEM): TEM was performed using a TESLA BS500 electron microscope operating at 90 kV. Approximatively 50 nm thick sections were microtomed from multilayered films with a Power Tome XL ultramicrotome equipped with a diamond knife. Again, cuts were perpendicular to the extrusion direction.

4.2.6 Property Measurements

4.2.6.1 Steady shear viscosity measurement

The apparent steady shear viscosity of all polymers and graphene formulations were determined using an ARES Rheometer (TA Instruments) with 25 mm diameter parallel plate fixture at a shear rate of $4s^{-1}$ to simulate the flow condition in the extrusion. In the mixing elements section, one can estimate the shear flow knowing the throughput of the extruder (around 6 kg/h), the density of the PMMA (1.18 g/cm^3) and the dimensions of the mixing elements (10 × 10 mm) and obtain a value close to 8 s^{-1}. The $4s^{-1}$ shear rate was chosen because the high viscosity system gave a torque at the limit of the instrument for this rate.

4.2.6.2 Mechanical Properties

Quasi-static mechanical properties of the multilayer films were determined in uniaxial extension using an Instron 4301 testing machine with a 1kN load cell. At least five specimens of each sample (0.3~0.5×10×110 mm^3), cut parallel and transverse to the extrusion flow direction, were tested at ambient temperature and 50% relative humidity at a cross head speed of 5 mm/min. Strain was obtained from the cross head displacement and original sample length (110 mm) between the grips of testing machine. Tensile modulus was calculated within the linear regime of strain (0.2-0.4 %) from the stress versus strain curves.

The dynamic moduli at a single frequency of 1.0 Hz were determined using a TA Instruments Q800 DMA with a rectangular specimen (0.3~0.5×5 ×20 mm^3). Compliance was calibrated with a stainless steel strip by using the internal instrument procedure. A dynamic temperature ramp at 2 °C/min was run at 1Hz and 0.5 % strain over the temperature range from

40 °C to 130 °C. It was verified that the measurement remained in the linear viscoelastic domain. Three samples were tested for each type of sample investigated.

4.2.6.3 Glass Transition Temperature Determination

The glass transition temperature T_g was determined from calorimetry as the limiting fictive temperature T_f'.[26-27] The calorimeter was a TA Q10 differential scanning calorimeter (DSC, TA Instruments) and the tests were run in heating at 10 °C/min after cooling at 10 °C/min from a temperature of 130 °C under nitrogen flow.

4.2.6.4 Annealing Test

Films were cut to 5 × 5 mm^2 and annealed at 125°C for 1 hour. The dimension change was obtained using optical microscopy to characterize de-orientation of the polymer chains.

4.3. Results and Discussion

4.3.1 Structure and morphology

Electron microscopy was used to confirm the existence of the continuous layer structure of the films. Multilayer coextrusion produces polymer films with alternating layers, and the thickness of the layers is controlled by varying the number of layers and keeping the total thickness of the films constant. The overall thicknesses of the films in the present study were approximately 0.5 mm and 0.3 mm for PMMA/PS and PMMA/PMMA systems, respectively. For example, taking into account the weight ratio of 9:1 for the two polymer layers, the multilayer films with 2049 layers contained individual layers with a theoretical thickness of 500 nm for the PMMA and 65 nm for the PS in the PMMA/PS-graphene films, and 290 nm and 35

nm for PMMA/PMMA-graphene films. The layers then provide the geometric constraints to orient the graphene nanoplatelets.

Due to these constraints, graphene nanoplatelets were expected to be oriented in the confinement by the thin layers. The layer and orientation were studied by SEM, STEM and TEM. It was found that the concentration of graphene influenced the alternating layer structure.

4.3.1.1 PMMA/PS-graphene system

The STEM and SEM images of Figure 4.2 show cross sections of the 2049-layer PMMA/PS films with 0 wt %, 0.5 wt %, 2 wt % and 4 wt % graphene nanoplatelets in the thin PS layers(e.g. 0 wt %, 0.05 wt %, 0.2 wt % and 0.4 wt % in the total film). The layer continuity was evidenced and the influence of graphene on the layer structure was studied, although the graphene confined in the thin PS layers was difficult to observe.

The PMMA and PS layers (white and black) are readily distinguished as continuous layers (Figure 4.2a), with the thickness close to expectation (PS: 60-90 nm; PMMA: 300-600 nm), although with some non-uniformity with the addition of 0.5 wt % graphene (Figure 4.2b). However, when the concentration of graphene is 2 wt % in the PS layers, some layers break and are no longer continuous. (Figure 4.2c). We also note that the addition of graphene swells the layer, which may lead to the break-up of layers at higher concentrations of graphene. When there is 4 wt % graphene in the PS layers, most of the layers are broken, with some aligned lamellae and some droplets. (Figure 4.2d) Therefore, 2 wt % graphene is found to be the upper limit in our filled layer to maintain the layer structure.

4.3.1.2 PMMA/PMMA-graphene system

We first used optical microscopy to characterize the morphology of the multilayer films at the micro-scale and to compare the dispersion of graphene nanoplatelets for films with different number of layers. To quantify the dispersion of graphene nanoplatelets, the fraction R of the total aggregates with diameter > 5 μm (area > 19.6 μm^2) over the total area of the sample was determined following the work of Pötschke.[25] Although the value obtained cannot be related to the real volume fraction of aggregates in the sample, concerning the thickness of the sample imaged, it is still observed that the large aggregation (particles > 5μm in diameter) fraction R decreases as the number of layers increases. Although it is clear that some large aggregates remain in the sample, which certainly results in the local perturbation of the nano-scaled layers even when 10 mixing elements are used, the dispersion of the graphene nanoplatelets and the breakage of aggregates in the relevant polymer matrix appears to increase upon increasing the number of layers. In the process of multi-layer co-extrusion, the mixing elements slice the melts with the result that the graphene aggregates are broken up to a large extent. In addition, due to the limitation of resolution, optical microscopy is not able to show the layers below 1μm.(For the PMMA/PMMA films, the thickness of the filled layers are 450 nm and 35 nm for the 129 and 2049 layer films, respectively). In addition, the contrast between PMMA layers is too low to show distinct layers using optical microscopy. These are the reasons that Figure 4.3 does not show a distinct layered structure.

STEM and TEM were used to study the graphene orientation and aspect ratio, when the layer thickness reaches the nano-scale in the 2049-layer films (see Figure 4.4). With no graphene, as expected (Figure 4.4a), there is no clear distinction between the thin PMMA and the thick PMMA layers. However, when there is 1 wt % graphene in the thin PMMA layers, the individual graphene nanoplatelets can be observed and appear mostly oriented in the plane of the layers

(horizontal direction in Figure 4.4b), with distribution of platelet length ranging from approximately 50 to 150 nm.

When there is 2 wt % graphene in the layers, similar to the PMMA/PS system, the concentration appears to reach an upper limit which starts to perturb the nanostructure (Figures 4.4c and 4.4d). Figure 4.4c displays some small or wrinkled graphene nanoplatelets which are still expected to be confined within the thin layers (dashed lines), similar to the results reported by Gupta, et al[18] for polypropylene/ 10 vol. % phosphate glass particle filled polypropylene multilayer films. On the other hand, Figure 4.4d shows a large and oriented graphene with a length of approximately 600 nm. Although there are some stacks of graphene nanoplatelets, e.g. 60 layers of graphene with 20 nm thickness, the stacks of graphene can still be confined in the thin layers (30-40 nm thick). It is also possible that the thick-looking graphene nanoplatelets are not stacks of graphene, but rather titled platelets.

It should be noted that the length of the graphene nanoplatelets is, in any case, smaller than the data provided by the suppliers, but the observed particles may not be totally flat (since thickness, on the contrary appears greater than the supplier provided information (see Table 1)). Extrusion is also known to result in the shortening and breakage of nanofibers[25] and nanoplatelets,[28] so this is not unexpected.

As seen in Figure 4.4, it is difficult to give an average aspect ratio for the graphene nanoplatelets, due to the variety of shapes, lengths and thicknesses, the precision of the apparatus, and the relatively small scale of the pictures. To obtain more quantitative information concerning the size and orientation of the nanoplatelets, indirect scattering methods could unfortunately not

be performed because the graphene concentrations in the samples are too low for simple scattering characterization.

In consequence we can approximate the aspect ratio assuming the graphene thickness is 2-10 nm as given by the material provider. Then the aspect ratio A_f = length / thickness, depending on whether one has a wrinkled or flat shape of the nanoplatelet, can be estimated to range from 5-10 (wrinkled particles) up to 100-300 (flatter ones). Since the outer layer of films is unfilled polymer, electrical conductivity cannot be measured to obtain the percolation information of graphene in inner filled layers. In the next section we compare these values of aspect ratio with estimates from mechanical reinforcement data and the Mori-Tanaka model of composite reinforcement.[29]

4.3.2 Glass transition temperature

Polymers are frequently used at ambient temperature or above and this can be a high fraction of the glass transition temperature.[30] Because of this a change in T_g can impact the thermo-viscoelastic response of the polymer matrix significantly.[9, 30] Hence it is important to establish that any observed stiffness increase in a nanocomposite relative to the neat resin is not simply the result of an increased T_g. As discussed in Chapter 2, for example, a 16 °C increase in T_g in poly(ethyl methacrylate) (PEMA) with 0.25 wt % graphene oxide gives an apparent 25 % reinforcement at room temperature, and this could be mistaken for a large graphene oxide reinforcement.[9] Therefore to quantitatively study the reinforcement of the planar oriented graphene, the glass transition temperatures of samples taken so that they comprised the entire film thickness were studied by DSC and normalized heat capacity was determined to compare T_g variations.[31] As shown in Figure 4.5, the T_g is observed to increase by approximately 1.5-2 °C

upon the addition of 2 wt % graphene to both the PMMA and PS thin layers. Hence the shift of the T_g due to the presence of graphene in the present work is small, unlike previous work with the nanocomposites of PEMA/graphene oxide.[9] Subsequently, we show that this small change of T_g results in only modest apparent reinforcement and that most of the reinforcement observed in the present work occurs due to the oriented graphene and not to the change in T_g due to confining effects of the nanofillers.

4.3.3 Mechanical properties

From the microscopy we can see that, as we hypothesized, the forced assembly method succeeds in orienting the graphene in the plane of the layers to some extent. Therefore, in the direction of the orientation, nanocomposites with such structures should provide enhanced stiffening of the composites in the plane directions in which the graphene platelets are aligned. To confirm the microscopic observations, we examine the stiffening or reinforcement of the multilayer composites in two ways. We first considered the modulus of the multilayer films, themselves. The results show, in this case, modest reinforcement because the individual reinforcing elements (individual layers filled with graphene) make up only 10% of the film itself and, so, are effectively diluted. We, therefore, then analyzed the results by estimating properties of the single, graphene-filled, layers. We have also analyzed the experimental results within the framework of the Mori-Tanaka model which gives an additional estimate of the graphene platelet aspect ratio. This was found to be in the same range as the estimates obtained from the microscopy measurements for flatter nanoplatelets.

4.3.3.1 Mechanical properties of multilayer films

Figures 4.6a and 4.6b show the relative stiffening of the multilayer films along extrusion flow direction based on the quasi-static tension tests and dynamic mechanical tests, respectively. The figures show the ratio E/E_m vs. weight fraction graphene of the composite modulus E to the modulus E_m of the corresponding unfilled multilayer film (for PMMA/PMMA, E_m= 2.89 GPa; for PMMA/PS, E_m= 2.71 GPa, as measured in our lab). The results are plotted as a function of the weight fraction of graphene in the full film. From the quasi-static tension tests, we see that as the addition of graphene increases to 0.2 wt % for the total film, the reinforcement is 11.0 % for the 2049-layer PMMA/PMMA-graphene film (E= 3.21 GPa) and 4.2 % for the 2049-layer PMMA/PS –graphene film (E= 2.82 GPa). In addition, as expected, the reinforcement due to the graphene in the 2049-layer film is greater than in 129-layer and 3-layer films, consistent with the idea that increasing the number of layers improves the graphene orientation. From Figure 4.6b we see that the DMA results give a similar trend, but somewhat weaker than the quasi-static tension test, i.e., approximately 8% increase in modulus for the 0.2% graphene in PMMA/PMMA system. The slight difference can possibly be explained because the DMA tests were performed at 1.0 Hz and 40 °C while the static tension tests were performed at a rather low strain rate of 7.6×10^{-4}/s and at room temperature. In addition, in fracture toughness tests (data not shown), up to 0.2 wt % graphene, the brittleness of the films does not change significantly.

The PMMA/PS-graphene films made from the commercial master batch appear to display weaker reinforcement than PMMA/PMMA-graphene made from the lab-made master batches. This might be due to the poor bonding between graphene and PS or the poor bonding between the PS and PMMA layers. We note that a significant spontaneous delamination between the PMMA and PS layers occurred after two months of the samples sitting at ambient conditions in the lab, apparently due to the low interfacial adhesion between the immiscible PS and PMMA

layers.[32] In addition, we note that the commercially supplied master batch has additives in the mix to improve the graphene dispersion and this could also be a factor in the lower reinforcement. Regardless, in what follows we consider only the PMMA/PMMA-graphene system in an examination of the reinforcement in terms of the individual graphene reinforced layers rather than the total film.

We have already used optical microscopy to compare the dispersion of the graphene nanoplatelets for varying the number of polymer film layers. In Figure 4.7, it was observed that the stiffening of films versus layer thickness, share a similar trend with the dispersion quality. By increasing the number of layers, the degree of dispersion of the graphene nanoplatelets and the possible breakage of aggregates in the polymer matrix appear to increase as the thickness of the confining layer decreases, and should confine the graphene nanoplatelets more efficiently, giving enhanced reinforcement.

Another mechanical property of interest is the fracture toughness, the ability of a material to resist fracture in the presence of cracks. As we know, incorporation of some stiff nanofillers such as carbon nanotubes may increase or maintain the polymer brittleness depending on the dispersion,[23] and silica nanoparticles can enhance the fracture toughness of epoxy.[33-34] When the crack propagation of PMMA films at room temperature occurs in the linear elastic region, fracture toughness K_{IC} can be obtained from the following equation,[34]

$$K_{IC} = \frac{P_c}{tw^{0.5}} Q \qquad (\mathbf{1})$$

where P_c is the load at crack propagation obtained from the load-displacement curve, t is the thickness, w is width, and Q is a dimensionless function of pre-crack length over width. Figure 4.8 shows both the fracture toughness results and reinforcements for the 2049-layer

PMMA/PMMA–graphene films. No change in fracture toughness was observed. Therefore the addition of graphene can reinforce the PMMA films without loss of toughness.

4.3.3.2 Reinforcement of a single, graphene filled PMMA layer

From the measurements on the multilayer films, we can estimate the modulus of the actual single, graphene filled layer (see equation 2). Although the microscopy was not conclusive that there are distinct filled/unfilled layers in the PMMA/PMMA-graphene system, it is still reasonable to assume, in a first order approximation, that the graphene nanoplatelets are mainly confined within the thin PMMA layers and aligned in the flow direction. Such an assumption is reasonable because of the short residence time of the melt streams and slow diffusion of the graphene nanoplatelets in the mixing elements (~2 minutes). Using the Stokes-Einstein equation[35] and an equivalent spherical diameter[36] for the graphene nanoplatelets. For example, for diameters of 28.8 nm (for a 5 nm x 50 nm x 50 nm platelet) and 72.6 nm (for a 5 nm x 200 nm x 200 nm platelet), the mean-square diffusion displacement in 2 minutes is estimated to be 1130 nm^2 ($d \approx 34$ nm) and 449 nm^2 ($d \approx 21$ nm), respectively, for a melt viscosity of 5367 Pa.s at a temperature of 225°C. Considering the concentration of graphene, the system is not a dilute dispersion, and we would, therefore, expect that the particle diffusion should be slower than the Stokes-Einstein estimate because of the particle interactions.[37] Hence, the actual diffusion displacement of the graphene nanoplatelets would be significantly less than the above estimates. In addition, even if there are stacks of graphene, the larger particles should have even slower diffusion than the simple Stokes-Einstein estimates above. To conclude, even not considering that the particles need to move laterally to the (apparent) orientation direction nor the fact that the diameter reductions would be greatest in the last stage of the process, the distance migrated

out of the confining layer by the graphene nanoplatelets should not be enormous. The examination of the reinforcement of the single PMMA layer containing the graphene, and the comparison with micromechanical predictions assuming alignment of the nanoplatelets, provides us with insight into the advantages of the forced assembly in orienting the graphene. It also provides information about the efficiency of orientation within the single layers. This is particularly relevant if one can eventually make multilayer systems in which all of the layers are of nanometer thickness and reinforced by graphene.

The tensile modulus E_{single} of a single graphene filled PMMA layer can be estimated using equation 1, which corresponds to the results from the Voigt upper bound mixing rule,[38] where V_{thick} and V_{single} are the volume fraction of the unfilled thick PMMA layers and single graphene filled PMMA layers, respectively.

$$E_{single}=\frac{E-V_{thick}E_m}{V_{single}} \qquad (2)$$

In order to obtain further insight into the single layer reinforcement, we used the Mori-Tanaka model[29] to analyze the graphene reinforcement in the single filled PMMA layer. Tandon and Weng[39] have derived an analytical form of the Mori-Tanaka model for the tensile modulus in composites with unidirectionally aligned isotropic platelets:

$$\frac{E}{E_m}=\frac{1}{(1+V_f(-2\nu_m A_3-(1-\nu_m A_4+(1+\nu_m)A_5 A))/2A)} \qquad (3)$$

where E_m , ν_m, and V_f are tensile modulus of PMMA, Poisson's ratio of PMMA and volume fraction of graphene, respectively. A and A_i are functions of V_f, ν_m and the Eshelby tensors provided by Tandon and Weng.[39] In the case of the single layer, $E_{single}=E$. We have assumed

E_m= 2.89 GPa, ν_m= 0.35. and the tensile modulus of the graphene sheet was taken as 1060 GPa (value measured by nanoindentation[40]). At low volume fraction, the Mori-Tanaka model is insensitive to the Poisson's ratio of the filler and we have assumed that graphene is isotropic with a Poisson's ratio of 0.006.[41]

In Figure 4.9, for the case of the 2 wt % graphene in the individual layer, the degree of apparent reinforcement is 118 % (from the quasi-static tension tests) and 86 % (from the DMA results). These results are close to the predictions from the Mori-Tanaka model with A_f = 225 or 137, for quasi-static or DMA testing, respectively. This is similar to values from 100 to 300 estimated from the electron microscopy images described previously for the flatter nanoplatelets. The high amount of reinforcement is significantly greater than previously reported for reinforcements in isotropic or random dispersions of graphene in polymer matrices. For example, a 2 wt % graphene dispersed in PMMA by *in situ* polymerization gave a 39 % reinforcement[8] and a 2 wt % graphene dispersed in polycarbonate by melt mixing gave a 21% reinforcement.[10] Importantly, the single layer analysis shows that we achieve significant reinforcement in the polymer by orientation induced by forced assembly.

With regard to the small increase in T_g, we modified the mechanical results versus temperature to give corrected reinforcement $E(T\text{-}T_g)/E_m(T\text{-}T_g)$,[9] and also compared the results with the Mori-Tanaka model. In that case the fitting parameter A_f gave values of 180 and 102 for quasi-static and DMA experiments respectively, as shown in Figure 8, again in the range of the estimated A_f values for aligned nanoplatelets, obtained from the electron microscopy images. For the 2 wt % graphene in the filled layer, the reinforcement is 101 % (from quasi-static tension test) or 69 % (from DMA), still higher than previously reported reinforcements in isotropic or random dispersions. A point worth making here is that comparison of the corrected reinforcement with

the apparent reinforcement shows that there is an extra 15-20 % reinforcement that arises from the relatively small change in T_g.

We have also examined the two-dimensional reinforcement in the single layer from the measurements of modulus perpendicular to the extrusion direction. Indeed, when the film leaves the extruder, its thickness is close to 1 mm, whereas the final film thickness obtained after the chill-roll is between 0.3 and 0.5 mm, indicating orientation of the polymer chains. A point of importance here is that annealing of the samples above T_g and watching them de-orient, gives the result that the deorientation is approximately the same for the graphene filled and unfilled system. We interpret this to imply that the addition of the graphene does not significantly change the orientation of polymer chains induced by the multilayer extrusion process. Hence, we can compare the reinforcement relative to the neat resin properties using the extruded film estimates and the neat PMMA/PMMA multilayer film properties of the tensile modulus of 2.89 GPa and 2.08 GPa, along flow and transverse directions, respectively. We compare the mechanical properties by considering the tensile modulus of the single graphene filled layer, along both flow and transverse directions. Figure 4.10 presents the T_g corrected reinforcements of flow and transverse directions. We see from the figure that the transverse reinforcement is weaker than that of the flow direction and the difference between the two gets larger the higher the graphene content. We discuss the possible mechanism in the next section.

4.3.3.3 Graphene Orientation

The ability to create a two-dimensional, maybe nacre-like, structure that gives isotropic in-plane stiffening through platelet orientation[42] is a promising advantage of the forced assembly method of making graphene or other platelet-like nanocomposites. In the previous section we

saw that we obtained very good reinforcement of the single graphene reinforced layers in the flow direction and more modest reinforcement in the perpendicular direction. To explain our observations of planar reinforcement and its anisotropy (which cannot be explained by the presence of wrinkled, almost isotropic, graphene nanoplatelets) we can apply the Krenchel's approach[43] and Brune and Bicerano's model of "small off-plane deviation: imperfect planar orientation".[44]

There are some studies that explore how platelet-like particles orient during flow.[43-46] Although numerical methods predict that the major axis of rectangular platelet-like particles aligns in the shear flow direction[45], in Paul's work of polymer/nanoclay composites produced by injection molding, a lower degree of alignment of platelets was observed by TEM in the transverse direction compared to the flow direction.[46] Paul also reported higher thermal expansion coefficients in the transverse direction, corresponding to the non-uniform orientation.[46] This work indicated an imperfect planar orientation of platelet-like particles, and there has been some theoretical work to predict the effect of imperfect alignment on the composites properties. Both Lele et al[43] using Krenchel's approach[47] and Brune and Bicerano[44] using a numerical method, showed that a small off-plane deviation from perfect planar orientation of platelet-like particles can reduce the reinforcement significantly.

When graphene nanoplatelets are in such an imperfect planar orientation or "tilted" in the transverse direction, we can estimate the transverse reinforcement from the axial reinforcement (Brune and Bicerano assumed that the axial reinforcement equals to the maximum reinforcement for perfect planar orientation) as being tilted at an angle θ to the flow direction with the following method: If we assume that the individual graphene filled PMMA layer thickness is 35 nm and the length of the graphene nanoplatelets confined in the layer is 120 nm, the maximum

tilted angle θ equals to $\sin^{-1}(35/120)=17$ °. Following Krenchel's approach,[43, 47] we can estimate the lateral tensile modulus using equation 4:

$$E=E_m V_m+\cos^4\theta E_f V_f \quad (4)$$

where θ is the tilted angle to the flow direction, equaling to the angle to the lateral tensile load direction E_f is the tensile modulus of the graphene sheet. Krenchel's approach (equation 4) gives a value of the transverse reinforcement $(E/E_m)_{transverse}=0.86\ (E/E_m)_{axial}$, which is somewhat higher than the experimental results presented in Figure 8. Brune and Bicerano[44] solved the full tensor constitutive equations numerically and, from their graphical solution we estimate that $(E/E_m)_{transverse}=0.75\ (E/E_m)_{axial,}$ closer to the experimental result. Future work should explore the possibility that this imperfect planar orientation could be improved by combining the multilayer coextrusion with an external biaxial stretch.[18]

4.4. Conclusions

We have used forced assembly through multilayer extrusion methods to create PMMA/PS-graphene and PMMA/PMMA-graphene multilayer films. A combination of microscopic analysis of the morphology of the multilayer films and mechanical property measurements provides evidence that the reinforced layers contain oriented graphene in the direction of extrusion and partially oriented in the transverse direction. The amount of reinforcement is greater than normally reported for graphene nanocomposites and has been attributed primarily to the graphene orientation and not to the small increase in the glass transition temperature of the reinforced matrix. For the PMMA/PMMA-graphene system with 2% by weight loading of graphene in the thinnest layers (35 nm), the room temperature, flow direction tensile modulus is 2.18 times that of the neat resin while accounting for the increased T_g reduces the estimated

reinforcement to approximately 2.01 times that of the neat polymer matrix, still a significant effect. For the 40 °C data from dynamic testing the similar relative moduli are 1.86 and 1.69 for the non T_g-adjusted and T_g-adjusted values, respectively. The lateral degree of reinforcement at the same graphene loading in the PMMA/PMMA-graphene system is approximately 75 % that of the flow direction reinforcement, leaving room for improvement in the properties in the transverse direction. The results suggest that forced assembly by multilayer extrusion offers the opportunity of creating layered structures with high degrees of in-plane reinforcement and further refinements of the method should be developed.

While some of the results for the PMMA/PS-graphene are similar to those of the PMMA/PMMA-graphene system, the material is not very strong and weakens with time, possibly due to poor adhesion between the PS and the graphene and the weak interface between PMMA and PS. It has been suggested that the interface can be improved by the use of block copolymer compatibilizers to prevent delamination in this system.[32, 48]

4.5 References

1. Kim, H.; Macosko, C. W., *Morphology and Properties of Polyester/Exfoliated Graphite Nanocomposites*. *Macromolecules* **2008,** *41* (9), 3317-3327.
2. Potts, J. R.; Dreyer, D. R.; Bielawski, C. W.; Ruoff, R. S., *Graphene-based polymer nanocomposites*. *Polymer* **2011,** *52* (1), 5-25.
3. Kim, H.; Abdala, A. A.; Macosko, C. W., *Graphene/Polymer Nanocomposites*. *Macromolecules* **2010,** *43* (16), 6515-6530.
4. Potts, J. R.; Murali, S.; Zhu, Y.; Zhao, X.; Ruoff, R. S., *Microwave-Exfoliated Graphite Oxide/Polycarbonate Composites*. *Macromolecules* **2011,** *44* (16), 6488-6495.
5. Padawer, G. E.; Beecher, N., *On the strength and stiffness of planar reinforced plastic resins*. *Polymer Engineering & Science* **1970,** *10* (3), 185-192.
6. Jackson, A. P.; Vincent, J. F. V.; Turner, R. M., *A physical model of nacre*. *Compos Sci Technol* **1989,** *36* (3), 255-266.
7. Ramanathan, T.; Abdala, A. A.; Stankovich, S.; Dikin, D. A.; Herrera-Alonso, M.; Piner, R. D.; Adamson, D. H.; Schniepp, H. C.; Chen, X.; Ruoff, R. S.; Nguyen, S. T.; Aksay, I. A.; Prud'Homme, R. K.; Brinson, L. C., *Functionalized graphene sheets for polymer nanocomposites*. *Nat Nanotechnol* **2008,** *3* (6), 327-31.
8. Potts, J. R.; Lee, S. H.; Alam, T. M.; An, J.; Stoller, M. D.; Piner, R. D.; Ruoff, R. S., *Thermomechanical properties of chemically modified graphene/poly(methyl methacrylate) composites made by in situ polymerization*. *Carbon* **2011,** *49* (8), 2615-2623.
9. Li, X. G.; McKenna, G. B., *Considering Viscoelastic Micromechanics for the Reinforcement of Graphene Polymer Nanocomposites*. *ACS Macro Letters* **2012,** *1* (3), 388-391.
10. Kim, H.; Macosko, C. W., *Processing-property relationships of polycarbonate/graphene composites*. *Polymer* **2009,** *50* (15), 3797-3809.
11. Carotenuto, G.; Nicola, S. D.; Palomba, M.; Pullini, D.; Horsewell, A.; Hansen, T. W.; Nicolais, L., *Mechanical properties of low-density polyethylene filled by graphite nanoplatelets*. *Nanotechnology* **2012,** *23* (48), 485705.
12. Wu, H.; Rook, B.; Drzal, L. T., *Dispersion optimization of exfoliated graphene nanoplatelet in polyetherimide nanocomposites: Extrusion, precoating, and solid state ball milling*. *Polym Composite* **2013,** *34* (3), 426-432.
13. Lepoittevin, B.; Pantoustier, N.; Devalckenaere, M.; Alexandre, M.; Calberg, C.; Jérôme, R.; Henrist, C.; Rulmont, A.; Dubois, P., *Polymer/layered silicate nanocomposites by combined intercalative polymerization and melt intercalation: a masterbatch process*. *Polymer* **2003,** *44* (7), 2033-2040.
14. Pötschke, P.; Bhattacharyya, A. R.; Janke, A., *Carbon nanotube-filled polycarbonate composites produced by melt mixing and their use in blends with polyethylene*. *Carbon* **2004,** *42* (5–6), 965-969.
15. Liu, R. Y. F.; Bernal-Lara, T. E.; Hiltner, A.; Baer, E., *Polymer interphase materials by forced assembly*. *Macromolecules* **2005,** *38* (11), 4819-4827.
16. Ponting, M.; Hiltner, A.; Baer, E., *Polymer Nanostructures by Forced Assembly: Process, Structure, and Properties*. *Macromolecular Symposia* **2010,** *294* (1), 19-32.
17. Wang, H. P.; Keum, J. K.; Hiltner, A.; Baer, E.; Freeman, B.; Rozanski, A.; Galeski, A., *Confined Crystallization of Polyethylene Oxide in Nanolayer Assemblies*. *Science* **2009,** *323* (5915), 757-760.

18. Gupta, M.; Lin, Y.; Deans, T.; Baer, E.; Hiltner, A.; Schiraldi, D. A., *Structure and Gas Barrier Properties of Poly(propylene-graft-maleic anhydride)/Phosphate Glass Composites Prepared by Microlayer Coextrusion*. *Macromolecules* **2010,** *43* (9), 4230-4239.
19. Liu, R. Y. F.; Jin, Y.; Hiltner, A.; Baer, E., *Probing Nanoscale Polymer Interactions by Forced-Assembly*. *Macromolecular Rapid Communications* **2003,** *24* (16), 943-948.
20. Ivan'kova, E. M.; Krumova, M.; Michler, G. H.; Koets, P. P., *Morphology and toughness of coextruded PS/PMMA multilayers*. *Colloid & Polymer Science* **2004,** *282* (3), 203-208.
21. Sekelik, D. J.; Stepanov, E. V.; Nazarenko, S.; Schiraldi, D.; Hiltner, A.; Baer, E., *Oxygen barrier properties of crystallized and talc-filled poly(ethylene terephthalate)*. *J Polym Sci Pol Phys* **1999,** *37* (8), 847-857.
22. Wen, M.; Sun, X.; Su, L.; Shen, J.; Li, J.; Guo, S., *The electrical conductivity of carbon nanotube/carbon black/polypropylene composites prepared through multistage stretching extrusion*. *Polymer* **2012,** *53* (7), 1602-1610.
23. Miquelard-Garnier, G.; Guinault, A.; Fromonteil, D.; Delalande, S.; Sollogoub, C., *Dispersion of carbon nanotubes in polypropylene via multilayer coextrusion: Influence on the mechanical properties*. *Polymer* **2013,** *54* (16), 4290-4297.
24. Ania, F.; Baltá-Calleja, F. J.; Henning, S.; Khariwala, D.; Hiltner, A.; Baer, E., *Study of the multilayered nanostructure and thermal stability of PMMA/PS amorphous films*. *Polymer* **2010,** *51* (8), 1805-1811.
25. Alig, I.; Pötschke, P.; Lellinger, D.; Skipa, T.; Pegel, S.; Kasaliwal, G. R.; Villmow, T., *Establishment, morphology and properties of carbon nanotube networks in polymer melts*. *Polymer* **2012,** *53* (1), 4-28.
26. Badrinarayanan, P.; Zheng, W.; Li, Q.; Simon, S. L., *The glass transition temperature versus the fictive temperature*. *Journal of Non-Crystalline Solids* **2007,** *353* (26), 2603-2612.
27. Moynihan, C. T.; Easteal, A. J.; DeBolt, M. A., *DEPENDENCE OF THE FICTIVE TEMPERATURE OF GLASS ON COOLING RATE*. *Journal of the American Ceramic Society* **1976,** *59* (1-2), 12-16.
28. Aguilera I, P.; Gómez, C. **2011**.
29. Mori, T.; Tanaka, K., *Average stress in matrix and average elastic energy of materials with misfitting inclusions*. *Acta Metallurgica* **1973,** *21* (5), 571-574.
30. McKenna, G. B., Dynamics of Materials at the Nanoscale: Small-Molecule Liquids and Polymer Films. In *Polymer Physics*, John Wiley & Sons, Inc.: 2010; pp 191-223.
31. Koh, Y. P.; Simon, S. L., *Structural relaxation of stacked ultrathin polystyrene films*. *Journal of Polymer Science Part B: Polymer Physics* **2008,** *46* (24), 2741-2753.
32. Zhang, J.; Lodge, T. P.; MacOsko, C. W., *Interfacial slip reduces polymer-polymer adhesion during coextrusion*. *Journal of Rheology* **2006,** *50* (1), 41-57.
33. Hsieh, T. H.; Kinloch, A. J.; Taylor, A. C.; Sprenger, S., *The effect of silica nanoparticles and carbon nanotubes on the toughness of a thermosetting epoxy polymer*. *J Appl Polym Sci* **2011,** *119* (4), 2135-2142.
34. Kinloch, A. J.; Shaw, S. J.; Tod, D. A.; Hunston, D. L., *Deformation and fracture behaviour of a rubber-toughened epoxy: 1. Microstructure and fracture studies*. *Polymer* **1983,** *24* (10), 1341-1354.
35. Einstein, A. F., R. ; Cowper, A. D., *Investigations on the theory of the Brownian movement*. Courier Dover Publications: Mineola, NY, 1956.

36. Floquet, S.; Brun, S.; Lemonnier, J. F.; Henry, M.; Delsuc, M. A.; Prigent, Y.; Cadot, E.; Taulelle, F., *Molecular weights of cyclic and hollow clusters measured by DOSY NMR spectroscopy*. *Journal of the American Chemical Society* **2009,** *131* (47), 17254-17259.
37. Banchio, A. J.; Nägele, G.; Bergenholtz, J., *Viscoelasticity and generalized Stokes-Einstein relations of colloidal dispersions*. *Journal of Chemical Physics* **1999,** *111* (18), 8721-8740.
38. Voigt, W., *Ueber die Beziehung zwischen den beiden Elasticitätsconstanten isotroper Körper*. *Annalen der Physik* **1889,** *274* (12), 573-587.
39. Tandon, G. P.; Weng, G. J., *The Effect of Aspect Ratio of Inclusions on the Elastic Properties of Unidirectionally Aligned Composites*. *Polym Composite* **1984,** *5* (4), 327-333.
40. Lee, C.; Wei, X. D.; Kysar, J. W.; Hone, J., *Measurement of the elastic properties and intrinsic strength of monolayer graphene*. *Science* **2008,** *321* (5887), 385-388.
41. Cho, J.; Luo, J. J.; Daniel, I. M., *Mechanical characterization of graphite/epoxy nanocomposites by multi-scale analysis*. *Compos Sci Technol* **2007,** *67* (11–12), 2399-2407.
42. Paul, D. R.; Robeson, L. M., *Polymer nanotechnology: Nanocomposites*. *Polymer* **2008,** *49* (15), 3187-3204.
43. Galgali, G.; Agarwal, S.; Lele, A., *Effect of clay orientation on the tensile modulus of polypropylene–nanoclay composites*. *Polymer* **2004,** *45* (17), 6059-6069.
44. Brune, D. A.; Bicerano, J., *Micromechanics of nanocomposites: comparison of tensile and compressive elastic moduli, and prediction of effects of incomplete exfoliation and imperfect alignment on modulus*. *Polymer* **2002,** *43* (2), 369-387.
45. Yamamoto, S.; Matsuoka, T., *Dynamic simulation of a platelike particle dispersed system*. *Journal of Chemical Physics* **1997,** *107* (8), 3300-3308.
46. Yoon, P. J.; Fornes, T. D.; Paul, D. R., *Thermal expansion behavior of nylon 6 nanocomposites*. *Polymer* **2002,** *43* (25), 6727-6741.
47. Krenchel, H., *Fibre reinforcement*. Akademisk Forlag: Copenhagen 1964.
48. Zhang, J.; Lodge, T. P.; Macosko, C. W., *Interfacial morphology development during PS/PMMA reactive coupling*. *Macromolecules* **2005,** *38* (15), 6586-6591.

Table 4.1 Material characteristics reported by manufacturers

Master batch	Graphene concentration	Graphene source	Graphene Thickness / nm	Graphene Size / μm	Graphene Aspect Ratio A_f
Lab made PMMA/Graphene	20 wt %	ACS Materials GnP	2-10	5-10	1000-2000
Lab made PS/Graphene	20 wt %	ACS Materials GnP	2-10	5-10	1000-2000
PS/Graphene from Ovation Polymers	15 wt %	X-GnP M15	5	15	3000

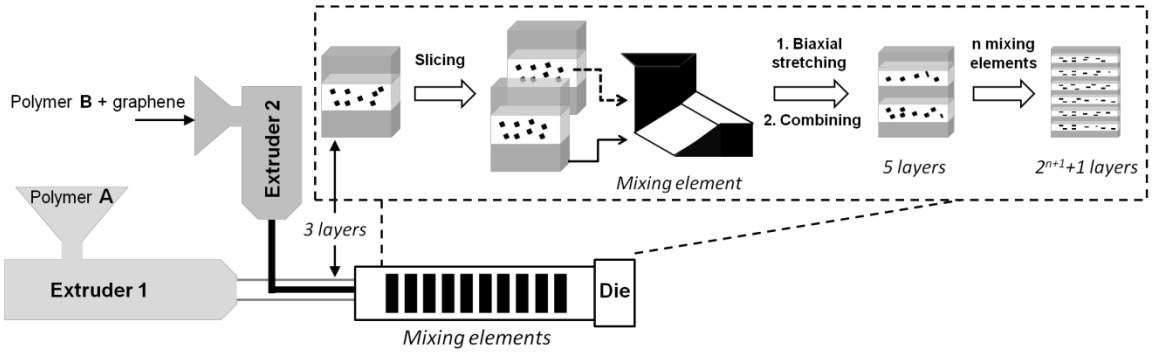

Figure 4.1 Schematic of the multilayer coextrusion process for production of multilayered polymer nanocomposites with alternating layers of unfilled polymer and polymer containing oriented graphene.

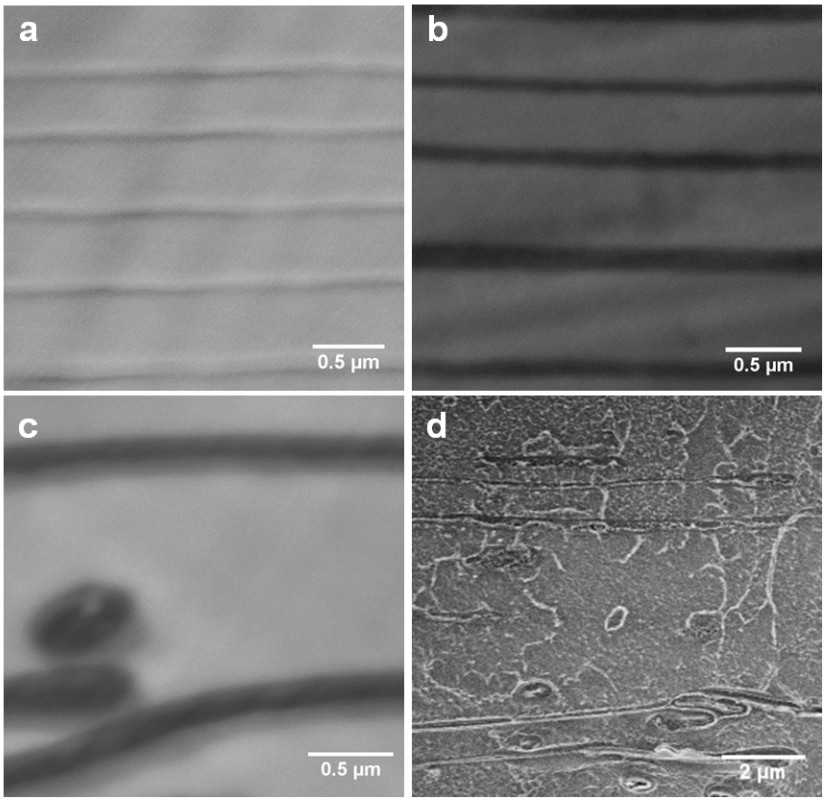

Figure 4.2 Cross section STEM images of 2049-layer PMMA/ PS filled with (a) 0 wt %; (b) 0.5 wt % graphene; (c) 2.0 wt % graphene; (d) SEM image for films with 4.0 wt % graphene (Here all films are made from the commercial graphene master-batch. The films with 4 wt % graphene were too brittle to microtome therefore they were immersed in liquid N_2 and cryogenically fractured before imaging by SEM)

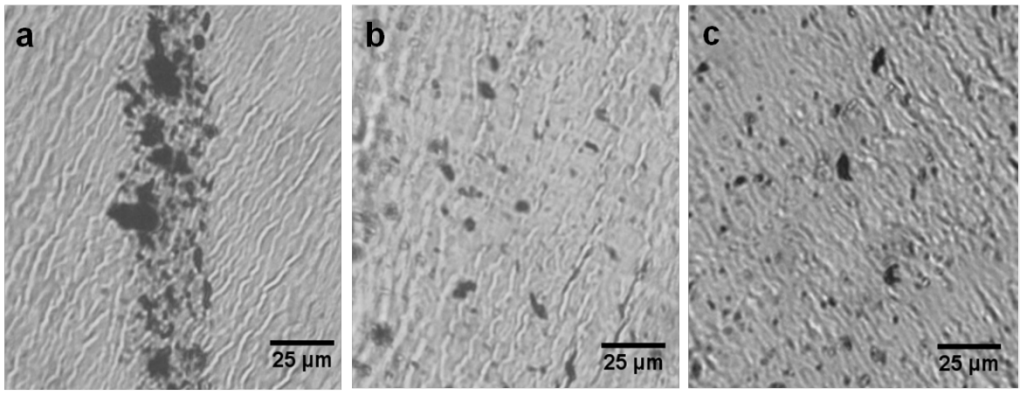

Figure 4.3 Optical images of PMMA/PMMA filled with 1 wt % graphene. (a: 3-layer, b: 129-layer and c: 2049-layer) and large aggregations fraction R

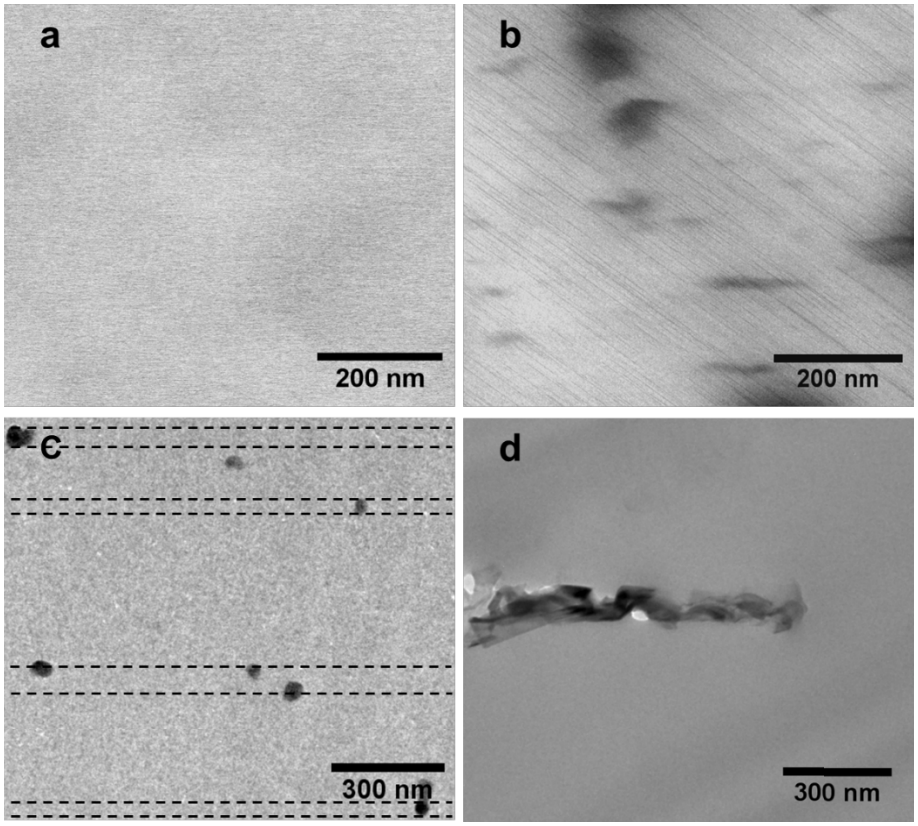

Figure 4.4 Cross section STEM images of 2049-layer PMMA/ PMMA film filled with (a) 0 wt %; (b) 1.0 wt % graphene; TEM images of 2049-layer PMMA/PMMA film filled with 2.0 wt % graphene (c) showing graphene confinement (dashed lines represent the tentative positions of the thin PMMA layers) (d) showing a single aligned graphene particle.

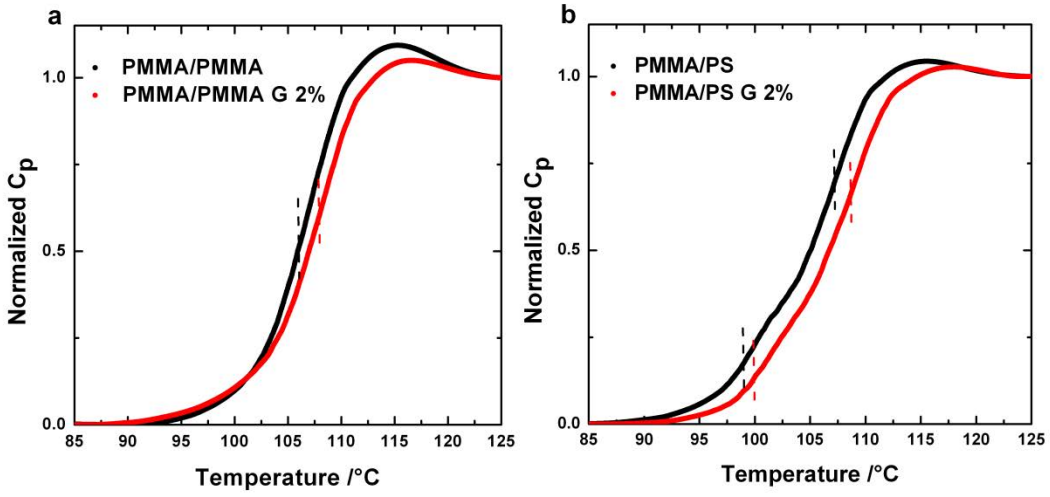

Figure 4.5 DSC results for the (a) 2049L PMMA/PMMA-graphene and (b) 2049L PMMA/PS-graphene systems. Reinforcing layers contain 2 wt % graphene.

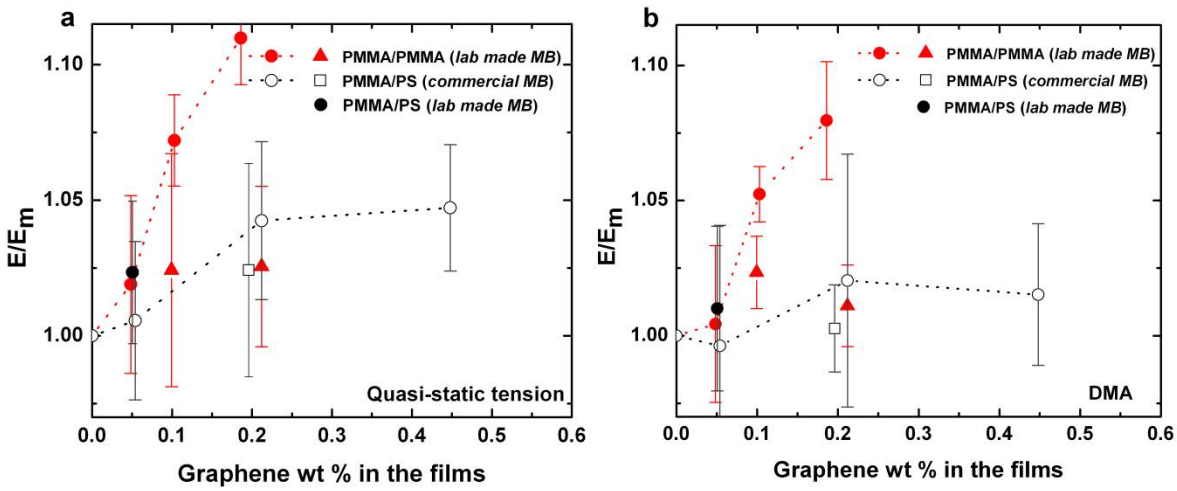

Figure 4.6 Reinforcement in the extrusion flow direction for PMMA/PMMA-graphene films and PMMA/PS-graphene films from (a) quasi-static tension tests at 23 °C and (b) DMA at 40 °C.(Circles: 2049-layer; Squares: 129-layer; Triangles: 3-layer.)

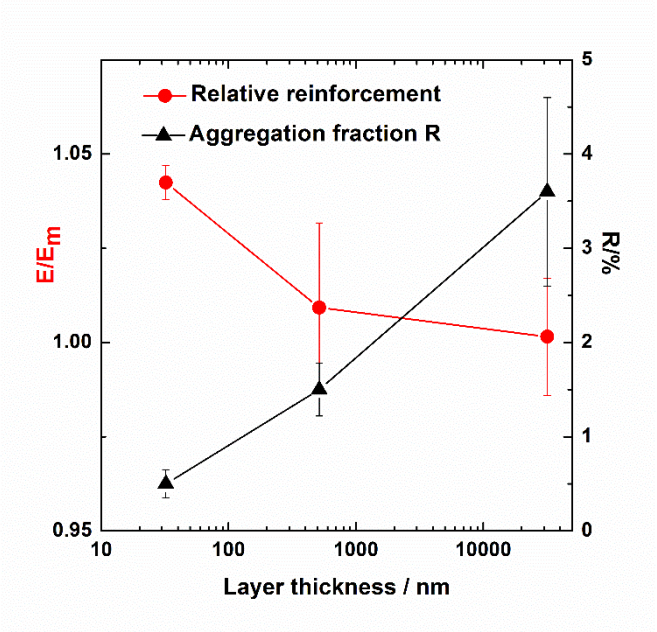

Figure 4.7 Relative reinforcement of PMMA/PMMA-1.0 wt % graphene from DMA at 40 °C and aggregation fraction R vs. layer thickness

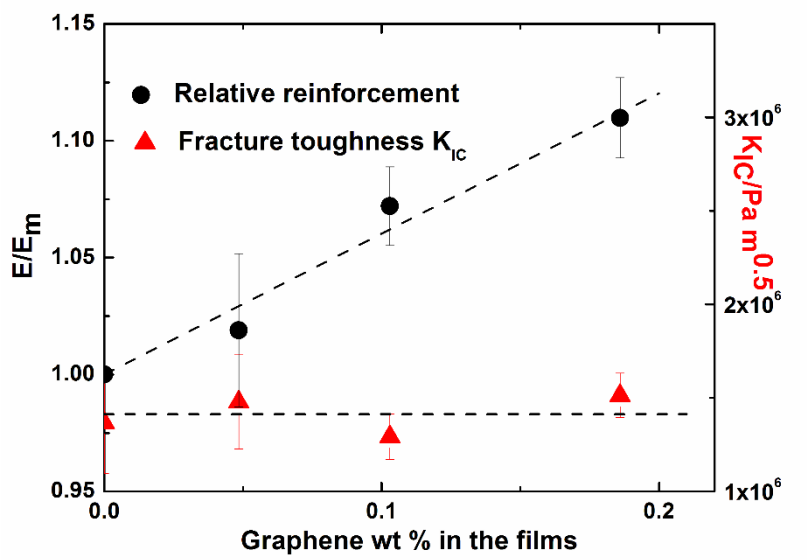

Figure 4.8 Relative reinforcement and fracture toughness K_{IC} in the extrusion flow direction for 2049L PMMA/PMMA-graphene films from quasi-static tension tests at 23 °C.

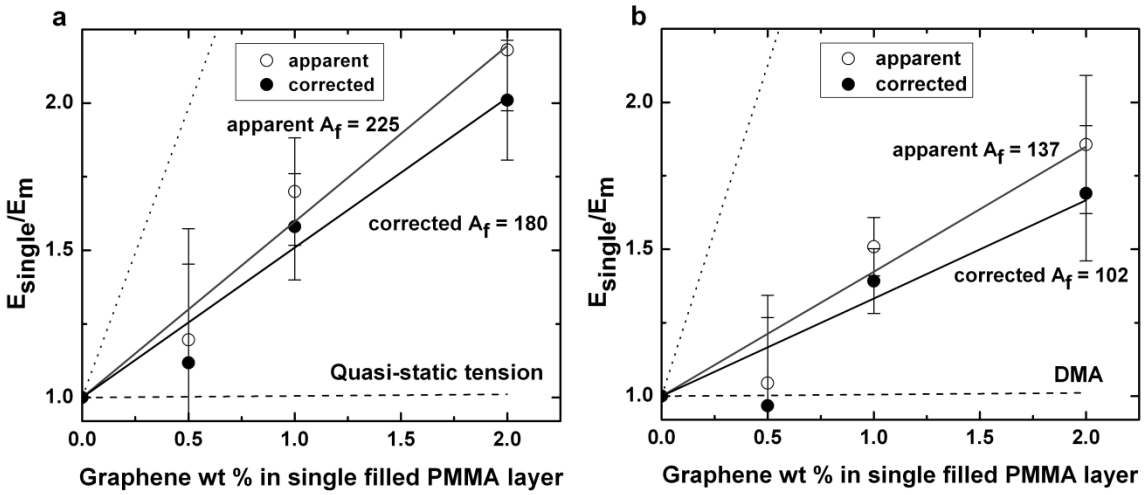

Figure 4.9 Experimental reinforcement and Mori-Tanaka calculations for the single graphene filled PMMA layers for 2049-layer PMMA/PMMA films. (Open circles: apparent reinforcement; Filled circles: corrected for changing T_g; Solid line: Mori-Tanaka prediction; Dotted line: Voigt upper bound; Dashed line: Reuss lower bound. Both of these bounds are estimated from the moduli of graphene and neat PMMA)

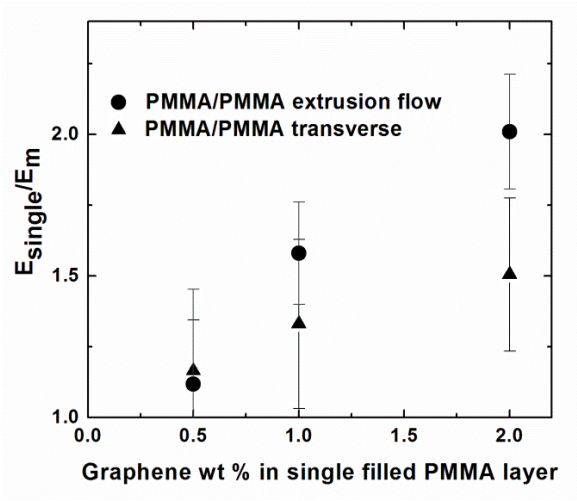

Figure 4.10 Comparison of T_g corrected reinforcements between flow and transverse directions for 2049-layer PMMA/PMMA

Chapter 5. Mechanical responses of a polymer graphene-sheet nano-sandwich

5.1 Overview and introduction

As previous chapters have shown, there has been significant interest in the reinforcement of polymer matrices by graphene over the past years.[1-3] And most of the work has focused on methods of obtaining good dispersion of the graphene in the polymer matrix[3-7]. Recently, however, there has been an attempt to understand the interfacial mechanics of single and multilayer graphene sheets in polymers using Raman spectroscopy[8-10]. In the present work we use a previously developed nano-bubble inflation method[11-15] to probe the interfacial mechanics between graphene and poly (ethyl methacrylate) (PEMA) in both its rubbery and glassy state. The method provides new information on the stiffness of a chemical vapor deposited (CVD) graphene in a novel nano-sandwich structure and provides new data related to the interfacial strength and internal stresses built up in the interface between the graphene and the polymer layers.

Young and co-workers used Raman spectroscopy to study graphene on polymeric substrates using a bending test[8-9]. Their work provided the first measurement of interfacial mechanics of a graphene/polymer system. However, Raman spectroscopy only provides indirect stress/strain responses of the graphene as a function of the beam surface strain[16-17], rather than through a direct measurement of the stress-strain responses of the graphene and the polymer matrix. Here a nano-sandwich built by layering a single CVD graphene sheet between two thin polymer films is proposed (Figure 5.1). There are three features of this unique nano-sandwich structure: first is that we can apply the nano-bubble inflation method developed in our laboratory previously[11-15] to obtain the stress-strain response of the graphene nano-sandwich directly. Hence we can probe the interfacial shear strength and internal stresses set up between the graphene and

the polymer matrix. Second is that single sheet, large-area CVD graphene[18-19] (graphene created by chemical vapor deposition, the area is > 1 x 1 mm^2) can be incorporated between the planes of two ultrathin polymer layers. The graphene reinforcing element has a large aspect ratio (A_f = length / thickness). Therefore the designed structure can also be used to estimate the properties of the CVD graphene.[20] In addition, we can use the nano-bubble inflation method at a temperature above the glass transition temperature of the polymer. In the previous Raman spectroscopy-based works[8-10] the polymer was in the glassy state.

Recently, Raman spectroscopy has been incorporated with the bulge test to monitor the biaxial strain of graphene bubbles.[21-22] However, to the best of our knowledge, the nano-bubble inflation or bulge testing methods have not been exploited to study such a nano-sandwich model composite as that investigated in the present work. Here we have applied the nano-bubble inflation method to obtain the mechanical response of the nano-sandwich as a function of inflating pressure. From the measured stress-strain behavior of the nano-sandwich we then extracted the interfacial shear strength and the internal stress built up between the graphene and polymer matrix, as well as the stiffness of the CVD graphene sheet.

5.2 Experiments

5.2.1 Materials:

Single layer CVD graphene sheets grown on copper foils were purchased from Graphene Laboratories, Inc, and characterized by micro-Raman spectroscopy. The measurements were performed using a Bruker Senterra dispersive Raman microscope spectrometer equipped with a 532 nm laser, and Figure 5.2a shows the Raman spectrum of a single layer CVD graphene transferred from the copper foil to a silicon wafer. The ratio of the integrated intensity of the 2D

peak to that of the G peak is greater than two, which suggests that the CVD graphene is single layer.[23] Furthermore, the defect density estimated from the ratio of $I_D/I_G < 0.3$ is low, and this confirms the quality of graphene. Poly(ethyl methacrylate) was purchased from Sigma Aldrich (PEMA, T_g = 65°C, M_w = 515 k, PDI = 1.52). Iron(III) chloride ($FeCl_3$) was purchased from Sigma Aldrich(sublimed grade, ≥ 99.9%).

5.2.2 Methods:

The method used to create the graphene nano-sandwiches has been developed in our laboratory. In Figure 5.3 we show schematically how we have used our expertise in polymer thin films and combined it with a recently reported transfer method for large-area CVD graphene[18-19, 23]. Each PEMA/toluene solution (0.8 % - 1.6 %, w/w) was spin coated onto the graphene side of a graphene/copper foil system at a speed of 2000 rpm for 30 s. The copper foil was then etched away using a 1M aqueous solution of $FeCl_3$ for 16 h. The PEMA/graphene bi-layer was then rinsed with deionized water. Another PEMA film of the same thickness was spin cast from toluene solution onto freshly cleaved mica sheets at the same condition, and was allowed to dry for 30 minutes at room temperature. The edges of the film were scraped off of the mica and the film was floated onto the water surface and lifted onto a clean silicon nitride filter template into which arrays of through-channels with a diameter of 10 μm have been etched (Aquamarijn Micro Filtration B. V.). This template (supporting the PEMA ultrathin layer) was then used to lift the PEMA/graphene stack from the water surface to create the nano-sandwich. The nano-sandwich structure was dried in a desiccator overnight and annealed at 80 °C for 15 mins to bond the film to the template surface. Film thicknesses were determined by the concentration of PEMA/toluene solution, and measured with an atomic force microscope (AFM) (Agilent SPM5500) as the step height across the score marks made on the template edges.[12] The

PEMA/Graphene/PEMA nano-sandwich was also transferred to a silicon wafer and characterized by micro-Raman spectroscopy. Figure 5.2b shows the Raman spectra of neat PEMA and a PEMA/Graphene/PEMA nano-sandwich. Although some of the peaks of PEMA overlap with that of graphene, the 2D peak of graphene is readily observed in the PEMA/Graphene/PEMA nano-sandwich, consistent with the high quality of the graphene as shown in Figure 5.2a.

The TTU nano-bubble inflation methods have been described thoroughly in prior works.[12-13] The filter template holding the nano-sandwich was mounted in a custom pressure cell using the adhesive and pressurized dry air was applied below the filter template to inflate the sample films into bubbles, and the AFM was used to measure the bubble profile. The AFM was operated in intermittent contact mode and the scan area was $40 \times 40\ \mu m^2$. The scan rate was 1.1 lines/ second.

5.3. Results and Discussion

5.3.1. Mechanical study of the graphene nano-sandwich

Figures 5.4a and 5.4b show the three-dimensional AFM images and center-line profiles of both PEMA bilayer and graphene reinforced nano-sandwich bubbles as a function of pressure. The main feature observed in Figure 5.4 is that the heights of the graphene nano-sandwich bubbles are significantly lower than those of the PEMA bilayer bubbles of the same thickness. This is a result of the graphene sheet reinforcing (stiffening) the nano-sandwich system. We also remark here that the measurements at 80 °C are above the glass transition temperature of the PEMA polymer, i.e., the polymer is in the rubbery state. It is also interesting to observe that only the neat PEMA bubbles show “dips” at the hole or channel boundaries. The reason is that for neat PEMA films the boundaries of the bubbles are below the template surface due to capillary

effects which pull the films approximately 100 nm into the channel during the previous annealing stage. However, due to the high graphene modulus, the nano-sandwich is too stiff to be pulled into the channel upon annealing.

To obtain the stress-strain response of the graphene nano-sandwich and investigate the interfacial mechanics of the single graphene layer in the PEMA, the biaxial strain of the bubbles as a function of pressure was obtained from their profiles. Since the present experiments were performed for bubble deflections larger than three times the film thickness (membrane limit[24]), the bubble deformation is dominated by the stretching stress of the membrane and the bending contribution is negligible[13]. In this case, following the analysis methods described previously[11-14], the radius of curvature R of the inflated bubble is calculated by fitting the bubble profile data to the equation of a circle:

$$R^2 = (x-a)^2 + (y-b)^2 \quad \textbf{(1)}$$

Where x and y are the x-position and height data, and a and b are offset constants for a circle not centered on the coordinate axes. The stress σ is related to the pressure P, the film thickness t_0 and the radius of curvature R of the bubble as Equation 2.

$$\sigma_{11} = \sigma_{22} = \frac{PR}{2t_0} \quad \textbf{(2)}$$

The biaxial strain $\varepsilon_{11}=\varepsilon_{22}$ at the pole of the bubbles is related to the geometry of the bubble by Equation 3 and 4,[11-12]

$$\varepsilon_{11} = \varepsilon_{22} = \frac{s}{2R_0} - 1 \quad \textbf{(3)}$$

$$s = 2R \sin^{-1}\left({R_0}/{R}\right) \quad \textbf{(4)}$$

where R_0 is hole radius and s is the segment length of the bubble. The total stress σ_{total} in the bubble is the sum of the elastic stress and pre-stress σ_0 (the stress at zero pressure, e.g. surface stress and residual stress) as given in Equation 5.[14]

$$\sigma_{total} = \sigma_{11} = E_{biax}\varepsilon_{11} + \sigma_0 \quad \textbf{(5)}$$

Therefore, a plot of σ_{total} versus ε_{11} should be a straight line and the biaxial modulus E_{biax} and pre-stress σ_0 can be obtained as the slope and intercept, respectively. In Figure 5.5a, we observe that the stress-strain curves of the graphene nano-sandwich systems show greater stiffness than do the neat PEMA films. These results show that in the rubbery state, the interfacial stress transfer between the graphene and PEMA is sufficient to achieve good stiffness reinforcement.

Since large-area CVD graphene is used in the nano-sandwiches, the aspect ratio A_f of the graphene is extremely large. Assuming good stress transfer between the graphene and polymer layers,[20] we used the Voigt upper bound mixing rule[25] to estimate the modulus of the graphene sheet by fitting the results for the nano-sandwich stress-strain information of Figure 5.5a using Equation 6.[20]

$$E_{biax} = E_g V_g + E_m V_m \quad \textbf{(6)}$$

Here V is the volume fraction of the relevant component; the subscripts g and m are for the graphene and the polymer matrix, respectively. The graphene volume fraction V_g is obtained from the ratio of the graphene thickness to that of the full nano-sandwich structure, that is, 0.34 nm/ total thickness. It is noteworthy that we also observe that the stiffness of the neat PEMA thin films increases with decreasing thickness. Similar results have also been reported for poly(vinyl acetate) (PVAc)[11, 26], polystyrene (PS)[26], poly(n-butyl methacrylate)[14], polycarbonate (PC),[15] and a segmented polyurethane[27] in the rubbery state. The slope α obtained from the linear fit of log

PEMA modulus vs. log thickness is α = -1.3, indicating a stiffening that is close to that of the polyurethane(α = -1.2)[27] and larger than that of the poly(n-butyl methacrylate)(α = -0.83)[14]. The PVAc, PS and PC all showed α values close to -2.0.

In Figure 5.5b, when a single layer of graphene is confined in the 69+69 nm thick PEMA bilayer (corresponding to 0.25 vol %), the biaxial modulus of the nano-sandwich increases from the 32.0 MPa for the neat resin films to 1.49 GPa. When the thickness of the PEMA layers decreases to 33+33 nm, the volume fraction of the graphene increases to 0.52 % and the biaxial modulus of the nano-sandwich increases from the 68.7 MPa of the neat resin (stiffer than 69+69 nm thick PEMA bilayer due to the rubbery stiffening we reported previously[14, 26-27]) to 3.22 GPa. By fitting these results with the Voigt upper bound (Equation 6), the biaxial modulus of the CVD graphene is obtained as 608 GPa. We then calculate the Young's modulus of the CVD graphene using Equation 7.

$$E = E_{biax}(1 - \nu) \quad \textbf{(7)}$$

Using a Poisson's ratio of ν=0.16[28], the Young's modulus of CVD graphene is found to be 511 GPa. Of interest is that recent work has shown that there are wrinkles in CVD graphene, which lower its Young's modulus to between 250 and 550 GPa [29-30], compared to the pristine graphene which has a reported Young's modulus of 1060 GPa.[31] The Young's modulus obtained in the present work is at the upper end of the results for CVD graphene.

The mechanical responses of graphene nano-sandwich with glassy PEMA layer has been also studied using nanobubble inflation method and similar results of AFM profiles were obtained (Figure 5.6a). In Figure 5.6b, stress-strain responses of 68~70 nm thick PEMA/Graphene/PEMA nano-sandwich were obtained at 35 °C and the biaxial modulus of the nano-sandwich increases from the 1.24 GPa of the neat resin films to 4.34 GPa. Therefore a

significant reinforcement of 250 % with 0.5 vol % loading of graphene has been observed for single graphene on glassy PEMA. Compared to the reinforcement of oriented graphene nanoplatelet in the filled PMMA layers in Chapter 4, here the reinforcement is much higher and reach the Voigt upper bound[32], because of the large aspect ratio of CVD graphene.

5.3.2. Interfacial mechanics between graphene and PEMA

The nano-bubble inflation method also provides a means to study the stress-strain behavior of the graphene nano-sandwich beyond the linear regime to investigate the interfacial mechanics of the graphene in PEMA. Figure 5.7a shows there is an interesting "yield-like" or instability phenomenon which occurs. For the single layer graphene confined in the bilayer PEMA (34+34 nm) at 80 °C, when the strain is below approximately 0.18 %, the stress increases linearly with the strain. The composite biaxial modulus E_{biax} is approximately 3.0 GPa. As the strain approaches 0.18 %, the stress goes through a maximum and drops sharply with increasing strain. It then increases with the strain but with a much smaller slope showing a biaxial modulus of around 0.2 GPa. Due to the experimental limitations for the stepwise pressure change loading procedure used in this work, the precise "yield" point is very difficult to obtain. If we assume the "yield" occurs near the peak obtained, the "yield" strain is estimated to be 0.18 %. In Figure 5.7b, similar "yield-like" phenomenon is also observed for graphene confined between glassy PEMA at 35 °C, with a critical strain around 0.23 %.

One reasonable explanation for this "yield-like" phenomenon is that there is a critical strain ε_c for interfacial slip between the graphene and the PEMA. Young and co-workers reported that above a critical strain, the atomically smooth interface between graphene and the glassy polymer is broken.[8] Therefore there is no longer sufficient interfacial stress transfer to reinforce the PEMA and a maximum in the stress is observed.

Shear lag theory has been used to analyze the interface behavior for fibers[33] and platelets[34-35] in polymer matrices. Recently, the interfacial strength between graphene and a glassy polymer matrix was estimated using shear lag theory[8, 10, 20]. Here we use the shear lag analysis and, first, calculate the strain in the graphene ε_g from the strain in the polymer matrix ε_m and the graphene aspect ratio A_f using Equations 8, and 9.[10, 20]

$$\varepsilon_g = \varepsilon_m\left(1 - \frac{\cosh(nA_f\frac{x}{l})}{\cosh(0.5nA_f)}\right) \quad \textbf{(8)}$$

$$n = \sqrt{\frac{2G_m}{E_{biax\,g}}\frac{t}{t_0}} \quad \textbf{(9)}$$

Where n is calculated from the shear modulus of the polymer matrix G_m, thickness ratio of graphene and polymer layer t/t_0, and biaxial modulus of graphene $E_{biax\,g}$. l is the length of graphene sheet and x is the position. The interfacial shear stress τ is given by Equation 10.[10, 20]

$$\tau = nE_{biax\,g}\varepsilon_m\frac{\sinh(nA_f\frac{x}{l})}{\cosh(0.5nA_f)} \quad \textbf{(10)}$$

$$G_m = \frac{E_{biax\,m}(1-\nu_m)}{2(1+\nu_m)} \quad \textbf{(11)}$$

Young and co-workers used shear lag analysis to study the interface of the graphene with free edges supported by a polymer beam[8], but in the nano-sandwich structure, there is no free edge for a CVD graphene sheet confined between two PEMA layers suspended on the template holes. However, when the nano-sandwich is inflated, due to the ridges and defect lines ("grain boundaries") on the CVD graphene sheet,[29, 36] there are some "weak points" between the graphene and the polymer, which would debond. This would effectively create "free edges" where the structure of the interface can be treated using the shear lag analysis. Since there are more ridges around the hole edge and the distance between the defect lines ("grain boundaries") on the CVD graphene have been reported to be between 500 nm and 4 μm,[36] we can estimate the

distance between the debonding points on the CVD graphene sheet as being between 500 nm and 10 μm (hole diameter), therefore the effective aspect ratio A_f would be approximately 1500~30000 (the distance between the debonding points / graphene thickness). Upon calculating the interfacial shear stress of the graphene nano-sandwich as a function of aspect ratio using equation 10, we find that the maximum shear stress at the "free edges" (x/l=0.5) is between 3.08 MPa and 2.87 MPa when the aspect ratio A_f is between 1500 and 30000. Therefore, using the $A_{f\,max} \cong 30000$, we obtain an upper bound for the interfacial shear strength between graphene and PEMA.[10]

For the stress-strain results shown in Figure 5.7a, we used the experimental value of $E_{biax\,m}$ = 68.7 MPa and assume a rubbery Poisson's ratio ν_m = 0.5 to obtain the G_m from Equation 11. Then we use our experimental value of $E_{biax\,g}$= 608 GPa, the just determined G_m =11.45 MPa and an aspect ratio $A_{f\,max}$ of 30000 for the 68 nm thick nano-sandwich. Figure 5.8a shows the plot of strain ratio $\varepsilon_g/\ \varepsilon_m$ and interfacial shear stress τ at a matrix strain of 0.18 % as a function of position along the graphene sheet between debonding points ("free edges"). We see that the maximum strain in the graphene is at the center of (x/l=0) and the maximum interfacial shear stress occurs at the "free edges" (x/l=0.5). When the strain reaches 0.18 %, the interfacial shear stress reaches a critical value and interfacial slip or failure occurs. At the critical matrix strain of 0.18 %, the shear stress maximum of 0.48 MPa provides an estimate of a upper bound of the interfacial shear strength between graphene and rubbery PEMA.[10]

In Figure 5.7b, when graphene is confined by two glassy PEMA layers, we used the experimental value of $E_{biax\,m}$ = 1.24 GPa and assume a glassy Poisson's ratio ν_m = 0.34 to obtain the G_m from Equation 11. Then we use our experimental value of $E_{biax\,g}$= 608 GPa, the just determined G_m =305 MPa and an aspect ratio $A_{f\,max}$ of 30000 in the shear lag analysis. The upper

bound of the interfacial shear strength between graphene and glassy PEMA is estimated as 3.08 MPa, at the critical matrix strain of 0.23 % (Figure 5.8b). This value of interfacial shear strength is close to the value reported by Young and co-workers(2.3 MPa for graphene and glassy PMMA)[8]. It is found that both the value of critical strain and interfacial shear strength for graphene and rubbery PEMA are lower than those of graphene and glassy PEMA. A plausible reason is that the graphene/rubbery PEMA interface is weaker than the interface between graphene and glassy PEMA.[37] This explanation is consistent with Gent's work on peeling polymer thin layers off of rigid substrates to test the different interface strengths of glassy and rubbery polymers.[38-39] He reported that the peel strength is higher at high peeling rates and increases as temperature decreases through the glass transition. Gent attributed the different behaviors to the rubber showing lower adhesive fracture energies than the glass.[38-39]

The results for the "yield" in the stress-strain curves of the nano-sandwich can help achieve a better understanding of the reinforcement mechanism of graphene in a polymer matrix. Brinson and co-workers[2] proposed that strong interactions between graphene and the polymer, e.g. hydrogen bonding, are important to achieve high reinforcement, which is supported by their work on a graphene oxide/PMMA system. However, Young and co-workers[8, 20] observed that even without strong interactions, the moderate adhesion that resulted simply from Van der Waals forces between graphene and the polymer matrix provides sufficient interfacial stress transfer to achieve high stiffening at small strains. In the graphene nano-sandwich studied here, even though there are no hydrogen bonds between the CVD graphene sheet and the PEMA, a large stiffness reinforcement is observed below the critical strain ε_c, supporting the opinion of Young and co-workers[8, 20] that significant stiffening can occur in graphene nanocomposites without strong (hydrogen bonding) interactions with the polymer matrix. On the other hand, the full

mechanical performance of graphene (and other) nanocomposites may depend in a complex manner on the interactions between graphene (particle) and polymer matrices to achieve a good balance between strength and toughness.[40-41]

5.3.3. Internal residual stress

The stress-strain curves obtained for the nano-sandwich structure not only give the biaxial modulus E_{biax} as the slope, but also give a pre-stress σ_0 (the stress at zero pressure) as the intercept. And the residual stress σ_r built up between the graphene and the PEMA faces can be obtained from the pre-stress σ_0 by considering both the pre-stress and the PEMA/air surface tension contribution. As shown in Equation 12[27],

$$\sigma_r = \sigma_0 - \frac{2\gamma_p}{t_0} \quad \textbf{(12)}$$

where γ_p and t_0 are the surface tension and thickness of the PEMA layers, the residual stress σ_r is then calculated by subtracting the external surface tension of the PEMA in air from the pre-stress σ_0. Since previous work[14, 27, 42] shows that the surface tension of polymer films is independent of film thickness, the surface tension of the PEMA in air was taken as the macroscopic value (44.9 mN/m) from the intercept of the stress-strain curve for the 140 nm thick PEMA films. In Figure 5.9, the residual stress σ_r of the 68 nm thick nano-sandwich is approximately -0.54 MPa at 80 °C.

The internal residual stress σ_r set up between the graphene layer and the PEMA faces can be estimated from the spreading parameter S[43] and compared with the experimental results that give the residual stress and the surface tension contribution as described above. A positive spreading parameter (S=6.87 mN/m) is obtained using Equation 12[43-44],

$$S = \gamma_G - \gamma_{GP} - \gamma_P \quad \textbf{(12)}$$

where γ is the surface energy of the components, the subscripts *G*, *P* and *GP* are for the graphene in air, the PEMA in air, and the interfacial energy between graphene and the PEMA. Here γ_G is equal to 54.8 mN/m[45], γ_P is equal to 44.9 mN/m, and γ_{GP} is equal to 3.03 mN/m[46]. (Due to the lack of data for the interfacial energy γ_{GP} between graphene and PEMA, here we use the reported value for carbon nanotubes and PMMA[46]) Therefore the PEMA is estimated to wet on the graphene and the spreading stress σ_s to cause the PEMA to wet on the graphene can be calculated using Equation 13,[47]

$$\sigma_s = 2\frac{S}{t_0/2} \tag{13}$$

where t_0 is the thickness of the nano-sandwich. Since the wetting of the PEMA on the graphene is constrained by the wrinkles of the CVD graphene, a residual stress σ_r equal to the negative of the spreading stress σ_s is estimated to build up between the graphene and the PEMA faces. In Figure 5.9, we compare values for σ_r estimated from σ_s with the experimental results in which the measured value of σ_0 and the surface tension stress are used to determine σ_r. For the 68 nm thick nano-sandwich, the experimental residual stress σ_r is close to the σ_r estimated from the spreading parameter. But for the 138 nm thick nano-sandwich, the experimental σ_r is greater in magnitude than the estimated σ_r. Hence, other factors than the spreading parameter and interfacial tensions may be playing a role in the residual stress development. Also graphene has a negative thermal expansion coefficient[40] and creation of the graphene nano-sandwich at room temperature and measurement at 80 °C can also introduce residual stresses due to the mismatch of thermal expansion between the graphene and PEMA. However, the system is annealed at 80 °C, which should mitigate these stresses.

5.4 Conclusions

We have created a novel nano-sandwich structure made of thin PEMA layer /single layer CVD graphene/ thin PEMA layer, and have applied a nano-bubble inflation method to obtain the interfacial mechanical response. Significant mechanical (stiffness) reinforcement has been observed at small strains in both the rubbery and glassy states of the PEMA and the results were used to estimate the stiffness of the large area, single sheet, CVD graphene. At larger, but still small, strains, a critical strain for a "yield-like" or instability phenomenon was observed and has been interpreted to be due to interfacial slip. A shear lag analysis shows that the interfacial shear strength between the CVD graphene and the rubbery PEMA is lower than that between the CVD graphene and glassy PEMA. The nano-bubble inflation method can also provide a measurement of the internal residual stress set up between graphene and rubbery PEMA faces, although different from the estimation from the spreading parameter for thicker films. In the future, the technique has the potential to be used to study other 2-D plate-like nanoparticles, e.g. hexagonal boron nitride[48], confined in polymer matrices. The interfacial mechanics of graphene / functional polymers can also be studied with this technique, and could be useful in other applications such as flexible electronics.[49]

5.5 References:

1. Kim, H.; Abdala, A. A.; Macosko, C. W., *Graphene/Polymer Nanocomposites*. *Macromolecules* **2010,** *43* (16), 6515-6530.
2. Ramanathan, T.; Abdala, A. A.; Stankovich, S.; Dikin, D. A.; Herrera-Alonso, M.; Piner, R. D.; Adamson, D. H.; Schniepp, H. C.; Chen, X.; Ruoff, R. S.; Nguyen, S. T.; Aksay, I. A.; Prud'Homme, R. K.; Brinson, L. C., *Functionalized graphene sheets for polymer nanocomposites*. *Nat Nanotechnol* **2008,** *3* (6), 327-31.
3. Potts, J. R.; Lee, S. H.; Alam, T. M.; An, J.; Stoller, M. D.; Piner, R. D.; Ruoff, R. S., *Thermomechanical properties of chemically modified graphene/poly(methyl methacrylate) composites made by in situ polymerization*. *Carbon* **2011,** *49* (8), 2615-2623.
4. Kim, H.; Macosko, C. W., *Processing-property relationships of polycarbonate/graphene composites*. *Polymer* **2009,** *50* (15), 3797-3809.
5. Li, X. G.; McKenna, G. B., *Considering Viscoelastic Micromechanics for the Reinforcement of Graphene Polymer Nanocomposites*. *ACS Macro Letters* **2012,** *1* (3), 388-391.
6. Wu, H.; Rook, B.; Drzal, L. T., *Dispersion optimization of exfoliated graphene nanoplatelet in polyetherimide nanocomposites: Extrusion, precoating, and solid state ball milling*. *Polym Composite* **2013,** *34* (3), 426-432.
7. Li, X.; McKenna, G. B.; Miquelard-Garnier, G.; Guinault, A.; Sollogoub, C.; Regnier, G.; Rozanski, A., *Forced assembly by multilayer coextrusion to create oriented graphene reinforced polymer nanocomposites*. *Polymer* **2014,** *55* (1), 248-257.
8. Gong, L.; Kinloch, I. A.; Young, R. J.; Riaz, I.; Jalil, R.; Novoselov, K. S., *Interfacial Stress Transfer in a Graphene Monolayer Nanocomposite*. *Adv Mater* **2010,** *22* (24), 2694.
9. Young, R. J.; Gong, L.; Kinloch, I. A.; Riaz, I.; Jalil, R.; Novoselov, K. S., *Strain Mapping in a Graphene Monolayer Nanocomposite*. *ACS Nano* **2011,** *5* (4), 3079-3084.
10. Jiang, T.; Huang, R.; Zhu, Y., *Interfacial Sliding and Buckling of Monolayer Graphene on a Stretchable Substrate*. *Advanced Functional Materials* **2014,** *24* (3), 396-402.
11. O'Connell, P. A.; McKenna, G. B., *Rheological measurements of the thermoviscoetastic response of ultrathin polymer films (vol 307, pg 1760, 2005)*. *Science* **2005,** *310* (5753), 1431-1431.
12. O'Connell, P. A.; McKenna, G. B., *Novel nanobubble inflation method for determining the viscoelastic properties of ultrathin polymer films*. *Rev Sci Instrum* **2007,** *78* (1), 013901.
13. O'Connell, P. A.; McKenna, G. B., *A novel nano-bubble inflation method for determining the viscoelastic properties of ultrathin polymer films*. *Scanning* **2008,** *30* (2), 184-196.
14. Xu, S.; O'Connell, P. A.; McKenna, G. B., *Unusual elastic behavior of ultrathin polymer films: Confinement-induced/molecular stiffening and surface tension effects*. *The Journal of Chemical Physics* **2010,** *132* (18), 184902.
15. O'Connell, P. A.; Wang, J.; Ishola, T. A.; McKenna, G. B., *Exceptional Property Changes in Ultrathin Films of Polycarbonate: Glass Temperature, Rubbery Stiffening, and Flow*. *Macromolecules* **2012,** *45* (5), 2453-2459.
16. Frank, O.; Mohr, M.; Maultzsch, J.; Thomsen, C.; Riaz, I.; Jalil, R.; Novoselov, K. S.; Tsoukleri, G.; Parthenios, J.; Papagelis, K.; Kavan, L.; Galiotis, C., *Raman 2D-Band Splitting in Graphene: Theory and Experiment*. *ACS Nano* **2011,** *5* (3), 2231-2239.
17. Frank, O.; Tsoukleri, G.; Riaz, I.; Papagelis, K.; Parthenios, J.; Ferrari, A. C.; Geim, A. K.; Novoselov, K. S.; Galiotis, C., *Development of a universal stress sensor for graphene and carbon fibres*. *Nature Communications* **2011,** *2*, 255.

18. Li, X. S.; Cai, W. W.; An, J. H.; Kim, S.; Nah, J.; Yang, D. X.; Piner, R.; Velamakanni, A.; Jung, I.; Tutuc, E.; Banerjee, S. K.; Colombo, L.; Ruoff, R. S., *Large-Area Synthesis of High-Quality and Uniform Graphene Films on Copper Foils*. *Science* **2009,** *324* (5932), 1312-1314.
19. Li, X. S.; Zhu, Y. W.; Cai, W. W.; Borysiak, M.; Han, B. Y.; Chen, D.; Piner, R. D.; Colombo, L.; Ruoff, R. S., *Transfer of Large-Area Graphene Films for High-Performance Transparent Conductive Electrodes*. *Nano Lett* **2009,** *9* (12), 4359-4363.
20. Young, R. J.; Kinloch, I. A.; Gong, L.; Novoselov, K. S., *The mechanics of graphene nanocomposites: A review*. *Compos Sci Technol* **2012,** *72* (12), 1459-1476.
21. Lee, J. U.; Yoon, D.; Cheong, H., *Estimation of Young's modulus of graphene by Raman spectroscopy*. *Nano Lett* **2012,** *12* (9), 4444-8.
22. Zabel, J.; Nair, R. R.; Ott, A.; Georgiou, T.; Geim, A. K.; Novoselov, K. S.; Casiraghi, C., *Raman spectroscopy of graphene and bilayer under biaxial strain: bubbles and balloons*. *Nano Lett* **2012,** *12* (2), 617-21.
23. Wang, Y. Y.; Burke, P. J., *A large-area and contamination-free graphene transistor for liquid-gated sensing applications*. *Appl Phys Lett* **2013,** *103* (5).
24. Timoshenko, S. P.; Woinowsky-Krieger, S., *Theory of Plates and Shells*. McGraw-Hill: New York, 1969.
25. Liu, B.; Feng, X.; Zhang, S. M., *The effective Young's modulus of composites beyond the Voigt estimation due to the Poisson effect*. *Compos Sci Technol* **2009,** *69* (13), 2198-2204.
26. O'Connell, P. A.; McKenna, G. B., *Dramatic stiffening of ultrathin polymer films in the rubbery regime*. *The European physical journal. E, Soft matter* **2006,** *20* (2), 143-50.
27. Zhai, M.; McKenna, G. B., *Elastic modulus and surface tension of a polyurethane rubber in nanometer thick films*. *Polymer* **2014** *55*, 2725-2733.
28. Blakslee, O. L., *Elastic Constants of Compression-Annealed Pyrolytic Graphite*. *Journal of Applied Physics* **1970,** *41* (8), 3373.
29. Ruiz-Vargas, C. S.; Zhuang, H. L.; Huang, P. Y.; van der Zande, A. M.; Garg, S.; McEuen, P. L.; Muller, D. A.; Hennig, R. G.; Park, J., *Softened elastic response and unzipping in chemical vapor deposition graphene membranes*. *Nano Lett* **2011,** *11* (6), 2259-63.
30. Lin, Q. Y.; Jing, G.; Zhou, Y. B.; Wang, Y. F.; Meng, J.; Bie, Y. Q.; Yu, D. P.; Liao, Z. M., *Stretch-Induced Stiffness Enhancement of Graphene Grown by Chemical Vapor Deposition*. *ACS Nano* **2013,** *7* (2), 1171-1177.
31. Lee, C.; Wei, X. D.; Kysar, J. W.; Hone, J., *Measurement of the elastic properties and intrinsic strength of monolayer graphene*. *Science* **2008,** *321* (5887), 385-388.
32. Voigt, W., *Ueber die Beziehung zwischen den beiden Elasticitätsconstanten isotroper Körper*. *Annalen der Physik* **1889,** *274* (12), 573-587.
33. Cox, H. L., *The elasticity and strength of paper and other fibrous materials British Journal of Applied Physics* **1952,** *3*, 72-79.
34. Kotha, S. P.; Kotha, S.; Guzelsu, N., *A shear-lag model to account for interaction effects between inclusions in composites reinforced with rectangular platelets*. *Compos Sci Technol* **2000,** *60* (11), 2147-2158.
35. Tsai, J.; Sun, C. T., *Effect of Platelet Dispersion on the Load Transfer Efficiency in Nanoclay Composites*. *Journal of Composite Materials* **2004,** *38* (7), 567-579.
36. Huang, P. Y.; Ruiz-Vargas, C. S.; van der Zande, A. M.; Whitney, W. S.; Levendorf, M. P.; Kevek, J. W.; Garg, S.; Alden, J. S.; Hustedt, C. J.; Zhu, Y.; Park, J.; McEuen, P. L.; Muller, D. A., *Grains and grain boundaries in single-layer graphene atomic patchwork quilts*. *Nature* **2011,** *469* (7330), 389-92.

37. Tandon, G. P.; Weng, G. J., *The Effect of Aspect Ratio of Inclusions on the Elastic Properties of Unidirectionally Aligned Composites*. *Polym Composite* **1984,** *5* (4), 327-333.
38. Gent, A. N.; Petrich, R. P., *Adhesion of Viscoelastic Materials to Rigid Substrates*. *Proc. Royal. Soc. A* **1969,** *310*, 433-448.
39. Gent, A. N., *Adhesion and strength of viscoelastic solids. Is there a relationship between adhesion and bulk properties? Langmuir* **1996,** *12* (19), 4492-4496.
40. Xu, Y. X.; Hong, W. J.; Bai, H.; Li, C.; Shi, G. Q., *Strong and ductile poly(vinyl alcohol)/graphene oxide composite films with a layered structure*. *Carbon* **2009,** *47* (15), 3538-3543.
41. Fang, M.; Zhang, Z.; Li, J. F.; Zhang, H. D.; Lu, H. B.; Yang, Y. L., *Constructing hierarchically structured interphases for strong and tough epoxy nanocomposites by amine-rich graphene surfaces*. *J Mater Chem* **2010,** *20* (43), 9635-9643.
42. O'Connell, P. A.; McKenna, G. B., *The stiffening of ultrathin polymer films in the rubbery regime: The relative contributions of membrane stress and surface tension*. *Journal of Polymer Science Part B: Polymer Physics* **2009,** *47* (24), 2441-2448.
43. Bodiguel, H.; Fretigny, C., *Viscoelastic dewetting of a polymer film on a liquid substrate*. *The European physical journal. E, Soft matter* **2006,** *19* (2), 185-93.
44. Wang, J.; McKenna, G. B., *Viscoelastic and Glass Transition Properties of Ultrathin Polystyrene Films by Dewetting from Liquid Glycerol*. *Macromolecules* **2013,** *46* (6), 2485-2495.
45. Shin, Y. J.; Wang, Y.; Huang, H.; Kalon, G.; Wee, A. T.; Shen, Z.; Bhatia, C. S.; Yang, H., *Surface-energy engineering of graphene*. *Langmuir* **2010,** *26* (6), 3798-802.
46. Raravikar, N. R.; Schadler, L. S.; Vijayaraghavan, A.; Zhao, Y. P.; Wei, B. Q.; Ajayan, P. M., *Synthesis and characterization of thickness-aligned carbon nanotube-polymer composite films*. *Chem Mater* **2005,** *17* (5), 974-983.
47. Vilmin, T.; Raphaël, E., *Dewetting of thin viscoelastic polymer films on slippery substrates*. *Europhysics Letters (EPL)* **2005,** *72* (5), 781-787.
48. Watanabe, K.; Taniguchi, T.; Kanda, H., *Direct-bandgap properties and evidence for ultraviolet lasing of hexagonal boron nitride single crystal*. *Nat Mater* **2004,** *3* (6), 404-409.
49. Kim, R. H.; Bae, M. H.; Kim, D. G.; Cheng, H.; Kim, B. H.; Kim, D. H.; Li, M.; Wu, J.; Du, F.; Kim, H. S.; Kim, S.; Estrada, D.; Hong, S. W.; Huang, Y.; Pop, E.; Rogers, J. A., *Stretchable, transparent graphene interconnects for arrays of microscale inorganic light emitting diodes on rubber substrates*. *Nano Lett* **2011,** *11* (9), 3881-6.

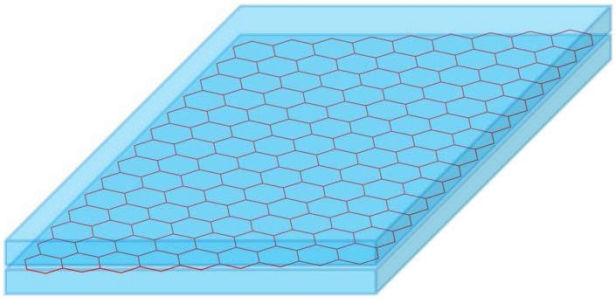

Figure 5.1 Schematic of a nano-sandwich of ultrathin polymer layer/single layer CVD graphene/polymer layer.

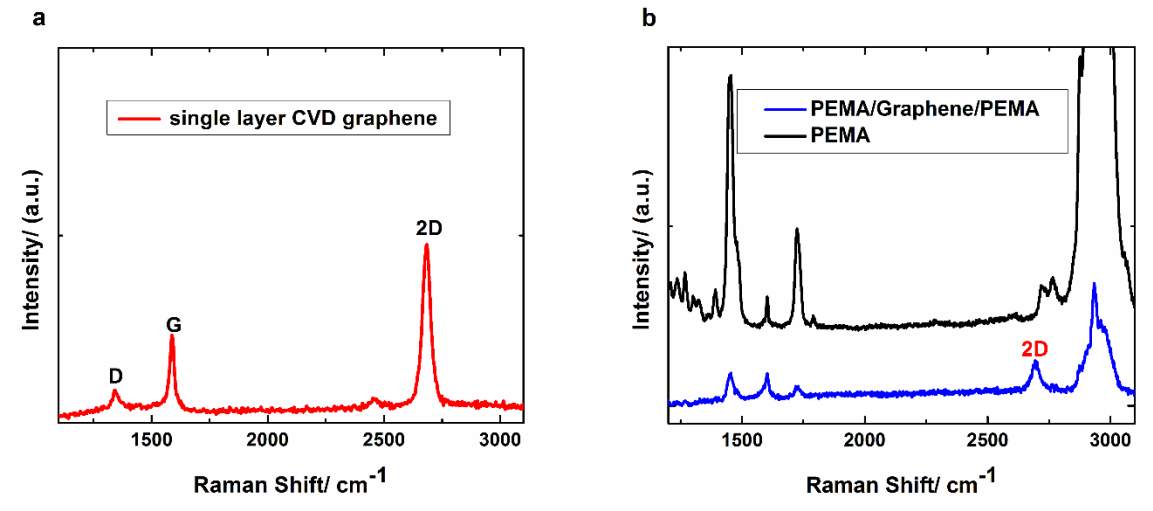

Figure 5.2 Raman spectrum of (a) single layer CVD graphene transferred onto silicon wafer and (b) neat PEMA and PEMA/Graphene/PEMA nano-sandwich

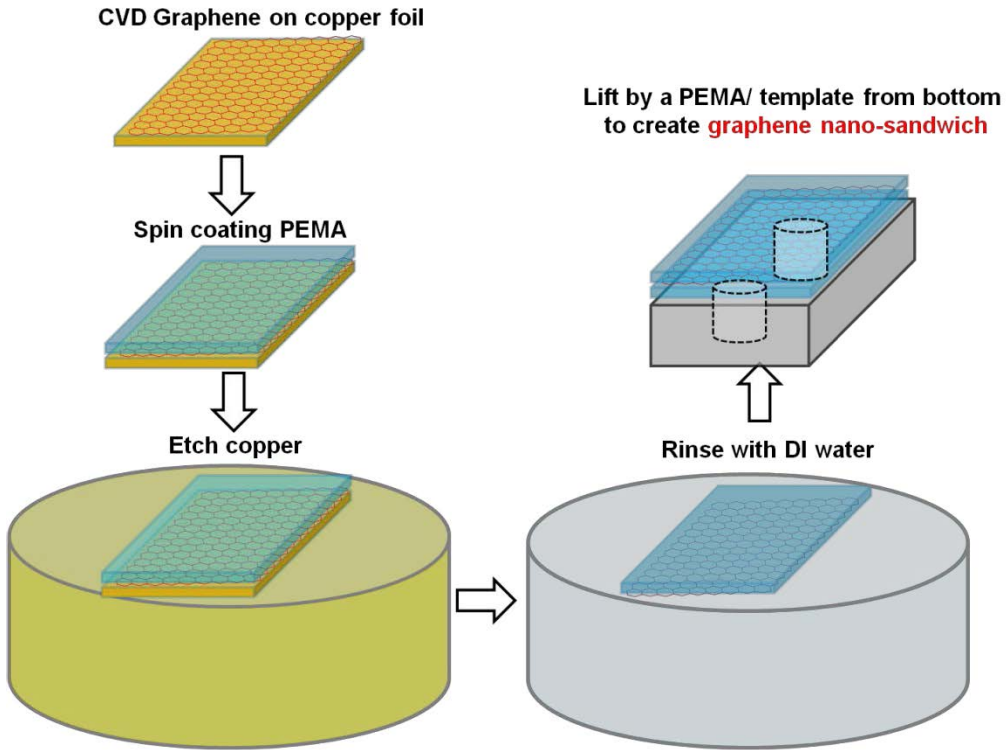

Figure 5.3 Schematic of the method to create the graphene nano-sandwiches

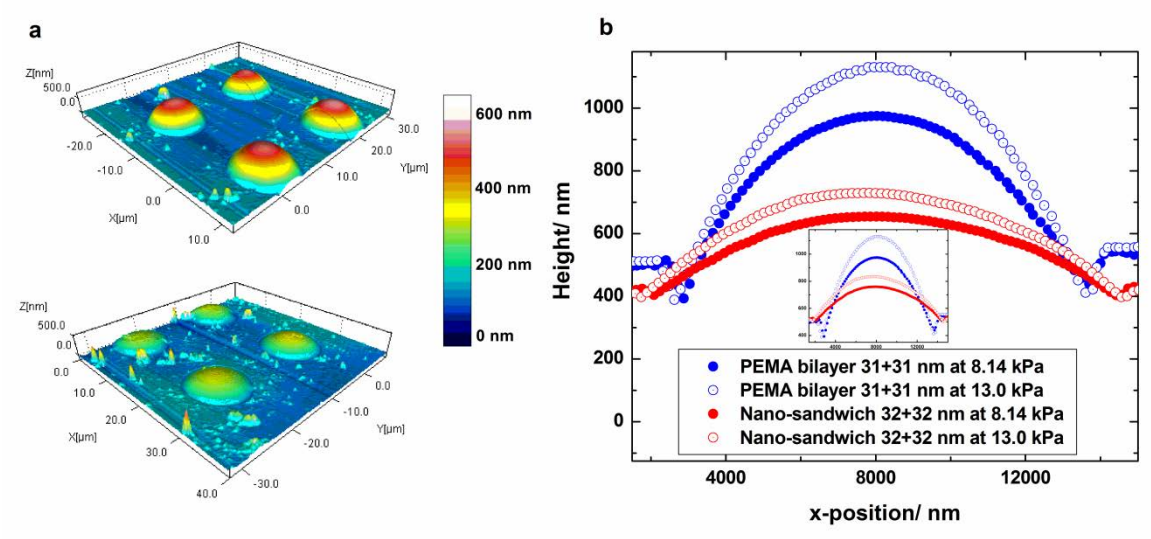

Figure 5.4 (a) Three-dimensional AFM images of 10 μm diameter bubbles of 62 nm thick PEMA bilayer (upper image) and 64 nm thick graphene nano-sandwiches (lower image) at 13.0 kPa. (b) Center-line profile of bubbles for PEMA bilayer and graphene nano-sandwich systems at different applied pressures, as indicated. Temperature is 80 °C. (The zero-positions of the nano-sandwich profiles have been shifted downwards from the template surface in order to have a clearer comparison with PEMA bilayer profiles for which the zero position is within the template channel. The insert shows the original, unshifted, nano-sandwich profiles)

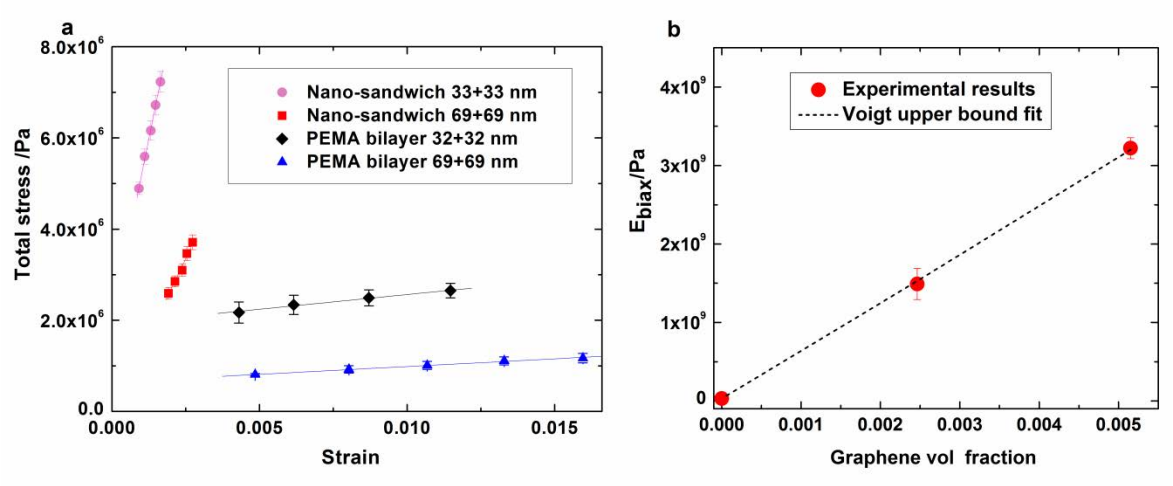

Figure 5.5 (a) Stress-strain responses for graphene nano-sandwich and PEMA bilayer films at 80 °C (b) Biaxial modulus vs. graphene volume fraction with Voigt upper bound fit.

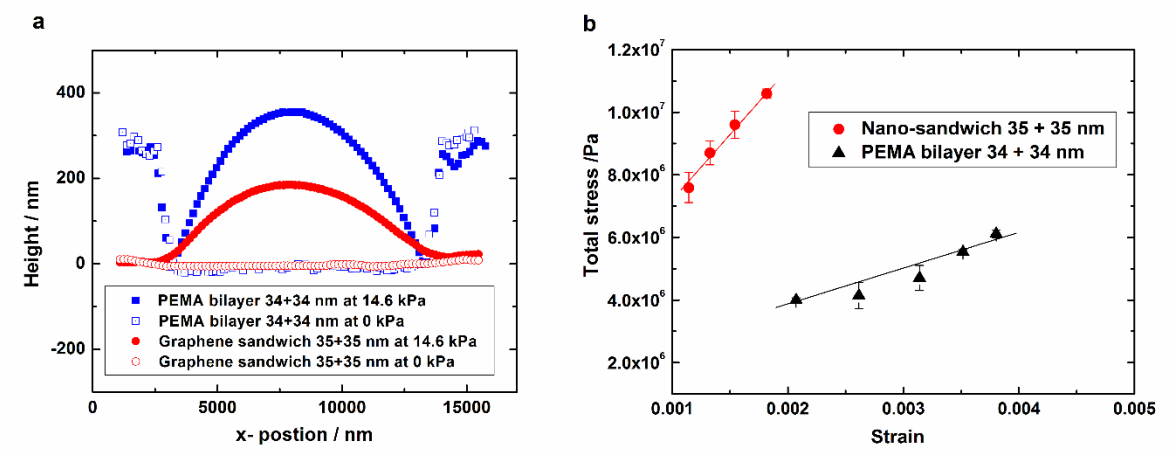

Figure 5.6 (a) Center-line profile of bubbles for 68~70 nm thick PEMA bilayer and graphene nano-sandwich systems at different applied pressures at 35 °C: (b) Stress-strain curves of corresponding bubbles with the PEMA layers in the glassy state

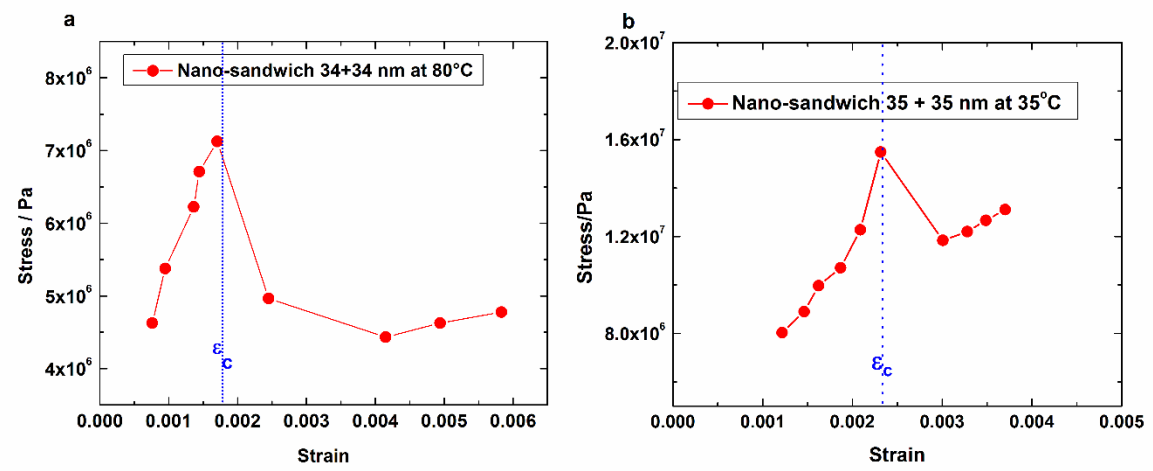

Figure 5.7 (a) Stress-strain behavior of a 68 nm thick nano-sandwich showing a "yield-like" instability related to the interfacial slip between graphene and PEMA at 80 °C; (b) Stress-strain behavior of a 70 nm thick nano-sandwich showing a "yield-like" instability at 35 °C.

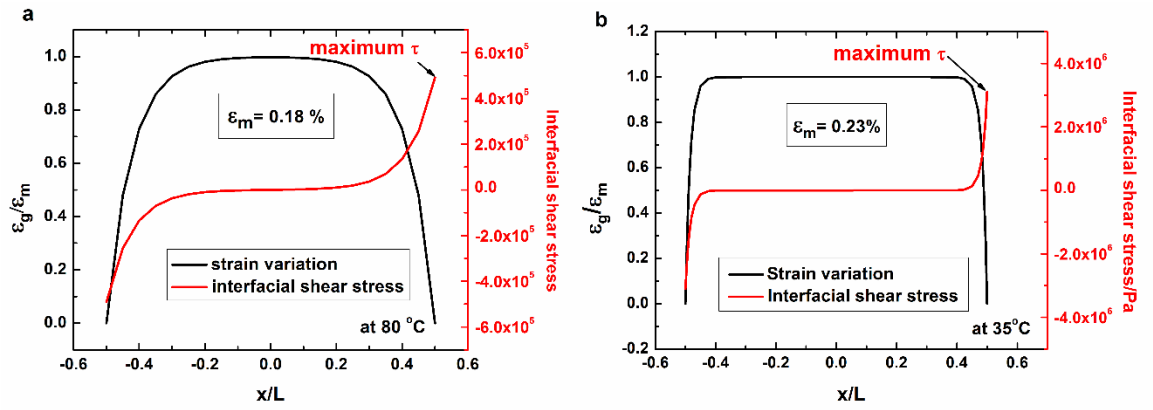

Figure 5.8 (a) Strain variation and interfacial shear stress at the matrix strain of 0.18 % for a 68 nm thick nano-sandwich with rubbery PEMA using shear lag analysis[33-35] (b) Strain variation and interfacial shear stress at the matrix strain of 0.23 % for a 70 nm thick nano-sandwich with glassy PEMA.

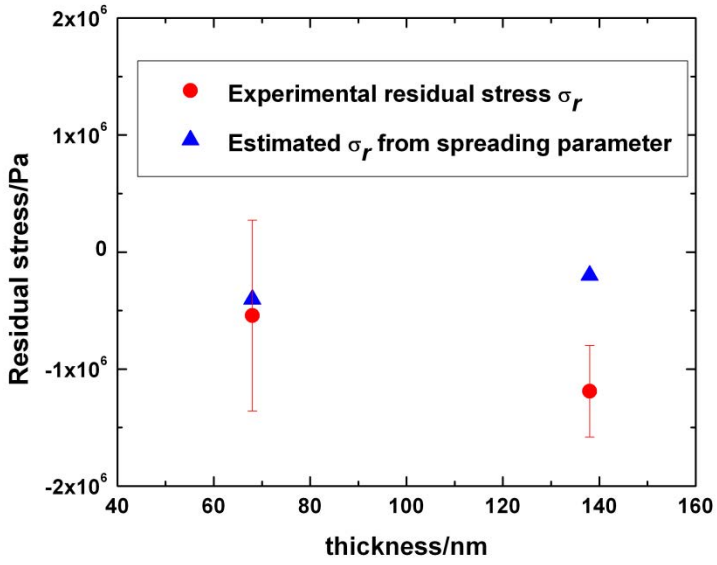

Figure 5.9 Residual stress between graphene and PEMA faces in the nano-sandwich structure compared with the values estimated from the spreading parameter, at 80 °C.

Chapter 6. Confinement Effects on the Properties of Ultrathin Poly (ethyl methacrylate) Films: Glass Transition Temperature and Rubbery Stiffening

6.1 Introduction

The dynamics of small molecules and macromolecules confined to nanometer geometries have attracted significant research interest over recent two decades.[1-13] Jackson and McKenna first reported the reduction of glass transition temperature for glass forming liquids in nano-pores [1] and Keddie et al first observed the T_g depression for polymer thin films.[14] Particularly, ultrathin polymer films have been widely studied due to the ease to control their thickness in nano-scale. To date, significant amount of work has been done for supported thin films and free-standing films using different experimental techniques, such as ellipsometry[3], fluorescence[15], DSC[16] and nano-bubble inflation method[8]. In the case of supported polymer thin films, T_g may increase or decrease depending on surface interactions between the substrates and polymer films.[3, 5] Comparing to that of the supported films (with one free surface), freestanding films which have two free surfaces are often seen to have much pronounced T_g depression.[6, 10, 17-18]

To date, polystyrene (PS) and poly(methyl methacrylate) (PMMA) have been widely studied for their nano-confinement behavior.[3, 5-6, 11, 18] For freestanding PMMA films, T_g reductions have been reported by Roth and Dutcher[6] but not as much as polystyrene[7]. Interestingly, chemical structure, i.e. tacticity of PMMA, has a large effect on the shift of T_g for thin films.[5] Grohens et al reported the ellipsometry work on the supported thin films to observe a large T_g increase (+40 K) for isotactic PMMA and decrease (-10 K) for syndiotactic PMMA, both with the film thickness of 35~40 nm.[19] However, the tacticity effect also depends on measurement methods. Fuako reported the dielectric results of decreased T_g for both isotactic and syndiotactic PMMA[20], with decreasing film thickness.

Moreover, the inherent differences in the chemical structure among polymers lead to different nanoconfinement behavior of thin films. The nano-bubble inflation work of O'Connell and McKenna shows no significant T_g change for free standing poly(vinyl acetate) (PVAc) thin films,[8, 17] significantly reduced T_g for polystyrene[17] and greatest T_g depression for polycarbonate[10]. In addition, using nano-bubble inflation method, enhanced stiffness at rubbery regime for polymer thin films has been reported and the thickness dependence of rubbery stiffening depends on the chemical structure of polymers. The slopes S obtained from the linear fit of log biaxial compliance vs. log thickness is used to describe the thickness dependence, such as S = 2 for polystyrene[21] and poly(vinyl acetate)[8], S = 1.93 for polycarbonate[10], S = 1.2 for segmented polyurethane[22] and S = 0.83 for poly(n-butyl methacrylate) (PBMA).[23]

To date, nano-bubble inflation method has not been exploited to study the nanoconfinement behavior of thin films of poly(alkyl methacrylates). In this chapter, we present the first nano-bubble inflation work on poly(ethyl methacrylate) (PEMA) ultra-thin films over thicknesses ranging from 112 to 21 nm. A reduction in glass transition temperature (T_g) with stiffening of the rubbery regime as film thickness decreases was observed. The results of thickness dependence of rubbery stiffening were used to examine Ngai's coupling model and Page's micromechanics approach, both proposed to explain the rubbery stiffening of thin films.

6.2 Experiments

Materials: Poly(ethyl methacrylate) (80% syndiotactic PEMA, T_g = 65°C, M_w = 515 k, PDI = 1.52; purchased from Sigma Aldrich).

Methods: PEMA/toluene solution (0.5 % - 2.1 %, w/w) was spin coated onto the fresh cut mica sheets at a speed of 2000 rpm for 30 s then dry for 30 mins at room temperature. The film was floated onto the water surface and lifted onto a clean silicon nitride filter template into which arrays of through-channels with diameters of 5 or 10 μm. The PEMA thin films were dried in a desiccator overnight and annealed at the actual T_g + 15 K for 15 mins to bond the film to the template surface. Film thicknesses were determined by the concentration of PEMA/toluene solution, and obtained by scoring made on the template edges and using an atomic force microscope (AFM) (Agilent SPM5500) to measure the step height.

The TTU nano-bubble inflation method has been described thoroughly in Chapter 2. The filter template holding the nano-sandwich was mounted in a custom pressure cell using the adhesive and pressurized dry air was applied below the filter template to inflate the sample films into bubbles, and the AFM was used to measure the bubble profile. The AFM was operated in intermittent contact mode and the scan area was 40 × 40 and 20 × 20 μm^2. The scan rate was 1.1 lines/ second.

6.3 Results and Discussions

6.3.1 Creep behavior and T_g reduction

Figure 6.1a shows a series of center-line profiles for a 21 nm thick PEMA film at 50 °C with a pressure of 20.3 kPa, obtained as a function of time. During the annealing stage, the capillary forces draw the film into the holes, hence the boundaries of the bubbles are observed below the substrate surface. As shown in Figure 6.1a, the 21 nm thick PEMA bubble continues to grow with time at 50 °C, illustrating a creep behavior. Figure 6.1b represents the creep

compliance for a 21 nm and 112 nm thick PEMA film at 65 °C (the macroscopic T_g of PEMA). It is observed that during the whole test the 112 nm thick PEMA film only shows a glass transition behavior but the 21 nm thick PEMA film begins to level out after 3000 s as the rubbery plateau is reached. Therefore, the hint of the T_g depression of PEMA with decreasing film thickness was observed.

To represent the creep results for a range of temperatures, we choose the reference curves in the glass transition region, then shift the other apparent creep compliance curves to construct a master curve using time-temperature superposition.[24] Figure 6.2a shows the creep master curves for the 21 nm thick film along with 4 other film thickness from 27 to 112 nm, and two trends can be observed. First when the film thickness is below 30 nm, PEMA can achieve creep below the macroscopic T_g of 65 °C, hence indicating the T_g depression. Second is that the rubbery plateau stiffens significantly as the film thickness decreases. Since the reference curve for each master curve is somewhat arbitrarily chosen, we will show a quantitative determination of T_g in next paragraph.

The glass transition temperature are determined using following procedure: For each thickness, the creep results at different temperatures were fitted to obtain retardation times using the modified Kohlrausch–Williams–Watts (KWW) equation[25],

$$D(t) = D_g + D_N \left[1 - \exp\left(-\left(\frac{t}{\tau}\right)^{\beta}\right)\right] \quad (1)$$

where D_g is the glassy biaxial compliance (2×10^{-10} Pa^{-1} from macroscopic data), D_N is the rubbery plateau biaxial compliance. τ and β are the retardation time and the stretching exponent, respectively, which can be obtained as fitting parameters. For 112 nm thick PEMA film, its retardation time τ is obtained as 1×10^5 s at 65 °C and we assume the 112 nm thick film has the T_g

same as macroscopic T_g of 65 °C. Therefore 1×10^5 s is chosen as the reference retardation time τ_{ref} and all shift factors are obtained using $a_T = \tau/ \tau_{ref}$. To determine the reduction of T_g of PEMA quantitatively, the temperature shift factors a_T vs. the reciprocal of temperature were plotted for each thickness and fitted using the Vogel-Fulcher-Tammann equation (VFT)[26-28] in Figure 6.2b. For each thickness, the T_g is determined as the temperature with the shift factor a_T equaling to zero, using the VFT equation.

The reduction of T_g as a function of film thickness is obtained and shown in Figure 6.3. For comparison, the ΔT_g vs. free-standing film thickness for atactic PMMA reported by Roth and Dutcher using ellipsometry,[6] and PS[17] and PVAc[17] reported by McKenna and co-workers using nanobubble inflation method were also plotted. As seen, very interestingly, T_g of PEMA thin films decreases slightly before the thickness approaching 30 nm. However, a significant reduction T_g (15.7 K) was observed for 21 nm thick PEMA. To date, PC thin films have been reported with the largest T_g reduction and PS thin films has the second largest T_g reduction,[10] but no T_g reduction was found for PVAc.[17] Here we observed that the thickness dependence of T_g depression of PEMA is smaller compared to that of PS. Although both PEMA and PMMA belong to the family of poly(alkyl methacrylates), and their extents of T_g reduction are similar when the thickness decreases from 120 to 20 nm, the trend is different since PEMA only shows a significant T_g reduction when the thickness approaching 30 nm. Therefore, the thickness dependences of T_g reduction of polymer thin films strongly depend on the chemical structures, as O'Connell and McKenna claimed.[17]

6.3.2 Rubbery stiffening

Enhanced stiffness at rubbery regime for polymer thin films is another interesting phenomenon reported by McKenna and co-workers using nanobubble inflation method (we call it "rubbery stiffening" [10, 17, 22-23] here), which also explicit a chemical structure dependence. Above the macroscopic T_g, the PEMA thin films are inflated by different pressures and the stress-strain response was obtained from the bubble shape and the applied pressure, using equations 7-10 in Chapter 2. The stress-strain responses for thin films at thicknesses ranging from 110 to 21 nm are shown in Figure 6.4a, and the linear relationship between stress and strain can be described using equation 2,

$$\sigma_{total} = \sigma_{11} = E_{biax}\varepsilon_{11} + \sigma_0 \quad (2)$$

where E_{biax} is the biaxial rubbery modulus and σ_0 is the surface stress due to the surface energy of PEMA.

As shown in Figure 6.4a, the rubbery modulus obtained as the slope of straight lines increases as the PEMA film thickness decreases. Further, the biaxial rubbery compliance can be determined from the biaxial rubbery modulus and the slopes S obtained from the linear fit of log biaxial rubbery compliance vs. log thickness are used to determine the thickness dependence of PEMA in Figure 6.4b. It was observed that the compliance of PEMA thin films are below the macroscopic value, and show a stiffening dependence of thickness of S = 1.34. In Figure 6.5, the stiffening dependence of thickness S is compared with PS, PVAc[17] and PBMA[23]. The stiffening of PEMA is higher than that of PBMA but lower than those of PS and PVAc.

Recently Ngai et al [29] have used the coupling model to explain the rubbery stiffening of thin polymer films. When the film thickness decreases, the degree of intermolecular cooperativity decreases as a consequence. Therefore Ngai proposed that the resultant increasing

separation of the segmental α relaxation and the Rouse modes consequence can lead to the observed rubbery stiffening.[29] Ngai et al further claimed that segmental α relaxation coupling parameter n_α indicates the extent of the separation of α relaxation and the Rouse modes, which is consistent with the rubbery stiffening dependence of thickness observed for PS, PVAc,[17] PC[10] and PBMA.[23] And very recently, Zhai and McKenna reported the rubbery stiffening of a segmented polyurethane (Estane)[22], which is also consistent with Ngai's analysis.

Here we discuss the results of PEMA with the literature values of coupling parameter n_α for PS, PVAc,[29] and poly(alkyl methacrylates).[30] In Figure 6.5, the sequence of n_α of PS, PVAc, PEMA, and PBMA is consistent with the rubbery stiffening dependence of thickness S. Therefore our results support Ngai's explanation that coupling parameter n_α is related to the rubbery stiffening. Particularly, although both belong to the family of poly(alkyl methacrylates), the degree of intermolecular cooperativity of PBMA is smaller than that of PEMA, due to the longer ester side chains.[29, 31] This can explain why PBMA has the smallest rubbery stiffening thickness dependence in Figure 6.5.

Very recently, Page et al[32] have provided another explanation on the rubbery stiffening of thin polymer films, using a micromechanics approach incorporating the stiffness of a single polymer chain. Because the single polymer chain is much stiffer than the bulk polymer,[33] Page et al consider the single polymer chain as a reinforcing element,[32] and treat the thin films as a mixture of soft bulk polymer and rigid single chain using a modified Halpin-Tsai equation.[34] As Page et al proposed, the ratio of the single chain (rigid phase) increase with decreasing film thickness, hence, the rubbery film stiffness increases.

Here we use the literature data of polymer chain stiffness and our rubbery stiffening results of PS, PVAc, PEMA and PC to examine above micromechanics approach. Back to the 1970s, X-ray diffraction[35-36] and Raman spectroscopy[37-38] were used to determine the stiffness of local crystalline region, thought to be a good estimation of the stiffness of aligned polymer chains. Tashiro[39] summarized the factors governing the polymer chain stiffness and we list the literature values of some polymers in Table 6.1. Three things are remarkable. First, chain conformation is the most dominant factor for chain stiffness. The conformation of planar zig-zag usually gives a much higher stiffness compared to that of helix[39], e.g PE (planar zig-zag) has a higher stiffness of 240 GPa than that of PP[39] (3/1 helix, 40 GPa). Second, the stiffness of polymer chain is mainly related to the backbone structure, e.g. PE and PVA have similar chain stiffness because both their backbone are $–CH_2CH_2–$.[39-40] Interestingly, polyesters e.g. PET, usually have a lower chain stiffness due to the oxygen atom in their backbones.[39] Third, intermolecular interactions through side groups have week effects on the chain stiffness. However, bulky side group might decrease the chain stiffness because of the large cross-sectional area.

As shown in Table 6.1, isotactic PS has a chain stiffness of 12 GPa due to its helix structure and bulky side group. With similar chemical structure, PEMA was reported to have a similar local helix structure to PMMA,[41] therefore it is reasonable to assume that PEMA has a similar chain stiffness to PMMA (10 GPa). In the same manner, PVAc should have a similar chain stiffness to PVA (255 GPa) due to their close chemical structure. And PC should have a similar chain stiffness to PET (118 GPa).

In Figure 6.6, the biaxial modulus of PS, PVAc,[17] PEMA and PC[10] are plotted as a function of film thickness, marked with their chain stiffness. However, the rubbery stiffening

dependence of thickness (slopes) are not consistent with the chain stiffness data of these polymers, i.e. PS and PEMA have similar low chain stiffness but PS has a larger slope of 2 than 1.34 of PEMA. Therefore, our results cannot support the micromechanics approach incorporating the chain stiffness, as strongly as Ngai's model.

The difference between Ngai's model and the micromechanics approach of Page et al is the role of interchain interactions. For Ngai's coupling model, the interchain cooperativity is an important factor of rubbery stiffening. However, in Page et al's micromechanics approach, the interchain interaction is neglected for the single chain stiffness.[39] This might be the reason that our results support Ngai's model better than the micromechanics approach.

6.4 Conclusion

The viscoelastic responses of poly(ethyl methacrylate) (PEMA) ultra-thin films over thicknesses ranging from 112 to 21 nm has been studied using nano-bubble inflation method. A reduction in glass transition temperature (T_g) as much as 15.7 K has been observed for 21 nm thick PEMA film. PEMA also has a rubbery stiffening as the film thickness decreases, with the thickness dependence between PS and PBMA. Finally, the thickness dependence of rubbery stiffening was analyzed using Ngai's coupling model and Page's micromechanics approach incorporating the stiffness of a single polymer chain. It is found that our experimental results can support Ngai's coupling model strongly.

6.5 References

1. Jackson, C. L.; McKenna, G. B., *The glass transition of organic liquids confined to small pores*. *Journal of Non-Crystalline Solids* **1991,** *131–133, Part 1* (0), 221-224.
2. Jackson, C. L.; McKenna, G. B., *The melting behavior of organic materials confined in porous solids*. *The Journal of Chemical Physics* **1990,** *93* (12), 9002-9011.
3. Keddie, J. L.; Jones, R. A. L.; Cory, R. A., *Interface and surface effects on the glass-transition temperature in thin polymer films*. *Faraday Discussions* **1994,** *98* (0), 219-230.
4. de Gennes, P. G., *Glass transitions in thin polymer films*. *The European Physical Journal E* **2000,** *2*, 201.
5. Grohens, Y.; Hamon, L.; Reiter, G.; Soldera, A.; Holl, Y., *Some relevant parameters affecting the glass transition of supported ultra-thin polymer films*. *The European physical journal. E, Soft matter* **2002,** *8* (2), 217-24.
6. Roth, C. B.; Dutcher, J. R., *Glass transition temperature of freely-standing films of atactic poly(methyl methacrylate)*. *The European physical journal. E, Soft matter* **2003,** *12 Suppl 1*, S103-7.
7. Alcoutlabi, M.; McKenna, G. B., *Effects of confinement on material behaviour at the nanometre size scale*. *Journal of Physics: Condensed Matter* **2005,** *17* (15), R461-R524.
8. O'Connell, P. A.; McKenna, G. B., *Rheological measurements of the thermoviscoetastic response of ultrathin polymer films (vol 307, pg 1760, 2005)*. *Science* **2005,** *310* (5753), 1431-1431.
9. Yang, Z.; Peng, D.; Clough, A.; Lam, C. H.; Tsui, O. K. C., *Is the dynamics of polystyrene films consistent with their glass transition temperature? The European Physical Journal Special Topics* **2010,** *189* (1), 155-164.
10. O'Connell, P. A.; Wang, J.; Ishola, T. A.; McKenna, G. B., *Exceptional Property Changes in Ultrathin Films of Polycarbonate: Glass Temperature, Rubbery Stiffening, and Flow*. *Macromolecules* **2012,** *45* (5), 2453-2459.
11. Gao, S.; Koh, Y. P.; Simon, S. L., *Calorimetric Glass Transition of Single Polystyrene Ultrathin Films*. *Macromolecules* **2013,** *46* (2), 562-570.
12. Ediger, M. D.; Forrest, J. A., *Dynamics near Free Surfaces and the Glass Transition in Thin Polymer Films: A View to the Future*. *Macromolecules* **2014,** *47* (2), 471-478.
13. Tress, M.; Erber, M.; Mapesa, E. U.; Huth, H.; Müller, J.; Serghei, A.; Schick, C.; Eichhorn, K.-J.; Voit, B.; Kremer, F., *Glassy Dynamics and Glass Transition in Nanometric Thin Layers of Polystyrene*. *Macromolecules* **2010,** *43* (23), 9937-9944.
14. Keddie, J. L.; Jones, R. A. L.; Cory, R. A., *Size-Dependent Depression of the Glass Transition Temperature in Polymer Films*. *EPL (Europhysics Letters)* **1994,** *27* (1), 59.
15. Ellison, C. J.; Torkelson, J. M., *The distribution of glass-transition temperatures in nanoscopically confined glass formers*. *Nat Mater* **2003,** *2* (10), 695-700.
16. Koh, Y. P.; Simon, S. L., *Structural relaxation of stacked ultrathin polystyrene films*. *Journal of Polymer Science Part B: Polymer Physics* **2008,** *46* (24), 2741-2753.
17. O'Connell, P. A.; Hutcheson, S. A.; McKenna, G. B., *Creep behavior of ultra-thin polymer films*. *Journal of Polymer Science Part B: Polymer Physics* **2008,** *46* (18), 1952-1965.
18. Forrest, J. A.; Dalnoki-Veress, K.; Stevens, J. R.; Dutcher, J. R., *Effect of Free Surfaces on the Glass Transition Temperature of Thin Polymer Films*. *PHY S I CAL REV I EW LETTERS* **1996,** *77*, 2002.

19. Grohens, Y.; Brogly, M.; Labbe, C.; David, M.-O.; Schultz, J., *Glass Transition of Stereoregular Poly(methyl methacrylate) at Interfaces*. *Langmuir* **1998,** *14* (11), 2929-2932.
20. Fukao, K., *Dynamics in thin polymer films by dielectric spectroscopy*. *The European Physical Journal E* **2003,** *12* (1), 119-125.
21. O'Connell, P. A.; McKenna, G. B., *Dramatic stiffening of ultrathin polymer films in the rubbery regime*. *The European physical journal. E, Soft matter* **2006,** *20* (2), 143-50.
22. Zhai, M.; McKenna, G. B., *Elastic modulus and surface tension of a polyurethane rubber in nanometer thick films*. *Polymer* **2014** *55*, 2725-2733.
23. Xu, S.; O'Connell, P. A.; McKenna, G. B., *Unusual elastic behavior of ultrathin polymer films: Confinement-induced/molecular stiffening and surface tension effects*. *The Journal of Chemical Physics* **2010,** *132* (18), 184902.
24. Ferry, J. D., *Viscoelastic Properties of Polymers*. Wiley: New York, 1980.
25. Williams, G.; Watts, D. C., *Non-symmetrical dielectric relaxation behaviour arising from a simple empirical decay function*. *Transactions of the Faraday Society* **1970,** *66* (0), 80-85.
26. Tammann, G.; Hesse, W., *The dependence of viscosity upon the temperature of supercooled liquids*. *Z. Anorg. Allg. Chem.* **1926,** *156*.
27. Fulcher, G. S., *ANALYSIS OF RECENT MEASUREMENTS OF THE VISCOSITY OF GLASSES*. *Journal of the American Ceramic Society* **1925,** *8* (6), 339-355.
28. Vogel, H., *The law of relation between the viscosity of liquids and the temperature*. *Phys. Z.* **1921,** *22*.
29. Ngai, K. L.; Prevosto, D.; Grassia, L., *Viscoelasticity of nanobubble-inflated ultrathin polymer films: Justification by the coupling model*. *J Polym Sci Pol Phys* **2013,** *51* (3), 214-224.
30. Ngai, K. L.; Gopalakrishnan, T. R.; Beiner, M., *Relaxation in poly(alkyl methacrylate)s: Change of intermolecular coupling with molecular structure, tacticity, molecular weight, copolymerization, crosslinking, and nanoconfinement*. *Polymer* **2006,** *47* (20), 7222-7230.
31. Hempel, E.; Hempel, G.; Hensel, A.; Schick, C.; Donth, E., *Characteristic Length of Dynamic Glass Transition near Tg for a Wide Assortment of Glass-Forming Substances*. *The Journal of Physical Chemistry B* **2000,** *104* (11), 2460-2466.
32. Page, K. A.; Kusoglu, A.; Stafford, C. M.; Kim, S.; Kline, R. J.; Weber, A. Z., *Confinement-driven increase in ionomer thin-film modulus*. *Nano Lett* **2014,** *14* (5), 2299-304.
33. Holliday, L.; White, J. W., The stiffness of polymers in relation to their structure. In *Pure and Applied Chemistry*, 1971; Vol. 26, p 545.
34. Halpin, J. C.; Kardos, J. L., *HALPIN-TSAI EQUATIONS: A REVIEW*. *Polymer Engineering and Science* **1976,** *16* (5), 344-352.
35. Sakurada, I.; Ito, T.; Nakamae, K., *Elastic moduli of the crystal lattices of polymers*. *Journal of Polymer Science Part C: Polymer Symposia* **1967,** *15* (1), 75-91.
36. Sakurada, I.; Kaji, K., *relation between the polymer conformation and the elastic modulus of the crystalline region of polymer*. *Journal of Polymer Science Part C: Polymer Symposia* **1970,** *31* (1), 57-76.
37. Strobl, G. R.; Eckel, R., *A raman spectroscopic determination of the interlamellar forces in crystalline n-alkanes and of the limiting elastic modulus Ec of polyethylene*. *Journal of Polymer Science: Polymer Physics Edition* **1976,** *14* (5), 913-920.
38. Pietralla, M.; Hotz, R.; Engst, T.; Siems, R., *Chain direction elastic modulus of PE crystal and interlamellar force constant of n-alkane crystals from RAMAN measurements*. *Journal of Polymer Science Part B: Polymer Physics* **1997,** *35* (1), 47-57.

39. Tashiro, K., *Molecular theory of mechanical properties of crystalline polymers*. *Progress in Polymer Science* **1993,** *18* (3), 377-435.
40. Tashiro, K.; Kobayashi, M.; Tadokoro, H., *Calculation of Three-Dimensional Elastic Constants of Polymer Crystals. 2. Application to Orthorhombic Polyethylene and Poly(vinyl alcohol)*. *Macromolecules* **1978,** *11* (5), 914-918.
41. Wind, M.; Graf, R.; Renker, S.; Spiess, H. W.; Steffen, W., *Structure of amorphous poly-(ethylmethacrylate): A wide-angle x-ray scattering study*. *The Journal of Chemical Physics* **2005,** *122* (1), -.
42. Urbanek, S.; Tashiro, K.; Kitayama, T.; Hatada, K., *Crystallite modulus of double-stranded helices of isotactic poly(methyl methacrylate): the X-ray measurement and the theoretical calculation*. *Polymer* **1999,** *40* (12), 3345-3351.

Table 6.1 The chain stiffness of some polymers

Polymer	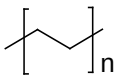 PE	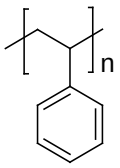 PS	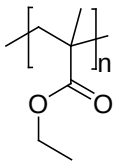 PEMA	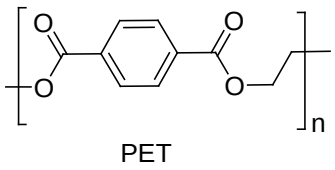 PET
Chain stiffness E_c	240 GPa Planar zig-zag[35, 39]	12 GPa isotactic, helix[35]	N/A	118 GPa Planar zig-zag[39]
Polymer	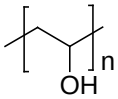 PVA	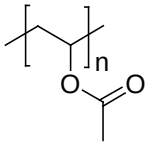 PVAc	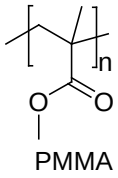 PMMA	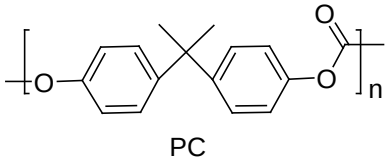 PC
Chain stiffness E_c	255 GPa Planar zig-zag[35]	N/A	10 GPa isotactic, helix[42]	N/A

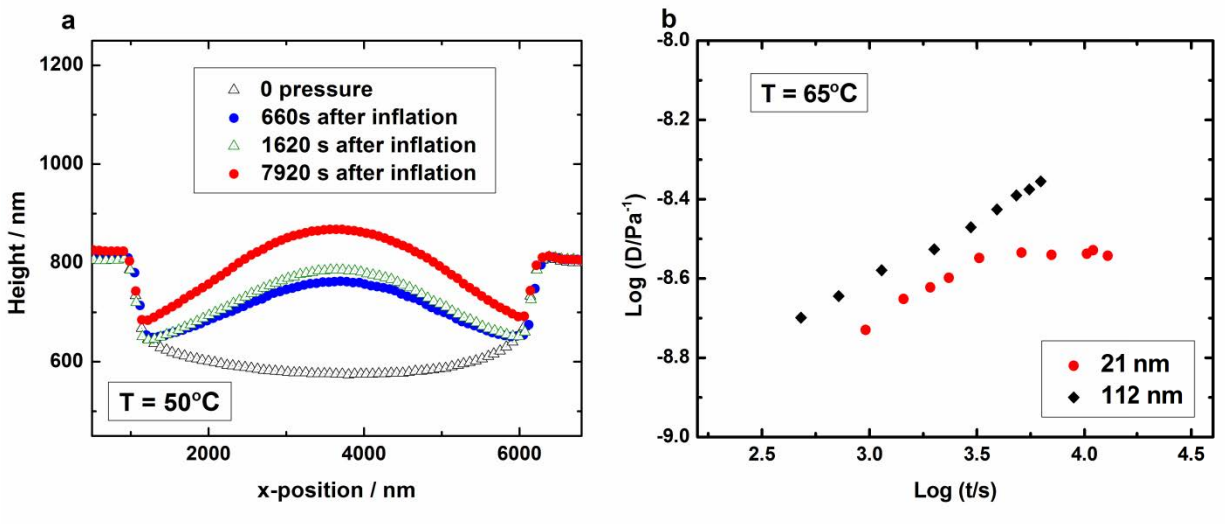

Figure 6.1 (a) Creep profiles of 5 μm diameter bubbles for a 21 nm thick PEMA film at 50 °C with the pressure of 20.3 kPa, with different creep times. (b) Creep compliance for a 21 nm and 112 nm thick PEMA film at 65 °C.

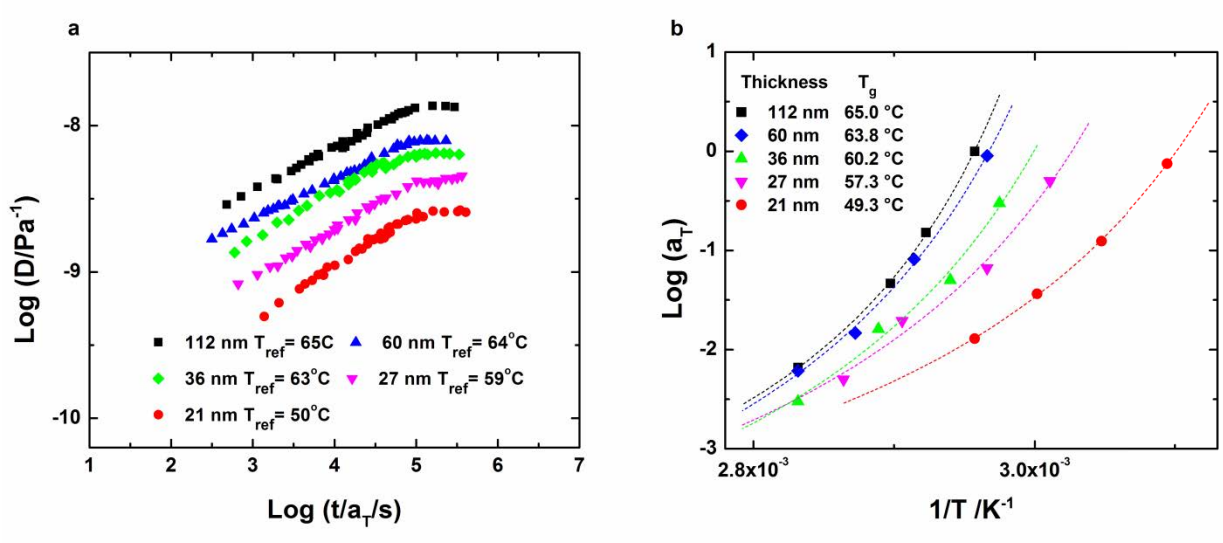

Figure 6.2 (a) Creep master curves for PEMA thin films. (b) Time-temperature shift factors vs. 1/T for PEMA thin films. Dashed lines are the VFT fitting curves.

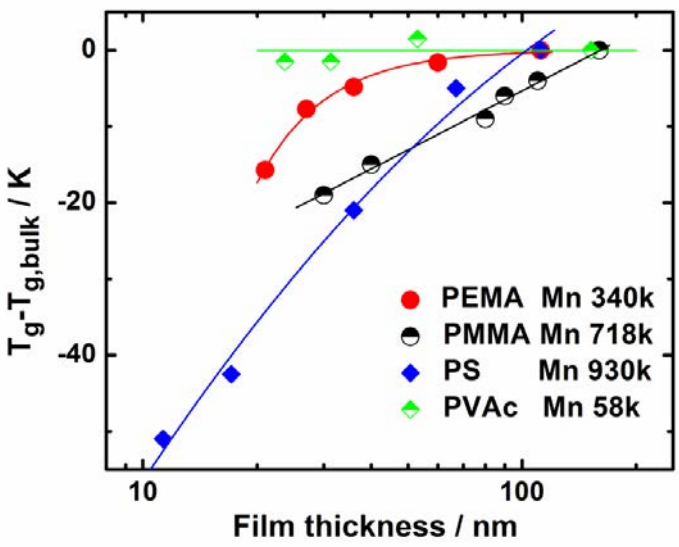

Figure 6.3 T_g reduction as a function of PEMA film thickness, comparing with PMMA[6], PS and PVAc[17].

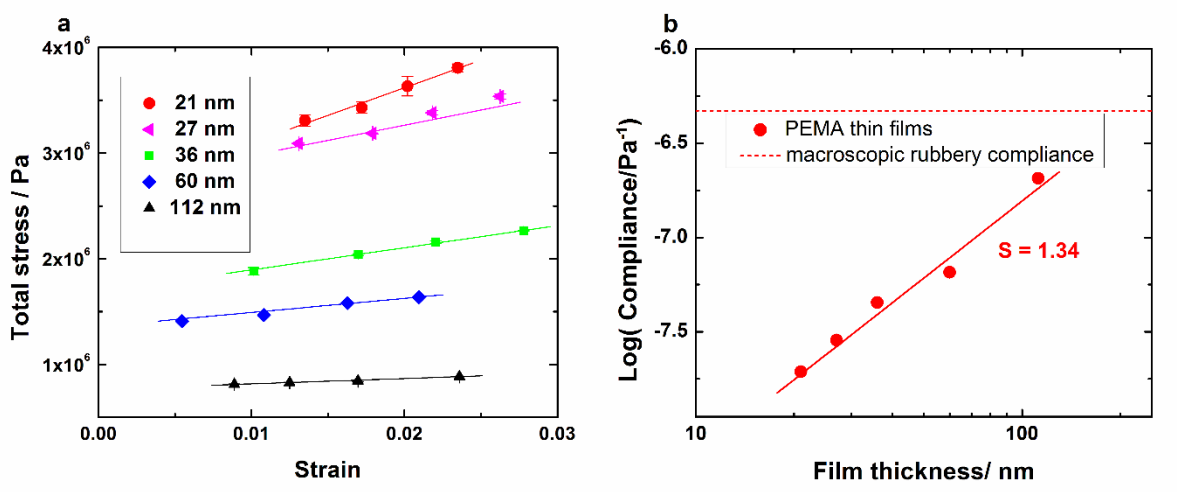

Figure 6.4 (a) Stress – strain responses for PEMA thin films at rubbery state; (b) Rubbery biaxial compliance vs. film thickness

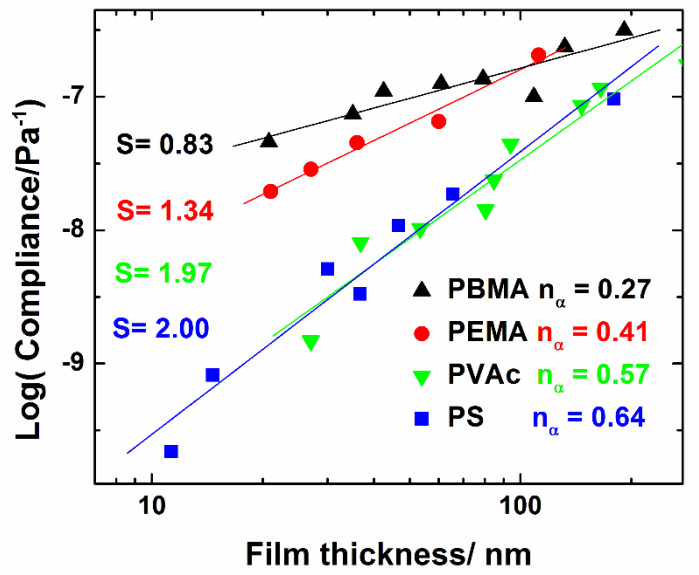

Figure 6.5 Rubbery stiffening dependence of thickness for polymer with different chemical structure

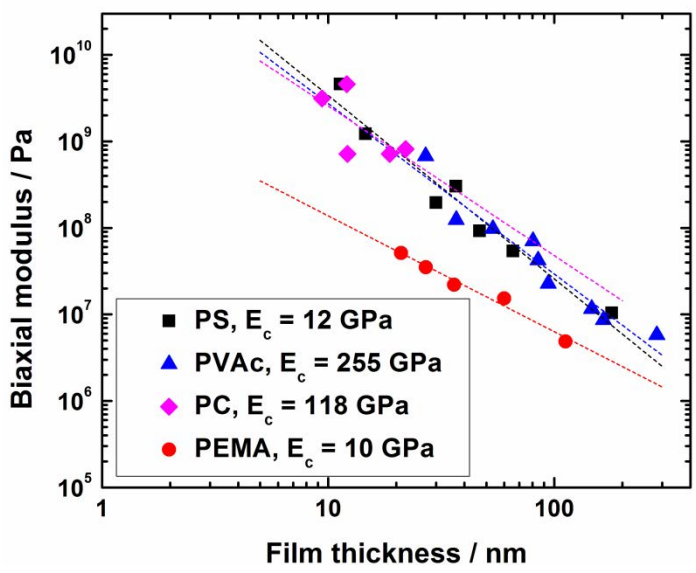

Figure 6.6 Rubbery stiffening of polymer thin films as a function of thickness, compared with their chain stiffness.

Chapter 7. Conclusion & Future work

7.1 Conclusion

The dissertation here addressed the problem of thermo-viscoelastic micromechanics and showed that it should be applied to account for the effects of T_g change in graphene reinforced polymer nanocomposites. This is recognized in order to decouple the reinforcement induced by the graphene itself from the one induced by the change in the viscoelasticity of the polymer matrix due to the addition of the graphene or graphene oxide. It was then demonstrated that a multilayer co-extrusion procedure, can maximize the mechanical stiffening of graphene nanocomposites by orienting the graphene in thin polymer layers created by forced assembly. Finally, we showed how to use a "graphene nano-sandwich" structure to investigate the interfacial mechanics between a single layer graphene sheet and the PEMA matrix. The viscoelastic responses of PEMA ultra-thin films over thicknesses ranging from 112 to 21 nm were also studied. The research methodology and major findings are highlighted as follows:

Rheological and glass transition temperature measurements demonstrate that graphene oxide stiffens the reinforced polymer matrices by increasing the T_g significantly and this change the thermo-viscoelasticity of the polymer matrices. Hence, much of the reported stiffening of graphene oxide polymer nanocomposites is due to the matrix itself stiffening as the T_g increases, rather than the extreme reinforcement of the matrix by the graphene oxide itself.

- In the work of Ruoff and co-workers,[1] the increase of T_g and reinforcement for PMMA/ graphene oxide nanocomposites share a similar trend with the increased loading of graphene oxide.

- In the present work, graphene oxide was incorporated into a poly(ethyl methacrylate) (PEMA) matrix at 0.25 wt % and a nearly 15 K increase of glass transition temperature T_g was observed.
- The addition of 0.25 wt % graphene oxide doesn't change the intensity of the β relaxation of PEMA, but increases the β relaxation by 6 ~ 8 K. Therefore the incorporation of graphene oxide further splits the glass transition and the β relaxation.
- Our thermo-viscoelastic micromechanics approach shows that most of the apparent extreme reinforcements in graphene oxide polymer nanocomposites can be attributed to the increased T_g of the polymer, and the corrected mechanical reinforcement from graphene oxide is much weaker than previously reported.[2]

Forced assembly multilayer co-extrusion was used to create films made of alternating layers of neat polymer / oriented graphene nanoplatelet filled polymer with the structure confirmed by a combination of microscopic analysis of the morphology of the multilayer films and mechanical property measurements:

- In the PMMA/PMMA-graphene multilayer films, the reinforced PMMA layers (35 ~ 40 nm thick) were shown to contain oriented graphene in the direction of extrusion and partially oriented in the transverse direction.
- The orientation of the graphene nanoplatelets in the PMMA thin layers (2 wt %), resulted in a significant reinforcement of 118 % increase in the tensile modulus along the flow direction. Upon accounting for the increased T_g (1~2 K), the corrected reinforcement is approximately 101 % that of the neat polymer matrix.

- The stiffening of PMMA/PMMA-graphene films versus layer thickness, share a similar trend with the dispersion quality. The reason is that, by increasing the number of layers, the degree of dispersion of the graphene nanoplatelets and the possible breakage of aggregates in the polymer matrix appear to increase as the thickness of the confining layer decreases, and should confine the graphene nanoplatelets more efficiently, giving enhanced reinforcement.
- PMMA/PS-graphene is a good system to demonstrate the morphology of distinct layer structure changes as the concentration of graphene nanoplatelets increases, but the weak adhesion between PMMA and PS needs to be improved.

A novel nano-sandwich structure made of thin PEMA layer /single layer CVD graphene/ thin PEMA layer was created, and the nano-bubble inflation method was applied to obtain the mechanical responses and investigate the interface mechanics between graphene and polymers:

- Significant mechanical (stiffness) reinforcements were observed at small strains in both the rubbery (45.9 times for 0.52 vol %) and glassy states (2.5 times for 0.48 vol %) of the PEMA.
- Above the critical strains (0.18% for rubbery and 0.23 for glassy PEMA), a “yield-like” phenomenon was observed and has been interpreted to be due to interfacial slip
- The interface shear strength can be estimated using shear lag analysis, and the interface built by Van der Waals forces can transfer the interface stress to achieve stiffening from graphene onto polymer matrices below the critical strain.

- The biaxial modulus of the large single CVD graphene sheet was obtained as 608 GPa from the mechanical responses of the graphene nano-sandwich. Therefore the Young's modulus of CVD graphene sheet was estimated as 511 GPa.
- The graphene nano-sandwich provides a measurement of the internal residual stress set up between graphene and rubbery PEMA layers.

The viscoelastic responses of poly(ethyl methacrylate) (PEMA) ultra-thin films over thicknesses ranging from 112 to 21 nm have been studied using nano-bubble inflation method:

- A reduction in glass transition temperature as much as 15.7 K has been observed for 21 nm thick PEMA film.
- PEMA shows a rubbery stiffening as the film thickness decreases, with the thickness dependence S between PS and PBMA.
- Our experimental results can support Ngai's coupling model better than the Page's micromechanics approach to explain the phenomenon of rubbery stiffening.

7.2 Future work

7.2.1 Influence of graphene oxide on the α and β relaxation of poly(n-alkyl methacrylate)

Excellent mechanical reinforcement of polymer nanocomposites (PNCs) and significant increases of T_g have been reported upon dispersing graphene oxide into polar polymer matrices at low loading (0.1 ~ 1.0 vol %)[1-3] and even at ultra-low loading (0.005 ~0.01 vol %)[4]. However, Macosko and co-workers have questioned Brinson's results for poly(methyl methacrylate)/ 0.005 vol % graphene oxide(PMMAGO) in which a solvent mixing method was used.[5] They reported that using Brinson's solution-mixing method, they do not observe a significant T_g change for

PMMA and most of the reinforcement and T_g increase reported by Brinson and co-workers result from the removal of low molecular weight additives in the original PMMA during the solvent mixing procedure to prepare the nanocomposites. The comparison of the neat PMMA containing additives with nanocomposites without additives leads to the apparently higher T_g and stiffness properties.[5] They also reported that only insitu-polymerization of MMA monomer with graphene oxide can raise T_g highly, due to the covalent bonds between graphene oxide and PMMA.

In our work, it was found that the T_g change of PMMA cannot be achieved to be as significant as PEMA via adding graphene oxide using solution-mixing method (Table 7.1). This result is consistent with Macosko and co-workers' conclusions. We propose here to explain the interesting difference between PEMA and PMMA in nanocomposites system. Both PEMA and PMMA are poly(n-alkyl methacrylates) and their α (glass transition) and β (side ester group rotation) relaxations have attracted great interest.[6-7] Williams an co-workers[7] reported that based on dielectric measurements, increasing pressure or decreasing temperature further separate the α and β relaxations of PEMA. In Chapter 3 we showed that graphene oxide can increase both α and β relaxation temperatures and also increase the distance between them. In future work, it would be of interest to investigate how graphene oxide can further split the α and β relaxations of a series of poly(n-alkyl methacrylates). We hypothesize the splitting issue is the reason that graphene oxide raises T_g more for PEMA than for PMMA. To study the splitting, one would compare the distance between T_g and T_β for PMMA and PEMA with the addition of the same loading of graphene oxide. Table 7.1 shows some preliminary results:

The preliminary results show that adding graphene oxide can further separate the T_g and T_β for PEMA but not for PMMA, which is consistent with our hypothesis. The reason might be

due to the fact that for PMMA with high T_g, α and β relaxations are already well separated therefore adding graphene oxide might not split them further.

To test our hypothesis, 95% isotactic-PMMA with a lower T_g compared to commercial atactic PMMA, has been chosen. Since the distance between the α and β relaxations is smaller than for commercial PMMA, it can then be split by adding graphene oxide, and give a significant increased T_g. So far preliminary results show that graphene oxide can also raise significantly the T_g of 95% isotactic-PMMA compared to the commercial atactic PMMA (Table 7.2) and in future work we are going to measure its β relaxation temperature to study the splitting.

7.2.2 Forced assembly multilayer co-extrusion

In the work from the present dissertation, when creating films of neat polymer / oriented graphene nanoplatelet filled polymer, the ratio of filled polymer / neat polymer is 1/9 ("asymmetric" alternating layers) and the highest graphene nanoplatelet concentration was 2 wt % in the filled polymer layers, which was regarded to maintain the thin layer structure. Therefore, the concentration of graphene nanoplatelets in the whole films was as low as 0.2 wt %. With modification and refinement of the multilayer co-extrusion facilities (installation of a new extrusion line in the PIMM lab at Arts et Métiers ParisTech in the fall of 2014), it would be possible to increase the ratio of filled polymer / neat polymer to 1/1, hence, creating films composed of "symmetric" alternating layers. In these films, when graphene nanoplatelet concentration is 2 wt % in the filled polymer layers, the concentration in the whole films can be as high as 1 wt %. (Figure 7.1) This new multilayer coextrusion line will also allow obtaining films where all the layers are in the 10 nm thickness range, which means that graphene

nanoplatelets can be incorporated into all the layers. In addition, not only reinforcement but also the gas permeability can be studied for these systems.

Another future work of interest is to incorporate block copolymer PS-b-PMMA to enhance the interface adhesion between the PS and PMMA. Although PMMA/PS-graphene is a good system to demonstrate the morphology of distinct layer structures with graphene nanoplatelets, the weak adhesion between PMMA and PS results in a spontaneous delamination and poor properties for PMMA/PS-graphene films. PS-b-PMMA as a compatibilizer would potentially strengthen the interface and therefore prevent delamination.[8-9]

7.2.3 Graphene nano-sandwich

Incorporating specific amphiphilic surfactants to bond graphene and polymer matrices, is an efficient strategy to disperse graphene in polymer matrices and increase their interaction to enhance properties.[10-11] However, it is of interest to evaluate the effects of different surfactants directly. Therefore, a potential future direction would be to use the nano-bubble inflation method to study the graphene nano-sandwich system with the addition of different surfactants to strengthen the interface between graphene and the polymer.

Amphiphilic surfactants usually have the structure of an aromatic core (graphene-philic) and polar chains (polar polymer-philic). However, with different surfactants, e.g. C10 triphenylene derivatives[10, 12-13] and 1-pyrenemethyl methacrylate, the interface between the graphene and polymers can be strengthened to different extents and this can be measured by nano-bubble inflation method to obtain different critical strains and interface strengths. Therefore strengthening of the graphene/polymer interface due to the surfactants could be investigated.

The nano-sandwich system also has the potential to be used to study other 2-D plate-like nanoparticles, e.g. hexagonal boron nitride (h-BN)[14-15] confined in polymer matrices. Hexagonal boron nitride has an excellent thermal conductivity with good dielectric properties.[14] And the future study of h-BN confined in polymer thin layer nano-sandwich could provide information about the interface mechanics between h-BN and polymers.

7.3 Reference

1. Potts, J. R.; Lee, S. H.; Alam, T. M.; An, J.; Stoller, M. D.; Piner, R. D.; Ruoff, R. S., *Thermomechanical properties of chemically modified graphene/poly(methyl methacrylate) composites made by in situ polymerization*. *Carbon* **2011,** *49* (8), 2615-2623.
2. Li, X. G.; McKenna, G. B., *Considering Viscoelastic Micromechanics for the Reinforcement of Graphene Polymer Nanocomposites*. *ACS Macro Letters* **2012,** *1* (3), 388-391.
3. Rafiee, M. A.; Rafiee, J.; Wang, Z.; Song, H.; Yu, Z.-Z.; Koratkar, N., *Enhanced Mechanical Properties of Nanocomposites at Low Graphene Content*. *ACS Nano* **2009,** *3* (12), 3884-3890.
4. Ramanathan, T.; Abdala, A. A.; Stankovich, S.; Dikin, D. A.; Herrera-Alonso, M.; Piner, R. D.; Adamson, D. H.; Schniepp, H. C.; Chen, X.; Ruoff, R. S.; Nguyen, S. T.; Aksay, I. A.; Prud'Homme, R. K.; Brinson, L. C., *Functionalized graphene sheets for polymer nanocomposites*. *Nat Nanotechnol* **2008,** *3* (6), 327-31.
5. Liao, K.-H.; Kobayashi, S.; Kim, H.; Abdala, A. A.; Macosko, C. W., *Influence of Functionalized Graphene Sheets on Modulus and Glass Transition of PMMA*. *Macromolecules* **2014**, 141028074543005.
6. Ngai, K. L.; Gopalakrishnan, T. R.; Beiner, M., *Relaxation in poly(alkyl methacrylate)s: Change of intermolecular coupling with molecular structure, tacticity, molecular weight, copolymerization, crosslinking, and nanoconfinement*. *Polymer* **2006,** *47* (20), 7222-7230.
7. Mpoukouvalas, K.; Floudas, G.; Williams, G., *Origin of the α, β, (βα), and "Slow" Dielectric Processes in Poly(ethyl methacrylate)*. *Macromolecules* **2009,** *42* (13), 4690-4700.
8. Zhang, J.; Lodge, T. P.; Macosko, C. W., *Interfacial morphology development during PS/PMMA reactive coupling*. *Macromolecules* **2005,** *38* (15), 6586-6591.
9. Zhang, J.; Lodge, T. P.; MacOsko, C. W., *Interfacial slip reduces polymer-polymer adhesion during coextrusion*. *Journal of Rheology* **2006,** *50* (1), 41-57.
10. Das, S.; Irin, F.; Tanvir Ahmed, H. S.; Cortinas, A. B.; Wajid, A. S.; Parviz, D.; Jankowski, A. F.; Kato, M.; Green, M. J., *Non-covalent functionalization of pristine few-layer graphene using triphenylene derivatives for conductive poly (vinyl alcohol) composites*. *Polymer* **2012,** *53* (12), 2485-2494.
11. Parviz, D.; Das, S.; Ahmed, H. S. T.; Irin, F.; Bhattacharia, S.; Green, M. J., *Dispersions of Non-Covalently Functionalized Graphene with Minimal Stabilizer*. *ACS Nano* **2012,** *6* (10), 8857-8867.
12. Yamamoto, T.; Motoyanagi, J.; Murakami, Y.; Miyauchi, Y.; Maruyama, S.; Kato, M., *Surfactant-Stabilized Single-Walled Carbon Nanotubes Using Triphenylene Derivatives Remain Individually Dispersion in Both Liquid and Dried Solid States*. *Applied Physics Express* **2009,** *2*, 055501.
13. Yamamoto, T.; Miyauchi, Y.; Motoyanagi, J.; Fukushima, T.; Aida, T.; Kato, M.; Maruyama, S., *Improved Bath Sonication Method for Dispersion of Individual Single-Walled Carbon Nanotubes Using New Triphenylene-Based Surfactant*. *Japanese Journal of Applied Physics* **2008,** *47* (4), 2000-2004.
14. Song, L.; Ci, L.; Lu, H.; Sorokin, P. B.; Jin, C.; Ni, J.; Kvashnin, A. G.; Kvashnin, D. G.; Lou, J.; Yakobson, B. I.; Ajayan, P. M., *Large scale growth and characterization of atomic hexagonal boron nitride layers*. *Nano Lett* **2010,** *10* (8), 3209-15.
15. Watanabe, K.; Taniguchi, T.; Kanda, H., *Direct-bandgap properties and evidence for ultraviolet lasing of hexagonal boron nitride single crystal*. *Nat Mater* **2004,** *3* (6), 404-409.

Table 7.1 Glass transition temperatures and β relaxation temperatures of PMMA/GO and PEMA/GO (Obtained from the G" peak in the rheological dynamic temperature test with the frequency at 6.28 rad/s)

Sample	T_β from G" /℃	T_g from G" /℃	Distance between T_g and T_β /℃
PMMA	4.0	94.8	90.8
PMMA/GO 0.12 vol %	7.4	98.4	91.0
PEMA	1.2	61.4	60.2
PEMA/GO 0.12 vol %	7.8	74.2	66.4

Table 7.2 Glass transition temperatures of atactic PMMA/GO, PEMA/GO and 95% isotactic-PMMA/GO (measured by DSC).

Sample	Mw	T_g from DSC/℃
Commercial PMMA (atactic)	100k	95.4
PMMA/GO 0.12 vol %	100k	99.6 ΔT_g=4.2
PEMA	515k	68.1
PEMA/GO 0.12 vol %	515k	81.7 ΔT_g=13.6
95% isotactic-PMMA	300k	56.2
95% isotactic-PMMA/GO 0.12 vol %	300k	67.2 ΔT_g=11.0

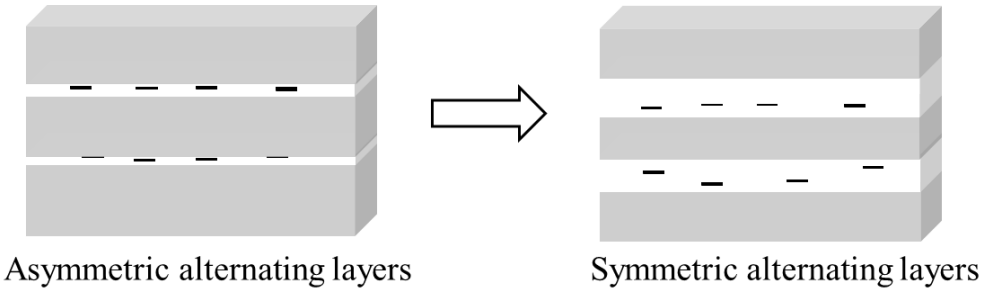

Figure 7.1 Refinement of the multilayer co-extrusion to create symmetric alternating layers with higher graphene nanoplatelets concentrations.

Résumé

Le graphène est une nanoparticule bidimensionnelle d'épaisseur atomique présentant des propriétés uniques, qu'elles soient mécaniques, électriques ou thermiques. Ceci ajouté à une faible densité et une très grande surface spécifique, fait que l'ajout de graphène et de nanoparticules dérivées (oxyde de graphène, graphite exofilé) pour renforcer des matrices polymères est devenu un sujet d'études d'intérêt majeur dans le domaine des nanocomposites. Cependant, l'influence de la variation de la viscoélasticité de la matrice due à l'ajout de graphène ainsi que la mécanique interfaciale reste aujourd'hui peu étudiée. De plus, il n'existe aujourd'hui pas de procédé permettant d'obtenir des nanocomposites présentant du graphène dans le plan orienté dans une matrice polymère afin de réaliser un renforcement à deux dimensions. Ce travail de thèse est composé principalement de trois projets portant sur ces problèmes.

La première partie de ce travail se concentre sur la façon d'utiliser l'approche micromécanique viscoélastiques pour soustraire l'effet de changement de T_g pour corriger la rigidité apparente de nanocomposites d'oxyde de graphène. On a ainsi trouvé que l'oxyde de graphène rigidifie « indirectement » les matrices polymères en augmentant de manière significative la T_g de la matrice, ce qui modifie largement la viscoélasticité du matériau. Le mécanisme de renforcement est ainsi largement causé par cet effet plutôt que du fait de la rigidité de l'oxyde de graphène lui-même.

La deuxième partie se concentre sur l'utilisation d'un procédé de mise en œuvre innovant, la coextrusion multinanocouches, ou assemblage forcé, pour créer des films nanocomposites constitués de couches alternées de polymères et de polymères chargés de nanoplaquettes de graphène orientées. Cette orientation est induite par le nanoconfinement imposé par le procédé. La morphologie des couches (35 ~ 40 nm d'épaisseur) contenant

du graphène orienté a été étudiée par microscopie électronique. Les propriétés mécaniques des matériaux ont été déterminées et le renforcement bidimensionnel a pu être corrélé à une orientation (imparfaite) des nanoplaquettes de graphène dans les films stratifiés.

La troisième partie se concentre sur l'utilisation de la méthode de l'inflation de nano-bulle pour obtenir les réponses mécaniques d'un « nano-sandwich » (nanofilm de polymère / feuille de graphène / nanofilm de polymère). Aux petites déformations, des renforts mécaniques significatifs ont été observées pour le système PEMA / graphène, tant à l'état caoutchouteux qu'à l'état vitreux. Les mécanismes d'interface entre le graphène et les polymères ont été étudiés et un glissement interfacial a été observé.

Nanocomposites graphène/polymères: rôle de la viscoélasticité, mise en oeuvre par assemblage forcé, et étude de l'interface

RESUME : Les nanocomposites ont un énorme potentiel pour une large gamme d'applications : ajouter des charges nanométriques aux propriétés intrinsèques extraordinaires dans un polymère est un moyen simple de modifier ses propriétés et d'obtenir de nouveaux matériaux. Le graphène est une nanocharge à deux dimensions d'épaisseur atomique, avec un fort potentiel dans les domaines mécaniques et électriques.

Dans ce travail, nous traitons plusieurs questions physiques concernant le mécanisme de renfort mécanique dans les nanocomposites à base de graphène et de ses dérivés : s'agit-il d'un effet dû aux propriétés intrinsèques des nanoparticules, ou dû aux modifications de la structure du polymère induit par l'ajout de ces charges ? Quel est le rôle de l'interface ? De nouvelles pistes pour la mise en oeuvre ont également été explorées : en utilisant un procédé innovant, des nanocomposites présentant des particules de graphène orientées et donc un renfort à 2 dimensions ont pu être obtenus.

Mots clés : nanocomposites, rhéologie, polymère, thin film.

GRAPHENE / POLYMER NANOCOMPOSITES:

VISCOELASTICITY, FORCED ASSEMBLY, AND NANOSANDWICH

ABSTRACT : Nanocomposites have a huge potential for a wide range of applications : adding fillers with nano-meter sizes and amazing intrinsic properties into polymers allow designing new materials. Graphene, is a planar nanofiller with atomic thickness, with high potential in the mechanical and electrical areas. In this work we deal with several physical questions to understand the mechanism for the mechanical reinforcement in graphene nanocomposites. In particular, this work aims at explaining if the effect is due to the intrinsic properties of the graphene or to the changes in the polymer properties induced by the addition of graphene. To do that, the effect of the graphene on the glass transition temperature and of amorphous polymers and the properties of the interface between graphene and the polymer were studied. We also designed nanocomposites presenting a nacre-like structure using an innovative processing tool to obtain a 2-dimensional reinforcement.

Keywords : polymer nanocomposites, multilayer film, processing, rheology, thin films, mechanical properties.

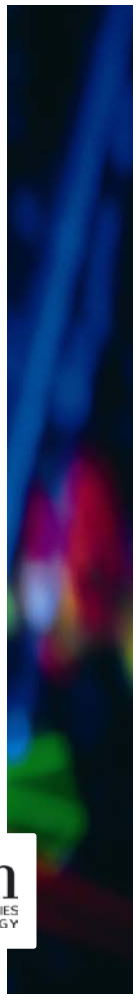

ARTS ET MÉTIERS ParisTech

ParisTech INSTITUT DES SCIENCES ET TECHNOLOGIES PARIS INSTITUTE OF TECHNOLOGY